

Mitigating Molecular Aggregation in Drug Discovery with Predictive Insights from Explainable AI

Hunter Sturm^{1,†}, Jonas Teufel^{2,†}, Kaitlin A. Isfeld¹, Pascal Friederich^{2,3,*}, Rebecca L. Davis^{1,*}

¹ University of Manitoba, Winnipeg, Canada

² Institute of Theoretical Informatics, Karlsruhe Institute of Technology, Karlsruhe, Germany

³ Institute of Nanotechnology, Karlsruhe Institute of Technology, Karlsruhe, Germany

[†] These authors contributed equally

*Corresponding authors: pascal.friederich@kit.edu, rebecca.davis@umanitoba.ca

Abstract

As the importance of high-throughput screening (HTS) continues to grow due to its value in early stage drug discovery and data generation for training machine learning models, there is a growing need for robust methods for pre-screening compounds to identify and prevent false-positive hits. Small, colloiddally aggregating molecules are one of the primary sources of false-positive hits in high-throughput screens, making them an ideal candidate to target for removal from libraries using predictive pre-screening tools. However, a lack of understanding of the causes of molecular aggregation introduces difficulty in the development of predictive tools for detecting aggregating molecules. Herein, we present an examination of the molecular features differentiating datasets of aggregating and non-aggregating molecules, as well as a machine learning approach to predicting molecular aggregation. Our method uses explainable graph neural networks and counterfactuals to reliably predict and explain aggregation, giving additional insights and design rules for future screening. The integration of this method in HTS approaches will help combat false positives, providing better lead molecules more rapidly and thus accelerating drug discovery cycles.

1. Introduction

High Throughput Screening (HTS) has become a cornerstone of early-stage drug discovery. With the advances in robotics and automation, millions of molecules are able to be rapidly screened against a biological target to assess activity and identify potential lead compounds. However, a persistent issue associated with HTS is the generation of false positives¹⁻³. False positives in HTS can be caused by many things, from alkylating agents to aggregation, promiscuity is almost always due to the physical properties of the molecules that cause the issue⁴. False positives pose serious issues in drug discovery as they can be found in most screening libraries and often results in additional resources and time being invested into nonproductive lead molecules^{5,6}. This issue is now exacerbated as HTS data is being used to train machine learning (ML) algorithms for the prediction of new lead compounds^{7,8}. The inclusion of false positives in these data sets again results in lost time and money in the identification of druggable molecules.

As of 2021, it was estimated that 15-20% of small molecules in publicly available databases undergo the phenomenon of molecular aggregation at a concentration of 30 μM , which is the typical screening concentration in an aqueous assay⁹. Small Colloidal Aggregating Molecules (SCAMs) are the most common class of molecules that give false positives in HTS⁵. Colloidal aggregation occurs once a compound reaches its critical aggregation concentration¹⁰. The colloid then binds to the surface of proteins which leads to local unfolding events and as such a loss of function of the protein¹¹. A second mechanism that aggregates can follow to interfere in biological assays is through a process called Aggregation-Induced Emission (AIE)¹². AIE occurs when molecules self-assemble and are then able to fluoresce¹³.

Due to the prevalence of SCAMs in HTS, there have been many methods established to predict and identify aggregating molecules¹⁴. SCAMs are identified experimentally through one of three common methods. The common experimental methods for SCAM detection are dynamic light scattering (DLS) running biological assays with and without an ionic detergent, as colloids tend to break up in detergent, and finally UV absorption spectroscopy can be used to detect AIE molecules. Experimental identification remains the most accurate method for aggregation detection, however the trade-off is that it is generally a slow process and would take weeks to screen all of the molecules in an HTS library. In order to speed up the identification process a number of *in silico* models have been developed for SCAM detection¹⁵⁻¹⁹. While each of these methods may be less accurate they make up for the issue with the speed.

While there are ways to predict if a molecule is a SCAM, *in silico* methods can provide greater than 80% accuracy but do not often provide the code necessary to be scaled to filter a large library of compounds¹⁶. Methods that can be scaled only correctly predict aggregation around 60-70% of the time^{15,16}. Therefore there is a need for a highly accurate method that can be scaled to filter large libraries of compounds. This study looked to fill this need by producing an accurate scalable model that can be utilized in the detection of SCAMs. Our model uses a multi-channel graph attention network (MEGAN)²⁰ to predict SCAMs with an accuracy of 82% and can be utilized in screening large libraries or single molecules. Additionally, our model outputs an explanation as to why it is classifying the compound as a SCAM or not. Our web server which screens single molecules also predicts the top user-specified number of counterfactuals, with explanations, for the input molecule. The counterfactuals explained in greater detail below are important as they tend to include at least one molecule that has its label flipped, meaning if your input molecule aggregates at least one of the counterfactuals will be predicted to not aggregate, and vice versa.

2. Methods

2.1 Dataset and cleaning process

In order to train our model, a dataset was curated and consisted of 12607 SCAMs downloaded from Aggregator Advisor¹⁷. In order to ensure our non-aggregating molecules were true non-aggregators, 432299 small molecules were obtained from the NIH Common Fund's Molecular Libraries Small Molecule Repository (MLSMR)²¹. The MLSMR dataset was utilized in this study as this library was used in one of the initial screens used to populate the aggregators

in Aggregator Advisor. Therefore any compound in the MLSMR dataset that is not an aggregator has been tested and experimentally validated as a non-aggregator¹¹.

From the initial list of 12607 aggregating and 432299 non-aggregating molecules, all SMILES codes were converted to canonical SMILES codes using Rdkit. If multiple fragments were present, the longest one was kept and the others (mostly counterions or solvents) were removed. If there was more than one long (>12 characters) fragment, the data point was discarded. After cleaning, the remaining lists of 12338 aggregating molecules and 371155 non-aggregating molecules were cross-checked to ensure they had no overlap.

From the initial 12607 aggregators, 20 were discarded due to the presence of large additional fragments, 2 caused Rdkit errors, and 247 were duplicates among the remaining molecules. Thus, the list was reduced from 12607 to 12338 molecules. From the initial 427630 non-aggregators, 5437 were discarded due to the presence of large additional fragments, none caused Rdkit errors, and there were 51038 duplicates among the remaining molecules. Thus, the list was reduced from 432299 to 371155 molecules.

2.2 Explainable graph neural networks, MEGAN

To reveal additional insights about the structure-property relationship behind molecular aggregation, we use a self-explaining graph neural network (GNN). To apply a GNN to the task of chemical property prediction, each molecule is first converted into a molecular graph where atoms are represented as nodes and bonds are represented as edges. All nodes and edges of the molecular graphs are additionally annotated with numeric feature vectors containing information about the corresponding elements and bond types. In particular, node feature vectors contain a one-hot encoding of the element as well as information about valence, charge, and aromaticity. Edge features include information about the bond type.

In this work, we use a multi-explanation graph attention network (MEGAN)²⁰. The MEGAN model uses attention mechanisms to directly produce multi-channel attributional explanations alongside each prediction. Attributional explanations assign an importance value of 0 to 1 to each node and edge of the input graph, which generally represent how important that particular element was towards the final outcome of the prediction. The MEGAN model employs multiple attention channels in parallel and produces one attributional explanation for each channel. In the case of binary classification problems (aggregator vs. non-aggregator), the model uses one explanation per class. Within each channel, the node and edge attribution masks are directly used as the weights of a global sum pooling operation to compute the global graph representation. A final fully-connected network is used to compute each channel's contribution to the final prediction result.

For the aggregation classification task, a molecule may be classified as one of the two classes "aggregator" or "non-aggregator". Consequently, the MEGAN model uses two separate explanation channels to represent these classes. The attributional node and edge explanations of these channels can thus be viewed as structural explanations for their respective classes.

An interactive version of the trained MEGAN model is available on <https://megan.aimat.science>, which allows single molecule predictions as well as batch predictions. Code and data are available on GitHub (See Data and Code Availability).

2.3 Counterfactuals

In addition to the attributional explanations generated by the MEGAN model, we use counterfactuals to explain the model behavior. Counterfactuals aim to intuitively explain the decision boundary of a model by providing counter examples of minimal input perturbations required to cause a maximum deviation of the model prediction. In the case of molecular classification, we define counterfactuals as molecular graphs which are structurally very similar to the original input graph, yet cause the greatest flip in the model's classification confidence.

To generate the counterfactuals for a given input molecule, we first compute all valid neighbor molecules. For this step we follow the procedure of generating single-edit molecular modifications described by Riley et al.²². All single-edit neighbors are then used as input to the model and sorted by the difference between their respective prediction results and the prediction of the original molecule. The generated counterfactuals are then ranked by prediction difference.

For all molecules in the test set, for which the model prediction was correct, we generated a fixed number of counterfactuals with one or two modification steps. For systematic analysis, we sorted the counterfactual molecules by the change in the model's prediction compared to the starting molecule, in order to find the modifications that lead to maximal changes in predicted aggregation behaviors. Full lists of molecules and counterfactuals can be found in the SI.

2.4 Fingerprint and descriptor based ensemble methods

To compare the accuracy of our model to the aggregation prediction model reported by Yang et al., we re-implemented their computational approach and trained it on the dataset presented in this work. We used three types of descriptors, namely fingerprint features (circular fingerprints as well as ECFP4/Morgan fingerprints as implemented in Rdkit²³), MACCS features as implemented in Rdkit²⁴, and CATS features²⁵ as implemented in <https://github.com/alexarnimueller/cats-descriptor>. Within each set of descriptors, we used a feature importance analysis based on a Random Forest classifier to determine how many features are required to achieve saturation in the test set accuracy. We set the numbers to 200, 200, 60, and 100 for circular fingerprints, ECFP4 fingerprints, CATS features, and MACCS features, respectively. After concatenation and hyperparameter optimization, we found the optimal hyperparameters of the Random Forest classifier to be an ensemble size of 500, with no limit on depth, and entropy as an impurity measure; of the Gradient Boosting classifier to be an ensemble size of 500, a maximum depth of 9, and a learning rate of 0.5; and of the xGBoost model to be an ensemble size of 500, a maximum depth of 8, and a learning rate of 0.1.

2.5 Feature Determination

Numerous molecular descriptors were explored to evaluate the differences in structural features and properties of the compounds in the aggregating and non-aggregating datasets. Using Rdkit, 111 molecular descriptors were calculated for both the aggregator and non-aggregator compounds (see SI for full list of descriptors). Of the 111 descriptors, 85 were fragment

descriptors which indicate the number of occurrences of specific fragments (e.g., halogens, carboxylic acids, nitro groups) in a given molecule. The remaining 26 descriptors were for general features (e.g., molecular weight, logP, ring count, number of hydrogen bond donors) of the molecules.

Histograms of each feature were plotted for both the aggregator and non-aggregator molecules to assess the distribution of the data (all histograms presented in SI). Nearly all 85 fragment descriptors, as well as 10 of the 26 general descriptors showed a non-normal distribution. As such, the fragment descriptors were analyzed separately from the general descriptors, and only the 16 general descriptors following a normal distribution were considered for further analysis.

In order to assess the statistical significance of each of the 16 general descriptors for the aggregating and non-aggregating molecules, p-values were calculated for each descriptor from a standard independent two sample t-test assuming equal population variances (calculated using `scipy.stats.ttest_ind`²⁶). All p-values were determined to be less than 0.005, indicating a high statistical significance for each descriptor, as such the effect size was computed for these features as the magnitude of the Cohen's d value.

$$\text{Cohen's } d = \frac{\mu_1 - \mu_2}{\sqrt{\frac{1}{2}((\sigma_1)^2 + (\sigma_2)^2)}} \quad (\text{Eq. 1})$$

Where μ_1 and μ_2 are the means of the descriptor values aggregators and non-aggregators, and σ_1 and σ_2 are the standard deviations. The p-values, means, standard deviations and Cohen's d values for the 16 general molecular descriptors can be found in the SI.

Analysis of the fragment descriptors through comparison of the relative frequency of each of the fragments between the aggregator and non-aggregator molecules revealed that the fragments provide little insight into the difference in the chemical nature of the aggregator and non-aggregator molecules (see SI for further information).

3. Results and discussion

3.1 Dataset Feature Analysis

While many studies have sought to determine which molecular features are responsible for aggregation of small molecules, to date, no consensus has been reached⁶. Molecular features often associated with SCAMS include logP, number of hydroxyl groups, number of sulfur atoms, and number of aromatic rings^{9,16,17}. To determine if there are significant differences in structural features and properties of the compounds in the aggregating and non-aggregating datasets used in this study, we analyzed both using the general and fragment molecular descriptors computed by RDKit.

All 16 of the normally distributed general molecular descriptors calculated had p-values of less than 0.005, indicating that they were statistically significant (see SI for details). The effect size was calculated to look for meaningful relationships between the molecules in the aggregating and non-aggregating datasets. As a measure of the difference in the mean of each descriptor of

the two data sets, Cohen's d values were calculated (**Figure 1**). The generally accepted interpretation of Cohen's d values is that a value of less than 0.2 is a small effect size, values near 0.5 are a medium effect size and values greater than 0.8 are a large effect size²⁷. The Cohen's d values indicate that two of the calculated descriptors (logP and number of aromatic rings) were considered to have high size effects. Analysis of the histograms for these features (see **Figure 2**) indicates that the molecules in the aggregator data set have a significantly higher logP and more aromatic rings per molecule, on average, than those in the non-aggregator data set. Three of the calculated descriptors (ring count, fraction of sp³ hybridized carbon atoms, and number of aromatic carbocycles) have medium size effects, again with the aggregators having higher average values in each category (see SI for details). Consistent with many other reports on aggregation features, our data indicates that both logP and the aromaticity are linked to aggregation. Alternatively, other features proposed in literature to be important to small molecule aggregation (i.e., number of sulfur atoms and number of hydroxyl groups) were not found to vary significantly between the molecules in the aggregating and non-aggregating datasets (see SI and **Figure 2d**)¹⁶.

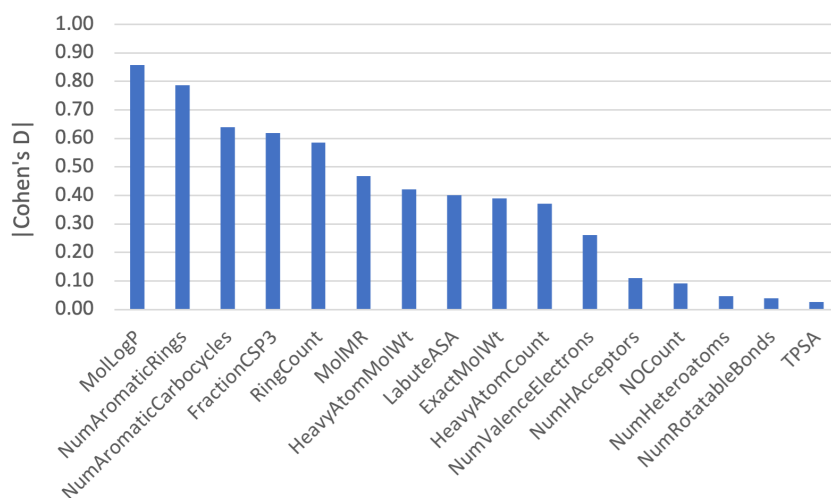


Figure 1. The absolute value of the Cohen's d for the 16 molecular descriptors.

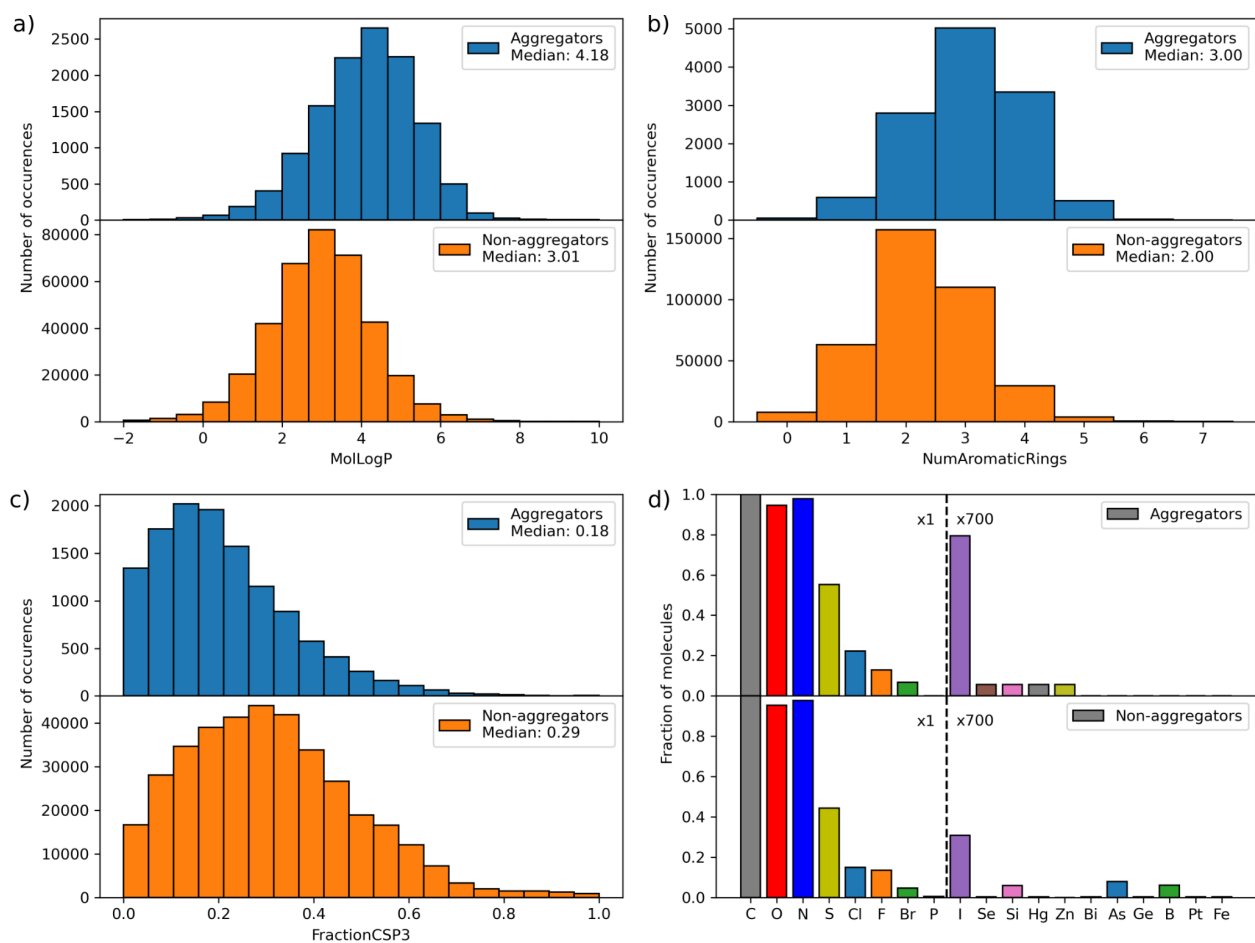


Figure 2. Histograms of a) MolLogP, b) Number of aromatic rings per molecule, c) Fraction of SP3 hybridized carbon, and d) element frequencies for the aggregator and non-aggregator datasets.

3.2 Prediction accuracy and benchmarking

We trained a MEGAN graph neural network model (see Methods) on the dataset described above. For a quantitative evaluation of our trained model, as well as a comparison to one of the previously best models in literature, we used a separate test set of 1500 aggregators and 1500 non-aggregators and computed the accuracy as well as the F1 score of the model. The results in **Table 1**, in particular a comparison of the first two lines, shows that the dataset presented here (or at least the balanced test split chosen here) is more difficult to predict than the dataset presented in Yang *et al.*¹⁶. However, when comparing the performance of the feature based XGBoost model used in Yang *et al.* (second line in **Table 1**) with the MEGAN model (third line), we see a clear advantage of the graph neural network. This can be due to the fact that the model input for the graph neural network is “complete” in a sense that the full molecular structure is modeled, which is not the case for the fingerprint and feature representations, or it can be related to the higher complexity and expressiveness of graph neural networks. Similar trends of superior performance of graph neural networks compared to classical machine

learning models can also be seen with many other datasets of molecules and materials of similar size²⁸.

While an accurate and reliable machine learning model can be used for screening and selection purposes in (multi-objective) molecular design tasks, we want to investigate in more detail what the MEGAN model learned and whether we can derive more generic design rules from it. To achieve that, we use a combination of the intrinsic explanations by the MEGAN model with a counterfactual analysis, and support both with additional analysis (e.g. through more detailed simulations) as well as with large language models (in this case ChatGPT and GPT3) to systematically and automatically generate possible explanations of aggregation behavior.

Table 1: Accuracy and F1 score of aggregation classifiers from literature (Yang *et al.*¹⁶), compared to our data and our MEGAN model.

| Model | Data | Accuracy (test) | F1 score (test) |
|---------------------------------|---------------------------------|-----------------|-----------------|
| Yang <i>et al.</i> | Yang <i>et al.</i> ¹ | 0.937 | 0.899 |
| Yang <i>et al.</i> ² | Ours (balanced test set) | 0.784 | 0.750 |
| Ours (MEGAN) | Ours (balanced test set) | 0.825 | 0.825 |

¹ The dataset used in Yang *et al.* is not published, which is why we could not reproduce the experiments with our model on their dataset.

² The code used in Yang *et al.* is not published, so we used a re-implementation based on the methodology described in Yang *et al.* However, not all 5 sets of descriptors could be re-implemented, which is why we used a subset of 3 sets of descriptors (see Methods). The best performance was achieved with a XGBoost model but the performance of random forest models and gradient boosting models was almost identical.

3.3 Explanations and counterfactuals from MEGAN: Presentation of few examples, discussion of insights gained.

The generation of counterfactuals for each aggregating and non-aggregating molecule in the test set highlighted several functional group modifications that were commonly used by the model to switch the label of a given molecule. Two of the most common modifications noted were the addition of a double bond and addition of a thiol to promote aggregation (see SI for details). To further assess the impact of these and other modifications on the predicted label, we performed a manual inspection of derivatives of molecules that were correctly predicted to be aggregators or non-aggregators. The data presented in this section is not a systematic evaluation of all molecules in our datasets but highlights some of the patterns we have noted in the evaluation of the counterfactuals.

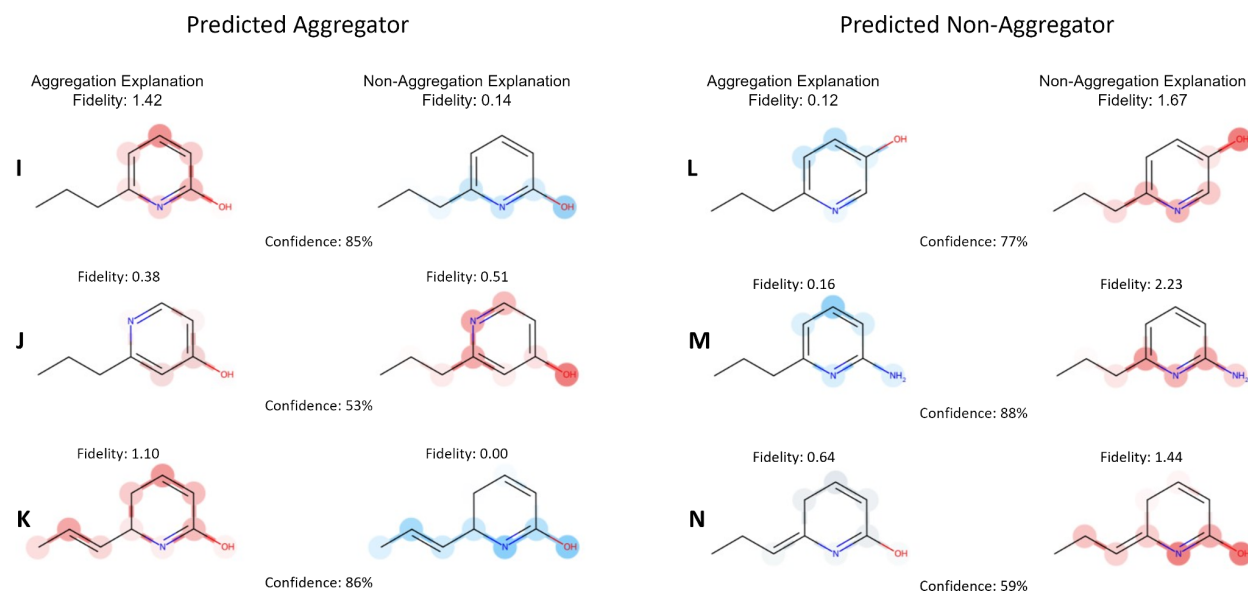


Figure 3. Compound **A** is a known aggregating compound, compound **E** is a known non-aggregating compound, compounds **B**, **C**, **D**, **F**, **G**, and **H** are all counterfactuals of compounds **A** and **E**.

To begin we assessed two compounds, **A** and **E**, that were each correctly predicted by the MEGAN model to be aggregators and non-aggregators, respectively (see **Figure 3**). Counterfactuals with a flipped label were generated for **A** and **E** in an effort to investigate what the MEGAN model deems important in predicting the aggregation label. The stark contrast between the aggregating abilities of the two compounds is based on the presence of a single methyl group. Thus, we first investigated the influence of location of the methyl group on the heteroaromatic polycycle. Compounds **F** and **G** are structural isomers to **A**, and were all found to produce flipped labels relative to **A** (i.e. convert an aggregator into a non-aggregator). This suggests that the presence of the methyl group is not in itself enough to flip the label, but that the location of the alkyl group is recognized to play a key role in assignment of the label.

The top two counterfactuals of **E**, predicted to have a flipped label, contained a hydroxyl (**B**) or thiol group (not shown). As previously noted, thiols have been identified as a common functional group for inducing aggregation both in our assessment of counterfactuals and by other models^{9,16,17}^{15,16,9,16,17}. With that in mind, compounds **C**, **D** and **H** were examined. The replacement of the methyl group in **A** with an alcohol increases confidence in the aggregator label (compare **A** and **C**). The confidence in the assignment of the aggregator label is further increased by replacement of the methyl with a thiol (compare **A** and **D**). It should be noted that the imidate and thioimidate substructures found in **C** and **D**, respectively, are often seen in aggregators predicted by our model. Examination of compound **H**, which contains a thiol and is geometrically similar to **D** but does not possess a thioimidate, shows that the thiol itself is not a predictor of aggregation.

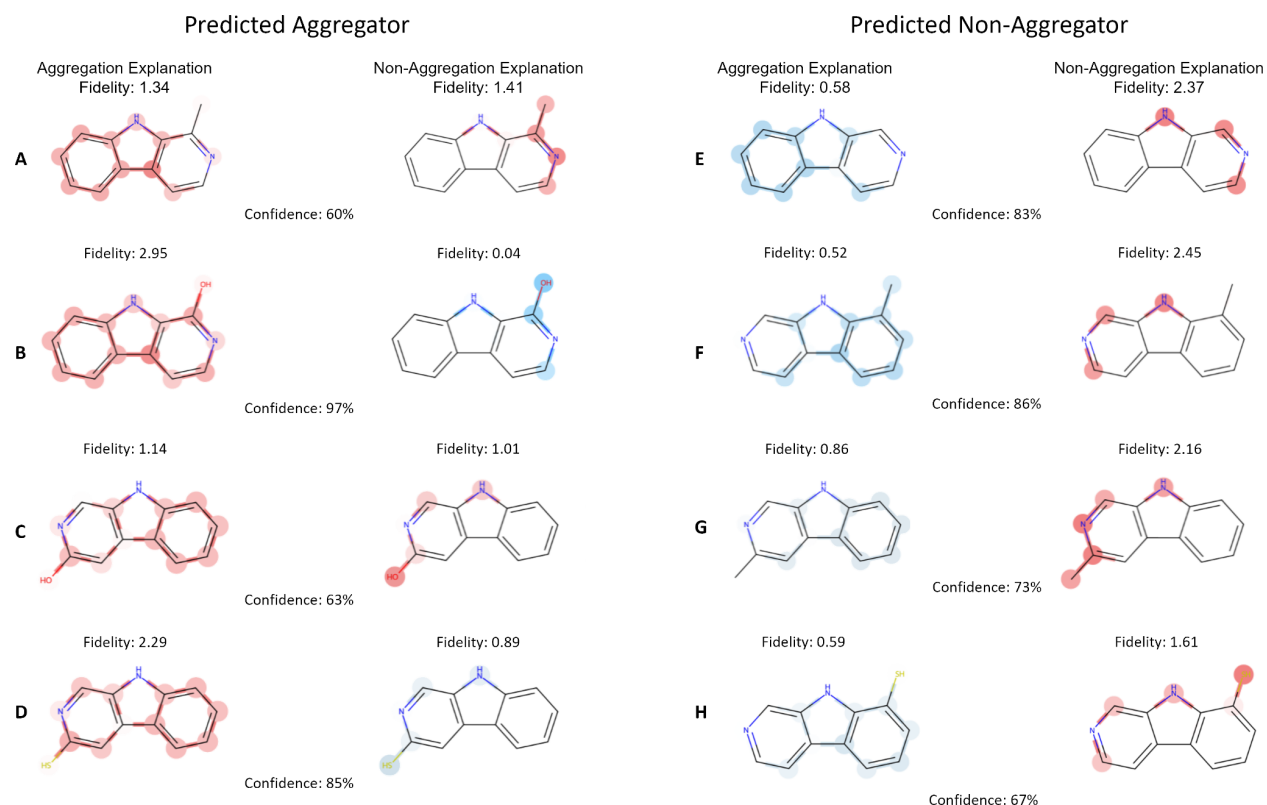


Figure 4. Counterfactual examples for pyridine derivatives.

Having demonstrated that the position of a functional group is key to prediction of a label, we wanted to further assess the sensitivity of the model to standard electronic effects. To do this we examined derivatives of pyridine (see **Figure 4**). Compound **I** is correctly predicted by the MEGAN model to be an aggregator. Moving the alcohol from the 2-position of the pyridine (**I**) to the 3-position (**L**) flips the label from aggregator to non aggregator. This could potentially be a sign of the model's ability to recognize the difference in the electronics of the 2 rings as in **L** the alcohol is no longer in conjugation with the pyridine nitrogen. However, it could also be the result of the loss of the imidate substructure that leads to **L** being classified as a non-aggregator. The assignment of **J**, which has the alcohol at the 3-position of the pyridine, as an aggregator suggests that the model may be sensitive to electronic effects and not just the presence of the imidate. While it has been shown that the imidates and thioimidates are commonly classified as aggregators by the MEGAN model, 2-amino pyridine **M** is predicted to be a non-aggregator. This suggests that the hydrogen bonding network, formed by the placement of a H-bond donor at the 2-position of the pyridine, is not solely responsible for the aggregation classification.

Finally, we evaluated the role of unsaturations in the classification of molecules as aggregators or non-aggregators. As noted in the analysis of our two data sets (**Figure 1**), aggregators contain significantly more aryl rings than non-aggregators. To test whether the presence of aromatic rings or the presence of unsaturations in the molecule has a stronger influence on classification, we assessed two structural isomers of **I** in which one of the unsaturations in the pyridine ring has been migrated out of the ring (**K**, **N**), thus breaking the aromaticity while maintaining the number of unsaturated carbons. In **N**, the conjugation of all 3 double bonds is

maintained however aromaticity is lost. In **K**, one of the double bonds is moved out of conjugation with the unsaturations in the ring. Interestingly, **N** is classified as a non-aggregator while **K** is classified as an aggregator. This suggests that the model is sensitive to the positions of the unsaturations in a molecule, potentially to a greater extent than it is to the presence of aromatic rings.

In order to further investigate the relationship between the predictions by the MEGAN model and potential formation of molecular aggregates, we performed calculations of dimer binding energies of a set of molecules derived from the compounds shown in **Figure 4**. We varied the position of the nitrogen atom in the pyridine ring as well as the presence and position of an hydroxyl group. Initial dimer geometries were constructed and conformer ensembles were generated using CREST²⁹ based on GFN2-xTB calculations³⁰. The lowest energy conformer (dimer as well as monomer) was optimized using density functional theory (B3-LYP^{31,32}/def2-SV(P)³¹) in Turbomole³¹⁻³³. **Figure 5** shows the correlation of dimer binding energies and MEGAN aggregation predictions. Despite slight outliers such as compound **X** (derived from compound **M**), there is a strong correlation between binding energy and aggregation prediction. This suggests that dimerization might be related to formation of molecular aggregates, and stronger dimer binding energies increase the likelihood of aggregation. Further calculations of more compounds are needed to further investigate this relationship.

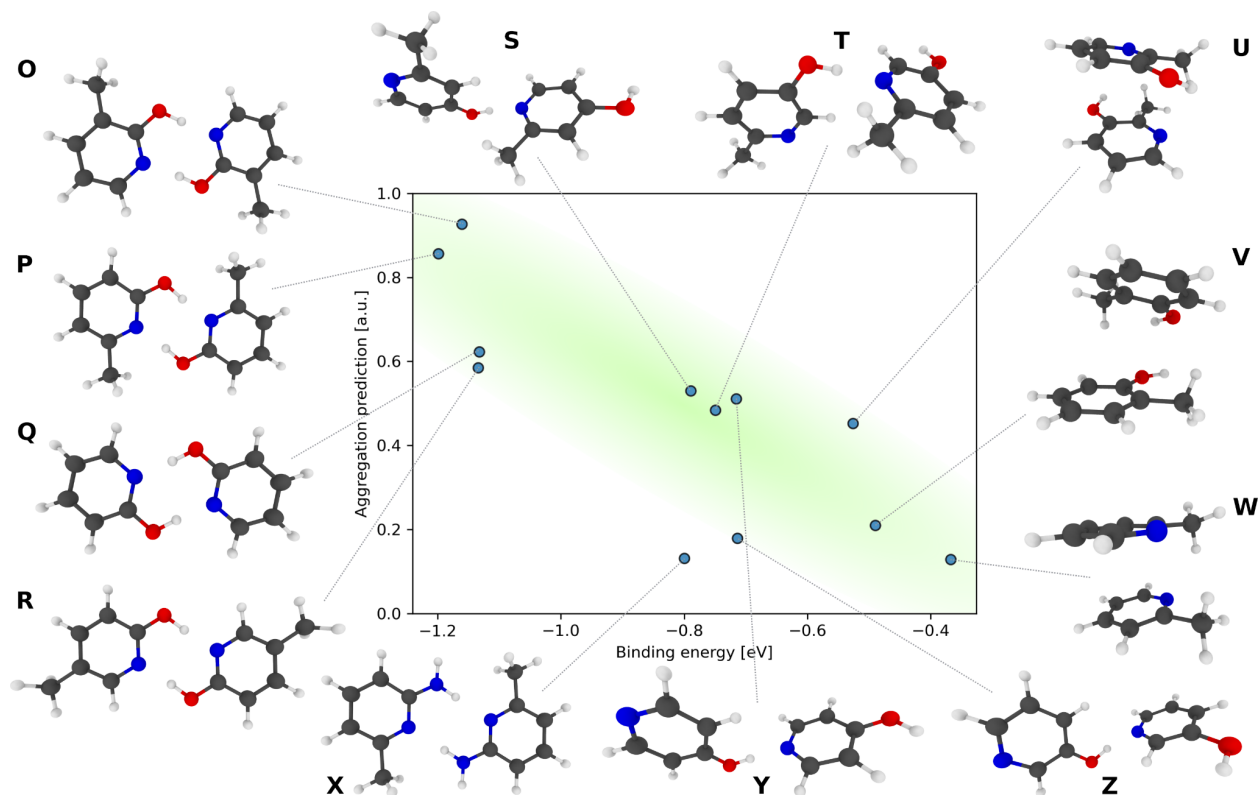


Figure 5. MEGAN prediction of aggregation on a scale from 0 to 1 vs. dimer binding energy calculation for compounds O - Y, derived/simplified from the compounds shown in **Figure 4**.

3.4 Automated generation of explanations using large language models

To analyze whether counterfactuals generated based on the MEGAN model can be explained in automated ways, we experimented with large language models, specifically GPT-3 and ChatGPT. The goal was to see whether counterfactuals, and in particular the associated molecular changes, can be automatically related to more broad chemical concepts and human-understandable explanations related to aggregation, in order to stimulate further ideas for more detailed studies and analysis by experts.

Prompts were created with the following template, which was adapted from OpenAI's examples:

"I am an expert in the field of chemistry with a specialization in the phenomenon of molecular aggregation. I generally explain circumstances by referencing specific rules of molecular dynamics or well-known interactions and molecular forces at play.

I have encountered a base molecule '{{ original.smiles }}' which is a {{ original.label }}.

This molecule is now modified to '{{ modified.smiles }}' and becomes a {{ modified.label }}.

Specifically the fragment '{{ original.fragment }}' is changed to '{{ modified.fragment }}'.

I will explain precisely how the small change in this fragment causes the change in its molecular aggregation behavior."

We manually used ChatGPT, through the openly accessible web interface, to generate explanations of selected counterfactuals and we integrated the GPT-3 API into automated workflows. In the following, a selection of interesting but also trivial GPT-generated explanations will be presented and discussed. Full texts can be found in the SI.

When asked about the role of a thiol group in aggregation in a specific small example, ChatGPT suggests that "[...] aggregation is often driven by noncovalent interactions, such as hydrogen bonding, pi-pi stacking, and hydrophobic interactions. The addition or removal of a specific atom can disrupt or alter these interactions, leading to different aggregation tendencies. [...]" and that "[...] the presence of the sulfur atom introduces additional opportunities for intermolecular interactions. The sulfur atom can participate in hydrogen bonding and form favorable interactions with other molecules or parts of the same molecule. These interactions contribute to the aggregation behavior observed. [...]"

When asked about differences between functions groups such as thiol, hydroxyl and nitrogen atoms, ChatGPT mentions multiple possible causes of increased aggregation behavior (full text in SI, here just a short summary): 1. The larger size and higher polarizability enable stronger intermolecular interactions. 2. The larger size and lower electronegativity of sulfur atoms compared to oxygen can make the sulfur lone pairs more prone to interactions with other molecules. 3. Sulfur is less electronegative than oxygen, making it more hydrophobic, which plays a significant role in aggregation processes, as nonpolar regions of molecules tend to associate with each other to minimize exposure to water. 4. Sulfur-containing groups, such as thiols (R-SH) and thioethers (R-S-R), can participate in pi-interactions and pi-stacking interactions, which can stabilize molecular assemblies and promote aggregation. 5. Sulfur atoms can readily form coordination bonds with metal ions, which is relevant in the context of

metalloproteins and metal-containing complexes, where the presence of sulfur can facilitate aggregation through metal-sulfur coordination interactions.

While most of these points are valid and relevant, they are also partially generic and trivial, and there are some caveats. The thioethers associated by the ChatGPT model with aggregation are statistically non-decisive in our dataset (occurring in 4.6% of aggregators and 4.3% of non-aggregators). However, sulfur atoms bridging any aromatic and non-aromatic systems occur in 22.4% of aggregators but only in 15.9% of non-aggregators, making them an interesting molecular motif worth further investigation. Furthermore, the metal atoms mentioned by the ChatGPT model are sequestered in the protein and not free to support aggregation. However, polarizability, hydrophobicity (logP), and pi-interactions are certainly related to aggregation and allow for further statistical analysis and potentially development of more refined design rules.

3.5 Predictions on external datasets

To further validate our model, a dataset of 91 structurally diverse molecules that have been experimentally determined as aggregating or non-aggregating was compiled and assessed with our model. This data set includes molecules that were previously unseen by the algorithm (i.e. not in the test or training set). The molecules, taken from literature sources, consisted of 52 aggregating and 39 non-aggregating compounds^{9,34–38}. Molecules in this external validation dataset were selected to be diverse structurally as well as in terms of mechanism of action of false positives. Of the aggregating molecules in this data set, 46 bind to an enzyme and kill activity, while the other 9 aggregators undergo aggregation-induced emission (AIE). As our model was only trained on aggregators that were identified through enzyme binding studies, this allowed us to test the model's ability to identify molecules that undergo AIE. Our model was able to correctly classify 69 out of 91 compounds correctly, leading to an accuracy of 75.8% (see **Figure 6**). 7 of the 9 molecules exhibiting AIE were correctly predicted to be aggregators.

| | | | |
|------------|----------------|-----------------|----------------|
| True Label | Aggregator | 42 | 10 |
| | Non-aggregator | 12 | 27 |
| | | Aggregator | Non-aggregator |
| | | Predicted Label | |

Figure 6. Confusion matrix of true and false predictions of the MEGAN model on external datasets.

Analysis of the counterfactuals produced for the true positives in the 91-molecule dataset revealed a slight pattern in the structures generated. It was frequently observed that the addition

of rigidity to the structures through double bonds and small rings systems, or the removal of a hydrogen bond donor, switched the label from non-aggregating to aggregating. Alternatively, the addition of a hydrogen bond donor, or the cyclization of the molecule into a macrocycle often switched the label from aggregating to non-aggregating. These observed trends provide further insight into what the MEGAN model deems important for aggregation.

Finally, a large dataset of FDA-approved drugs was compiled from the ZINC20 database to further validate our method³⁹. **Figure 7** shows the results of MEGAN predictions on a test set as well as on a dataset of FDA-approved drugs. While 154 molecules of the FDA dataset are predicted by the model to be aggregating, the confidence of the model is low compared to the predictions on the test dataset, where a substantial fraction has a likelihood much larger than 0.5 (which is the threshold). Only 41 of the FDA-approved drugs are predicted to be aggregating with a confidence of >0.9. This is inline with what would be expected as most of the molecules were predicted to be non-aggregators with high confidence, as mentioned above aggregators are false positives so it makes sense that there would not be many SCAMS as approved drugs. However, it is possible that some of the FDA drugs do aggregate, but just not at the concentration they are prescribed, or are unidentified to means of adsorption (i.e. topologically applied drugs).

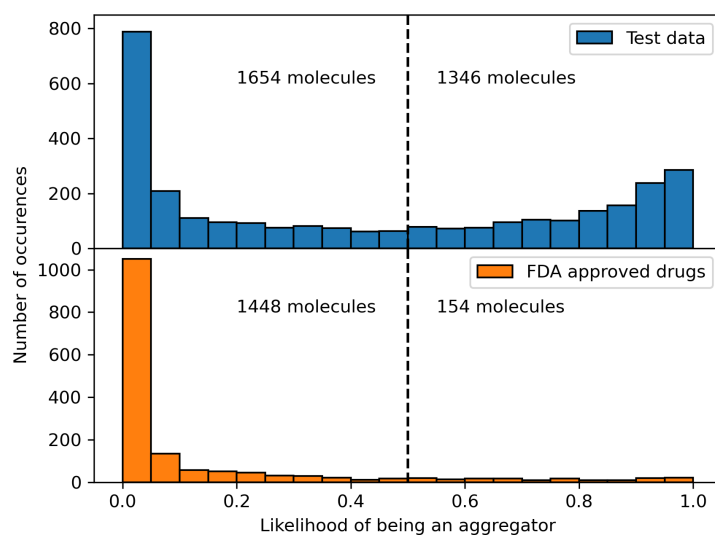


Figure 7. FDA predictions: The upper panel shows the distribution of raw outputs of the MEGAN model on a balanced test set of 1500 aggregating and 1500 non-aggregating molecules, while the lower panel shows the predictions on the FDA dataset.

4. Conclusions and Outlook

The MEGAN model presented in this work was able to accurately predict SCAMS with an accuracy of 82.5% on a balanced in-distribution test data set and similar accuracies on smaller external data sets. While traditional features, e.g. logP values or number of aromatic rings are relevant to detect SCAMS, the high accuracy of the MEGAN model can only be explained if we assume that the model learns more complex relations between molecular structure and aggregating behavior. Using intrinsic model explanations as well as counterfactuals, we

identified and further analyzed selected motifs that were found through systematic analysis of the model. Using expert knowledge driven interpretations, further simulations, as well as automatic interpretations with large language models, we show that additional insight into molecular aggregating can be obtained.

We find specific molecular motifs to be strongly related to aggregation while at the same time the MEGAN model helps to reveal small modifications that strongly change aggregating behaviour which can be used in molecular design approaches. We furthermore find that the predictions by the MEGAN model are strongly correlated with molecular binding energies, indicating that dimerization can play a relevant role in the formation of larger molecular aggregates. First tests of combining large language models with model predictions and counterfactuals shows that interesting additional insight can be obtained which potentially accelerates or inspires further manual analysis by experts.

The accuracy of the MEGAN model coupled with the accessibility and extra functionality provided through a publicly available web interface allows for reliable detection of SCAMs. Furthermore, molecular counterfactuals, where minimal structural changes reverse the aggregation prediction, can be utilized in the design of alternatives for compounds that are likely to aggregate that will still maintain the main structure of the scaffold. This overall allows for the filtering of HTS libraries to combat false positives in the actual screens.

Acknowledgments

P.F. acknowledges support by the Federal Ministry of Education and Research (BMBF) under Grant No. 01DM21001B (German-Canadian Materials Acceleration Center), as well as support by the Helmholtz Association within the Helmholtz Core Informatics Initiative. R.D acknowledges support from the National Science and Engineering Council Discovery Grant Program and the Canadian Institutes of Health Research.

Data and code availability

Our code for model training and counterfactual analysis can be found on Github https://github.com/aimat-lab/megan_aggregators. In our repository, we also include a persistent representation of the already trained model, which can be used directly. The dataset can be downloaded at <https://bwsyncandshare.kit.edu/s/pGExzNEkjbAdKHw>. Furthermore, we provide an interactive web interface for the manual prediction of the aggregation behavior of single molecules at https://megan.aimat.science/predict/megan_aggregator. Given a SMILES representation of a molecule, the interface shows the predicted classification, visualization of local explanations, and the top counterfactuals.

References

1. Sink, R., Gobec, S., Pečar, S. & Zega, A. False positives in the early stages of drug discovery. *Curr. Med. Chem.* **17**, 4231–4255 (2010).

2. Klumpp, M. Non-stoichiometric inhibition in integrated lead finding - a literature review. *Expert Opin. Drug Discov.* **11**, 149–162 (2016).
3. Thorne, N., Auld, D. S. & Inglese, J. Apparent activity in high-throughput screening: origins of compound-dependent assay interference. *Curr. Opin. Chem. Biol.* **14**, 315–324 (2010).
4. Baell, J. B. & Nissink, J. W. M. Seven Year Itch: Pan-Assay Interference Compounds (PAINS) in 2017-Utility and Limitations. *ACS Chem. Biol.* **13**, 36–44 (2018).
5. Ganesh, A. N., Donders, E. N., Shoichet, B. K. & Shoichet, M. S. Colloidal aggregation: from screening nuisance to formulation nuance. *Nano Today* **19**, 188–200 (2018).
6. Reker, D., Bernardes, G. J. L. & Rodrigues, T. Computational advances in combating colloidal aggregation in drug discovery. *Nat. Chem.* **11**, 402–418 (2019).
7. Dreiman, G. H. S., Bictash, M., Fish, P. V., Griffin, L. & Svensson, F. Changing the HTS Paradigm: AI-Driven Iterative Screening for Hit Finding. *SLAS Discov* **26**, 257–262 (2021).
8. Rahman, A. S. M. Z. *et al.* A machine learning model trained on a high-throughput antibacterial screen increases the hit rate of drug discovery. *PLoS Comput. Biol.* **18**, e1010613 (2022).
9. Lee, K. *et al.* Combating small-molecule aggregation with machine learning. *Cell Rep. Phys. Sci.* 100573 (2021).
10. Coan, K. E. D. & Shoichet, B. K. Stoichiometry and physical chemistry of promiscuous aggregate-based inhibitors. *J. Am. Chem. Soc.* **130**, 9606–9612 (2008).
11. Doak, A. K., Wille, H., Prusiner, S. B. & Shoichet, B. K. Colloid formation by drugs in simulated intestinal fluid. *J. Med. Chem.* **53**, 4259–4265 (2010).
12. Hong, Y., Lam, J. W. Y. & Tang, B. Z. Aggregation-induced emission: phenomenon, mechanism and applications. *Chem. Commun.* 4332–4353 (2009).
13. Mei, J., Leung, N. L. C., Kwok, R. T. K., Lam, J. W. Y. & Tang, B. Z. Aggregation-Induced Emission: Together We Shine, United We Soar! *Chem. Rev.* **115**, 11718–11940 (2015).
14. Yang, Z.-Y., He, J.-H., Lu, A.-P., Hou, T.-J. & Cao, D.-S. Frequent hitters: nuisance artifacts in high-throughput screening. *Drug Discov. Today* **25**, 657–667 (2020).
15. Alves, V. M. *et al.* SCAM Detective: Accurate Predictor of Small, Colloidally Aggregating Molecules. *J. Chem. Inf. Model.* **60**, 4056–4063 (2020).
16. Yang, Z.-Y. *et al.* Structural Analysis and Identification of Colloidal Aggregators in Drug Discovery. *J. Chem. Inf. Model.* **59**, 3714–3726 (2019).
17. Irwin, J. J. *et al.* An Aggregation Advisor for Ligand Discovery. *J. Med. Chem.* **58**, 7076–7087 (2015).
18. Ryan, A. J., Gray, N. M., Lowe, P. N. & Chung, C.-W. Effect of detergent on ‘promiscuous’ inhibitors. *J. Med. Chem.* **46**, 3448–3451 (2003).
19. Feng, B. Y. & Shoichet, B. K. A detergent-based assay for the detection of promiscuous inhibitors. *Nat. Protoc.* **1**, 550–553 (2006).
20. Teufel, J., Torresi, L., Reiser, P. & Friederich, P. MEGAN: Multi-Explanation Graph Attention Network. (2022).
21. McCarthy, A. The NIH Molecular Libraries Program: identifying chemical probes for new medicines. *Chem. Biol.* **17**, 549–550 (2010).

22. Zhou, Z., Kearnes, S., Li, L., Zare, R. N. & Riley, P. Optimization of Molecules via Deep Reinforcement Learning. *Sci. Rep.* **9**, 10752 (2019).
23. Rogers, D. & Hahn, M. Extended-connectivity fingerprints. *J. Chem. Inf. Model.* **50**, 742–754 (2010).
24. Durant, J. L., Leland, B. A., Henry, D. R. & Nourse, J. G. Reoptimization of MDL keys for use in drug discovery. *J. Chem. Inf. Comput. Sci.* **42**, 1273–1280 (2002).
25. Reutlinger, M. *et al.* Chemically Advanced Template Search (CATS) for Scaffold-Hopping and Prospective Target Prediction for ‘Orphan’ Molecules. *Mol. Inform.* **32**, 133–138 (2013).
26. Virtanen, P. *et al.* SciPy 1.0: fundamental algorithms for scientific computing in Python. *Nat. Methods* **17**, 261–272 (2020).
27. Sullivan, G. M. & Feinn, R. Using Effect Size-or Why the P Value Is Not Enough. *J. Grad. Med. Educ.* **4**, 279–282 (2012).
28. Reiser, P. *et al.* Graph neural networks for materials science and chemistry. *Commun Mater* **3**, 93 (2022).
29. Pracht, P., Bohle, F. & Grimme, S. Automated exploration of the low-energy chemical space with fast quantum chemical methods. *Phys. Chem. Chem. Phys.* **22**, 7169–7192 (2020).
30. Bannwarth, C., Ehlert, S. & Grimme, S. GFN2-xTB-An Accurate and Broadly Parametrized Self-Consistent Tight-Binding Quantum Chemical Method with Multipole Electrostatics and Density-Dependent Dispersion Contributions. *J. Chem. Theory Comput.* **15**, 1652–1671 (2019).
31. Weigend, F. & Ahlrichs, R. Balanced basis sets of split valence, triple zeta valence and quadruple zeta valence quality for H to Rn: Design and assessment of accuracy. *Phys. Chem. Chem. Phys.* **7**, 3297–3305 (2005).
32. Becke, A. D. A new mixing of Hartree–Fock and local density-functional theories. *J. Chem. Phys.* **98**, 1372–1377 (1993).
33. Ahlrichs, R., Bär, M., Häser, M., Horn, H. & Kölmel, C. Electronic structure calculations on workstation computers: The program system turbomole. *Chem. Phys. Lett.* **162**, 165–169 (1989).
34. Han, T. *et al.* Aggregation-induced emission: A Rising Star in chemistry and materials science. *Chin. J. Chem.* **39**, 677–689 (2021).
35. Peng, Q. & Shuai, Z. Molecular mechanism of aggregation-induced emission. *Aggregate (Hoboken)* **2**, (2021).
36. O'Donnell, H. R., Tummino, T. A., Bardine, C., Craik, C. S. & Shoichet, B. K. Colloidal Aggregators in Biochemical SARS-CoV-2 Repurposing Screens. *J. Med. Chem.* **64**, 17530–17539 (2021).
37. Zalmi, G. A., Jadhav, R. W., Mirgane, H. A. & Bhosale, S. V. Recent Advances in Aggregation-Induced Emission Active Materials for Sensing of Biologically Important Molecules and Drug Delivery System. *Molecules* **27**, (2021).
38. Wu, W. & Liu, B. Aggregation-induced emission: challenges and opportunities. *Natl Sci Rev* **8**, nwa222 (2021).
39. Irwin, J. J. *et al.* ZINC20-A Free Ultralarge-Scale Chemical Database for Ligand Discovery. *J. Chem. Inf. Model.* **60**, 6065–6073 (2020).

Supporting Information

Mitigating Molecular Aggregation in Drug Discovery with Predictive Insights from Explainable AI

Hunter Sturm, Jonas Teufel, Kaitlin A. Isfeld, Pascal Friederich, Rebecca L. Davis

SI. List of all RDKit molecular descriptors calculated for all compounds in the aggregator and non-aggregator datasets.

SII. Histograms of normally distributed general molecular descriptors for the aggregator and non-aggregator datasets.

SIII. Histograms of non-normally distributed general molecular descriptors for the aggregator and non-aggregator datasets.

SIV. Histograms of fragment molecular descriptors for the aggregator and non-aggregator datasets.

SV. p-values, means, standard deviations and Cohen's d values for the 16 general molecular descriptors calculated for the aggregator and non-aggregator datasets.

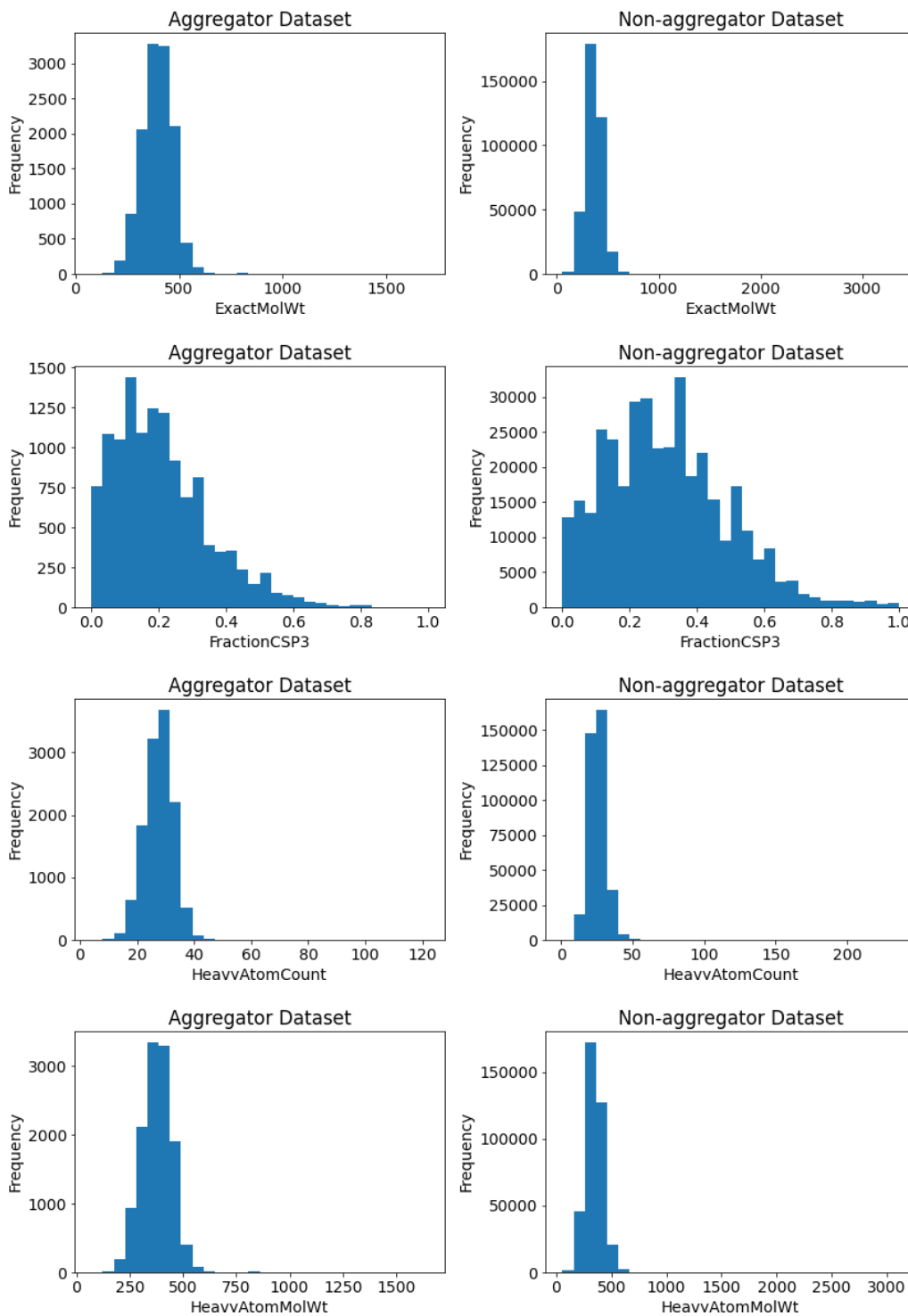
SVI. Comparison of the relative frequency of each of the fragments described by the fragment descriptors for the aggregator and non-aggregator molecules.

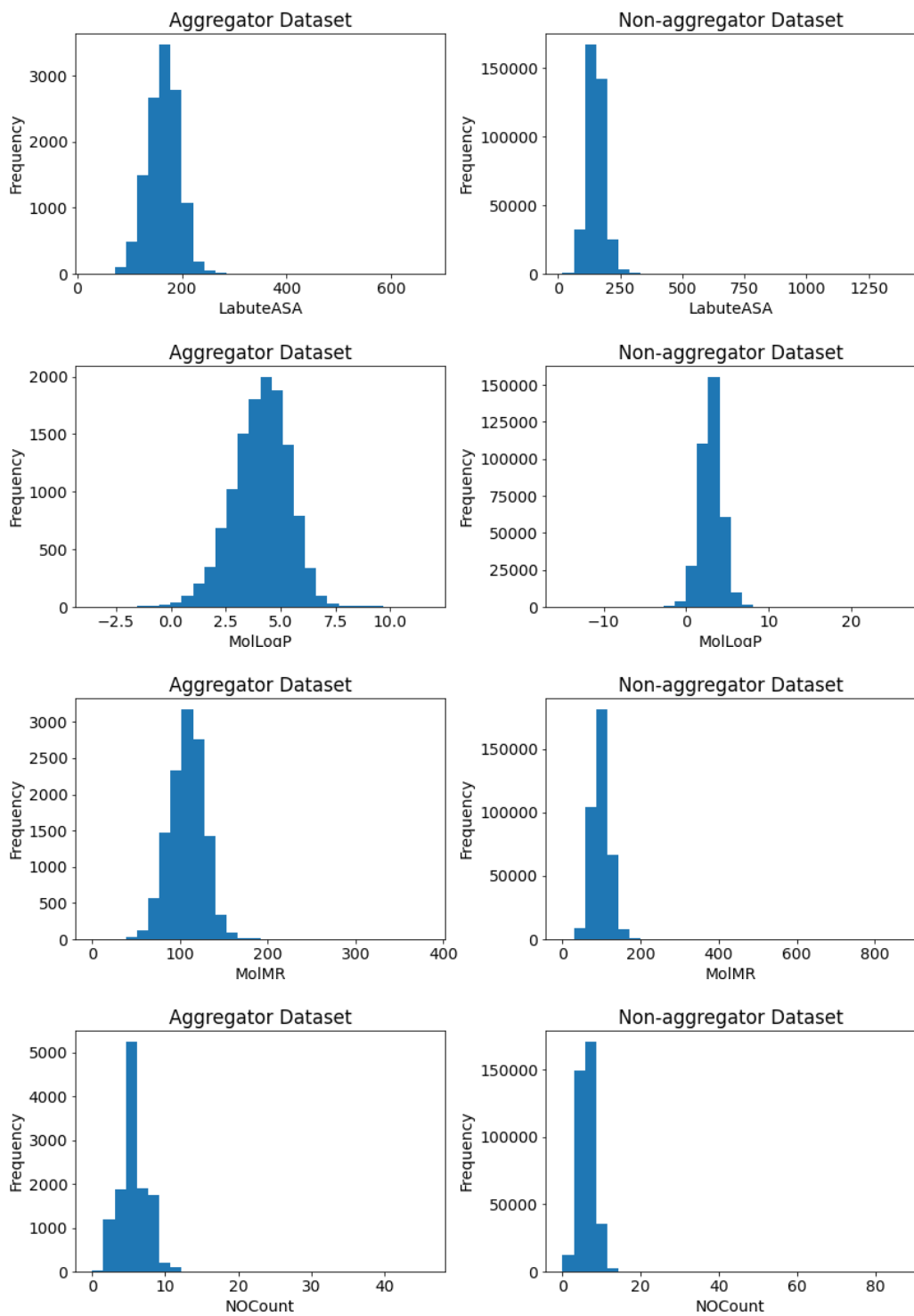
SVII. GPT-based explanations: Full texts.

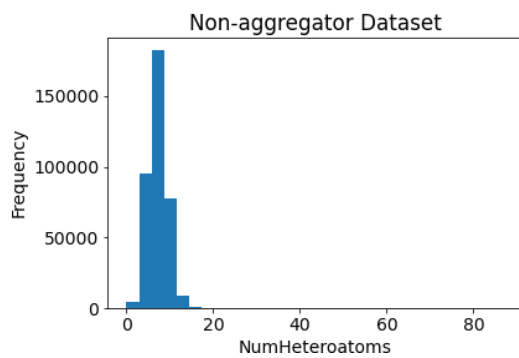
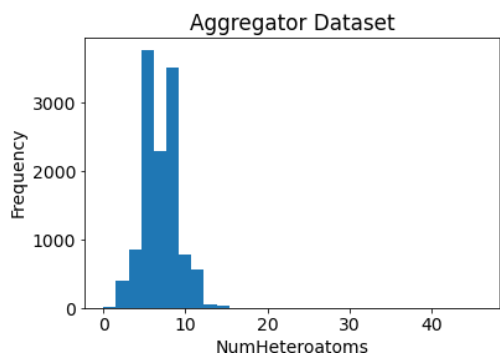
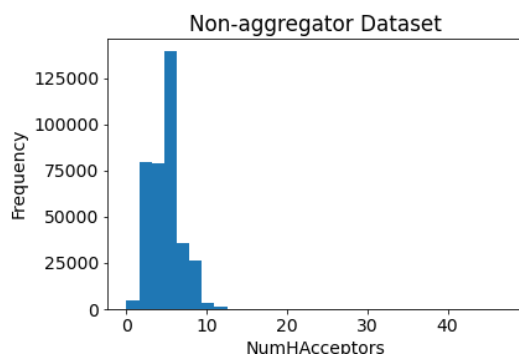
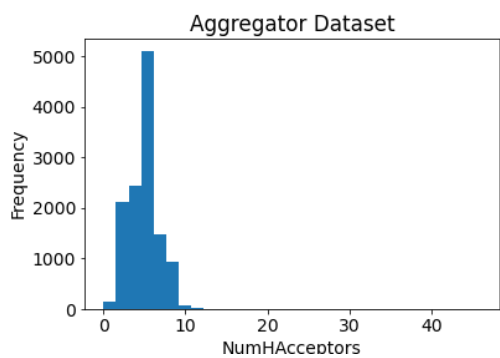
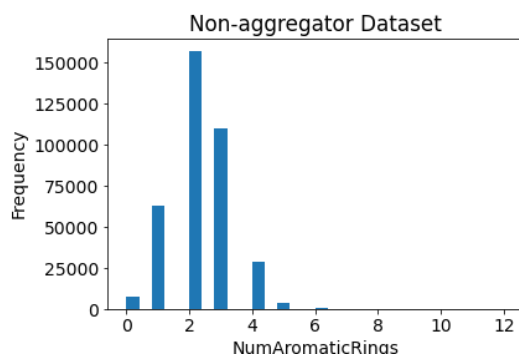
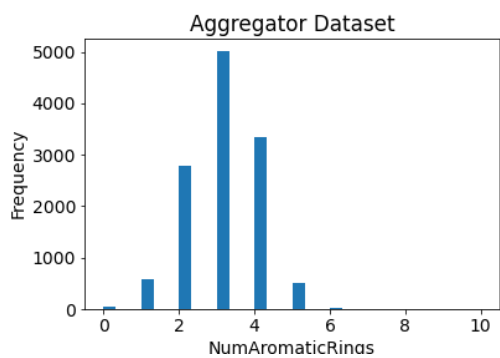
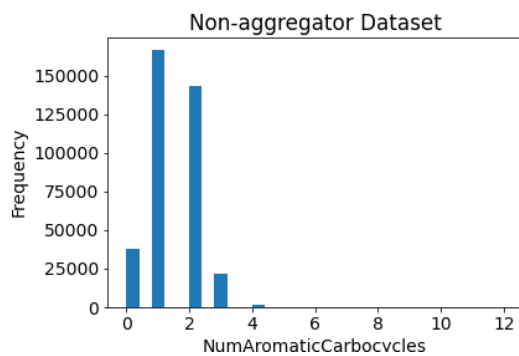
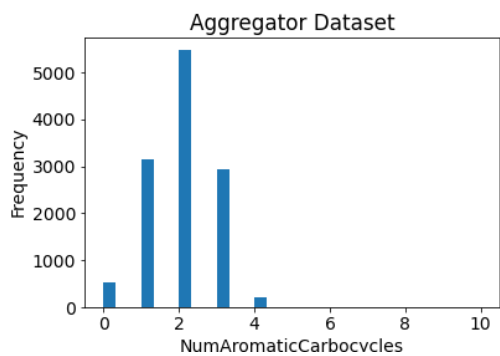
SI. List of all RDKit molecular descriptors calculated for all compounds in the aggregator and non-aggregator datasets.

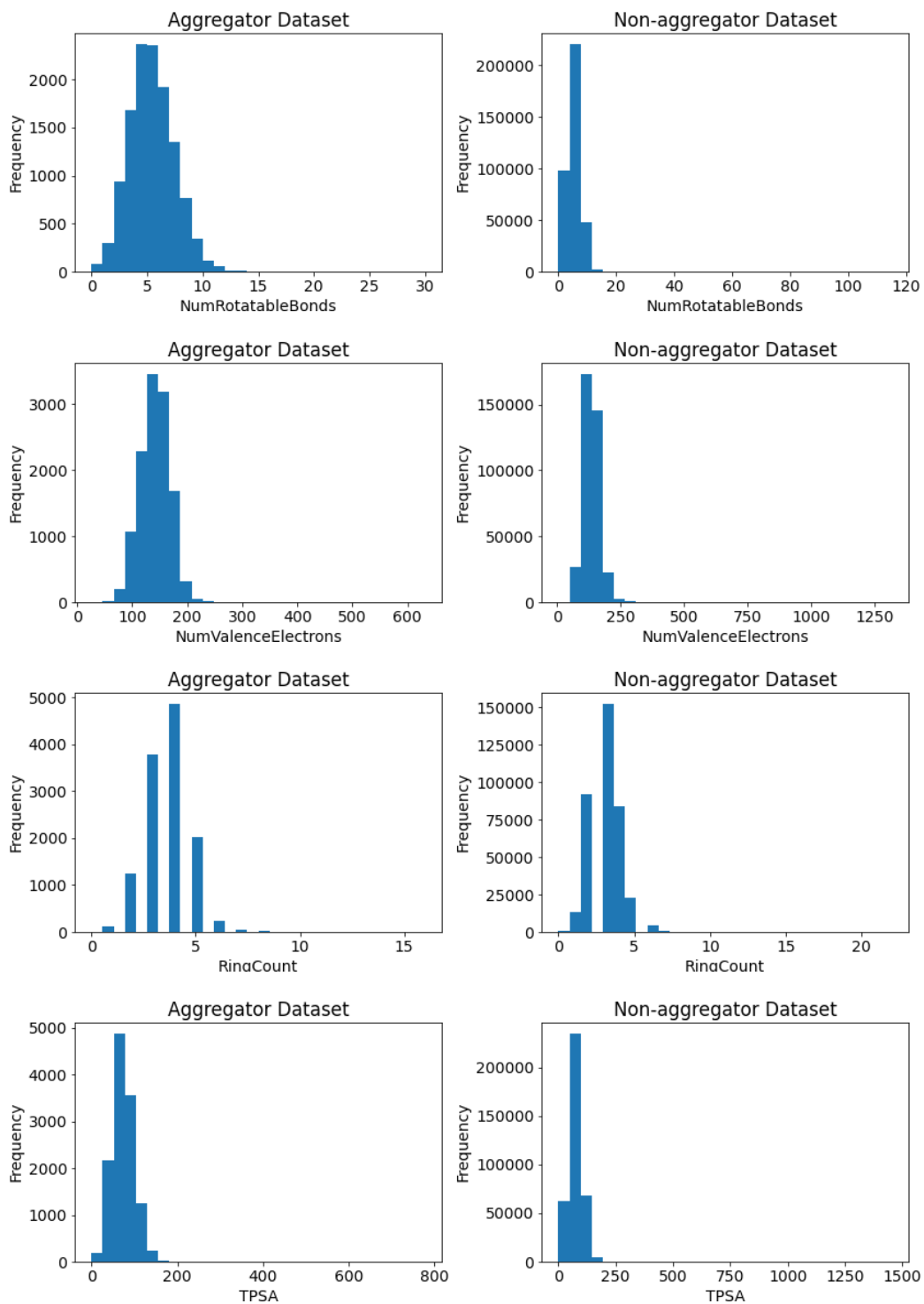
ExactMolWt, FractionCSP3, HeavyAtomCount, HeavyAtomMolWt, LabuteASA, MolLogP, MolMR, NHOHCount, NOCount, NumAliphaticCarbocycles, NumAliphaticHeterocycles, NumAliphaticRings, NumAromaticCarbocycles, NumAromaticHeterocycles, NumAromaticRings, NumHAcceptors, NumHDonors, NumHeteroatoms, NumRadicalElectrons, NumRotatableBonds, NumSaturatedCarbocycles, NumSaturatedHeterocycles, NumSaturatedRings, NumValenceElectrons, RingCount, TPSA, fr_Al_COO, fr_Al_OH, fr_Al_OH_noTert, fr_ArN, fr_Ar_COO, fr_Ar_N, fr_Ar_NH, fr_Ar_OH, fr_COO, fr_COO2, fr_C_O, fr_C_O_noCOO, fr_C_S, fr_HOCCN, fr_Imine, fr_NH0, fr_NH1, fr_NH2, fr_N_O, fr_Ndealkylation1, fr_Ndealkylation2, fr_Nhpyrrole, fr_SH, fr_aldehyde, fr_alkyl_carbamate, fr_alkyl_halide, fr_allylic_oxid, fr_amide, fr_amidine, fr_aniline, fr_aryl_methyl, fr_azide, fr_azo, fr_barbitur, fr_benzene, fr_benzodiazepine, fr_bicyclic, fr_diazo, fr_dihydropyridine, fr_epoxide, fr_ester, fr_ether, fr_furan, fr_guanido, fr_halogen, fr_hdrzine, fr_hdrzone, fr_imidazole, fr_imide, fr_isocyan, fr_isothiocyan, fr_ketone, fr_ketone_Topless, fr_lactam, fr_lactone, fr_methoxy, fr_morpholine, fr_nitrile, fr_nitro, fr_nitro_ arom, fr_nitro_ arom_nonortho, fr_nitroso, fr_oxazole, fr_oxime, fr_para_hydroxylation, fr_phenol, fr_phenol_noOrthoHbond, fr_phos_acid, fr_phos_ester, fr_piperdine, fr_piperzine, fr_priamide, fr_prisulfonamd, fr_pyridine, fr_quatN, fr_sulfide, fr_sulfonamd, fr_sulfone, fr_term_acetylene, fr_tetrazole, fr_thiazole, fr_thiocyan, fr_thiophene, fr_unbrch_alkane, fr_urea

SII. Histograms of normally distributed general molecular descriptors for the aggregator and non-aggregator datasets.

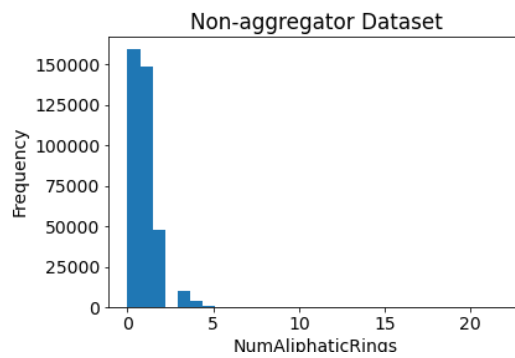
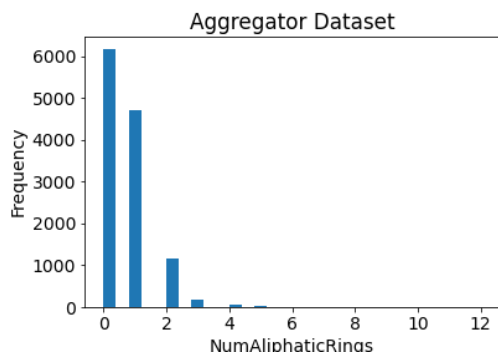
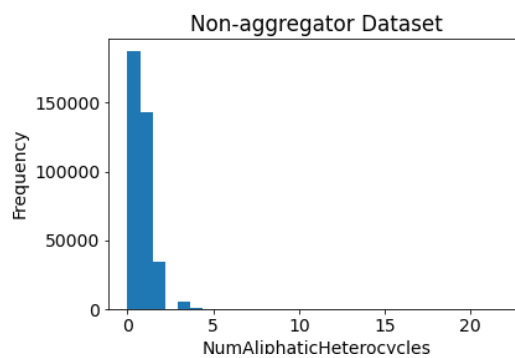
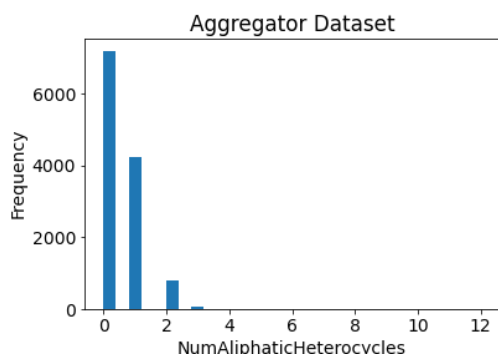
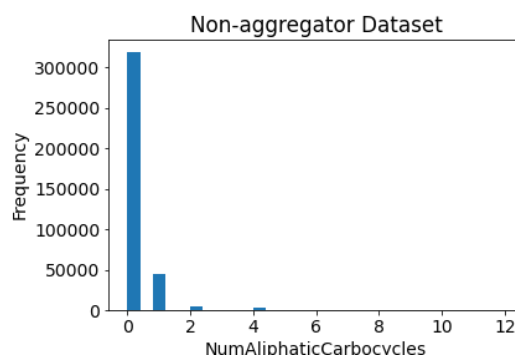
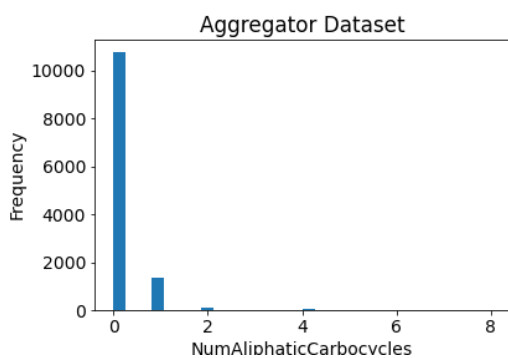
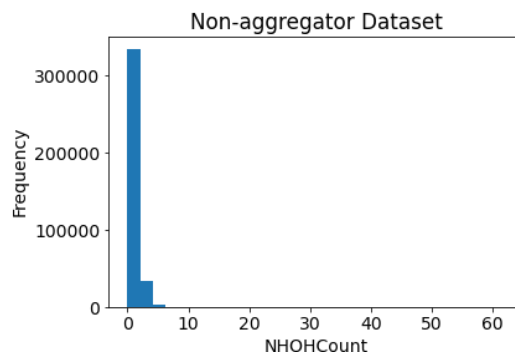
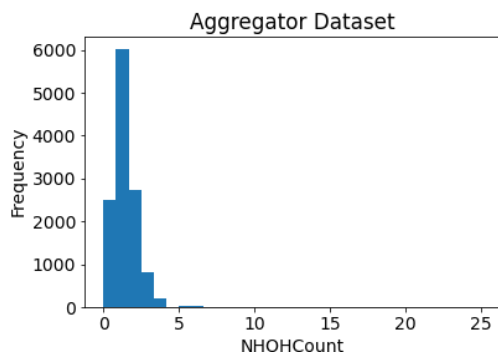


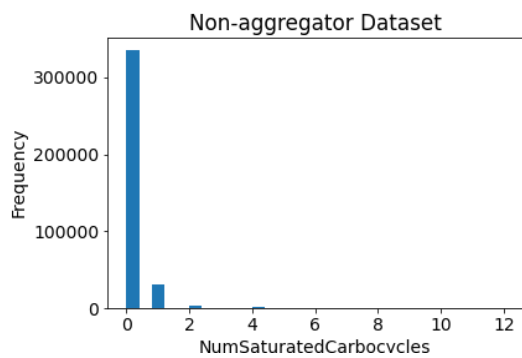
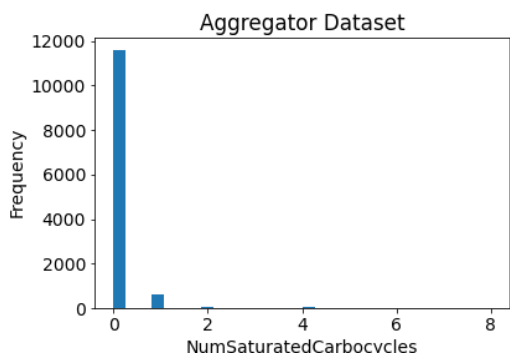
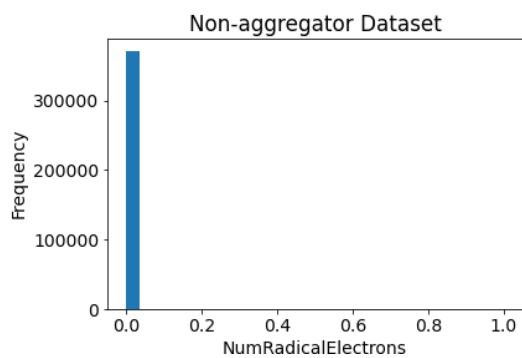
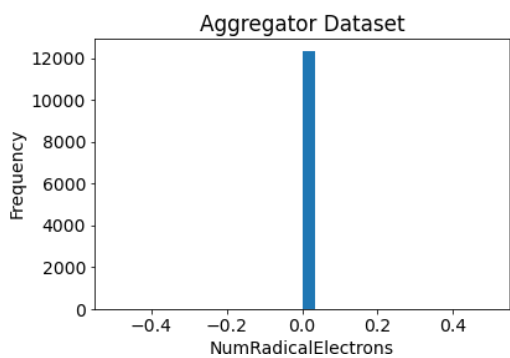
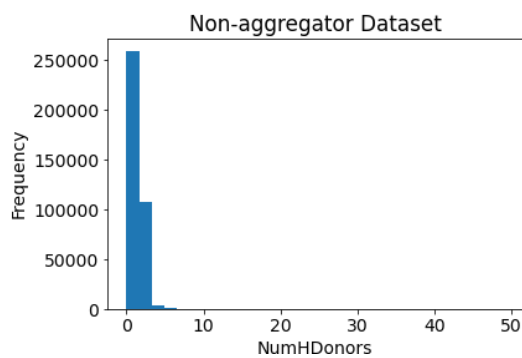
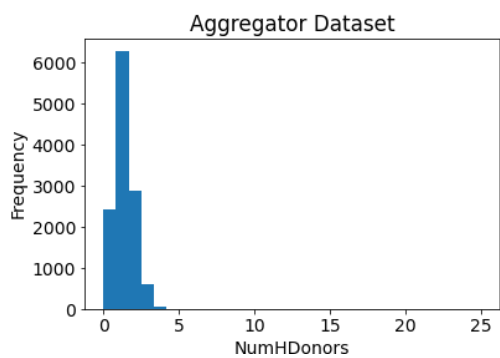
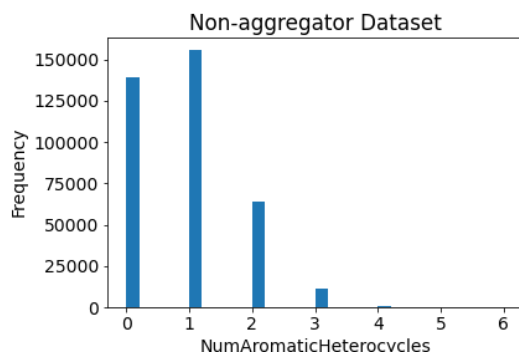
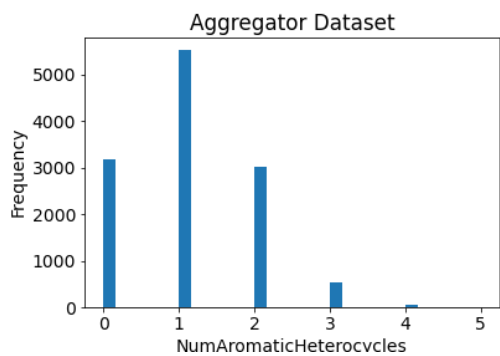


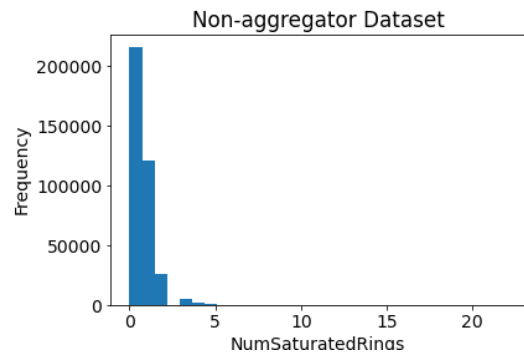
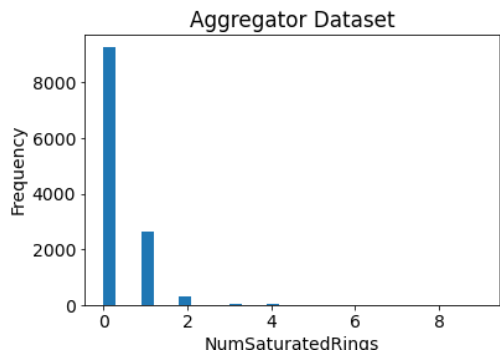
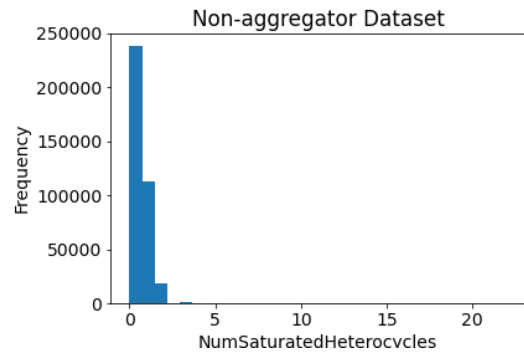
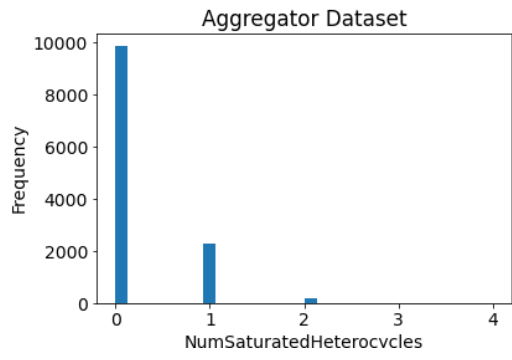




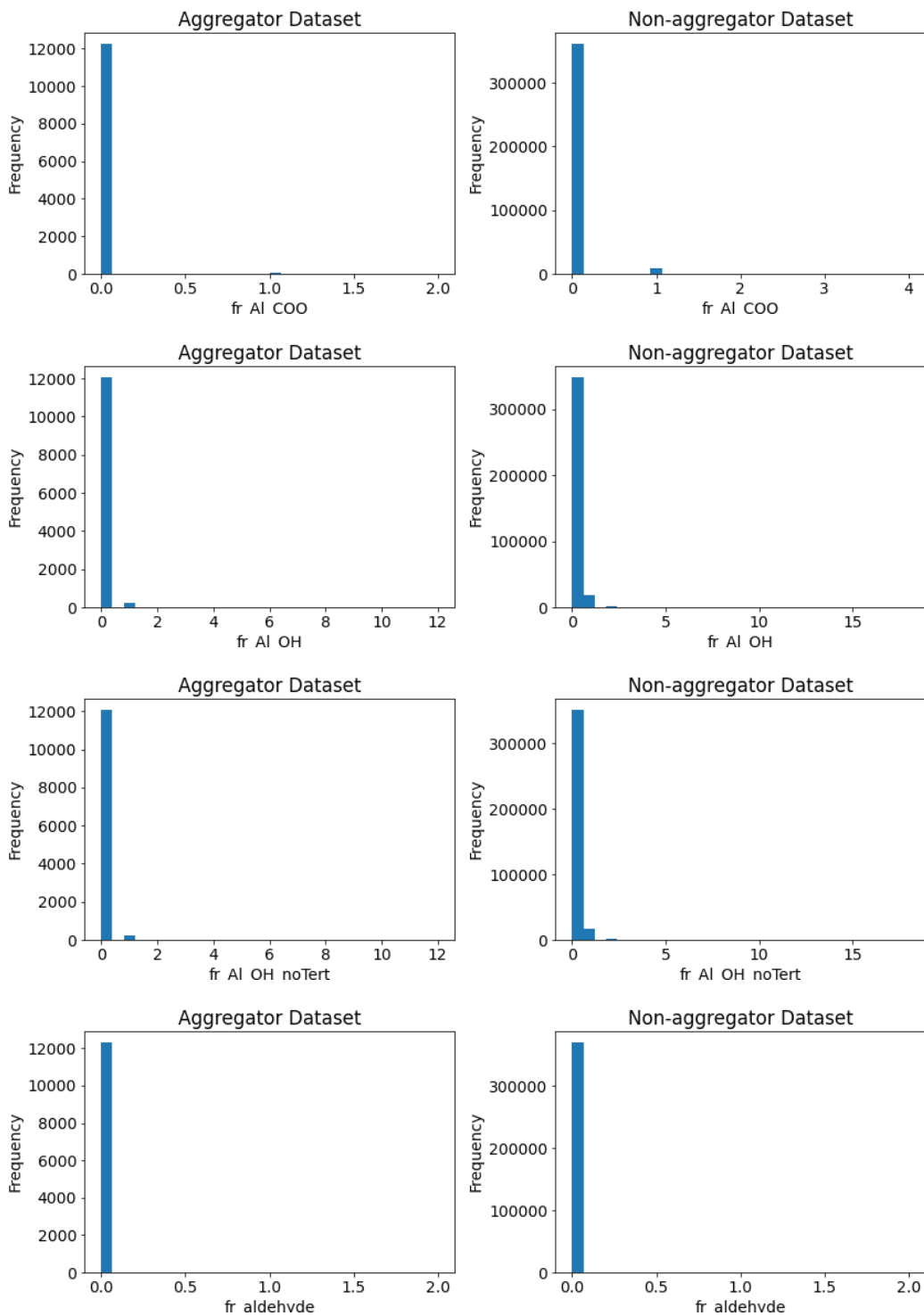
SIII. Histograms of non-normally distributed general molecular descriptors for the aggregator and non-aggregator datasets.

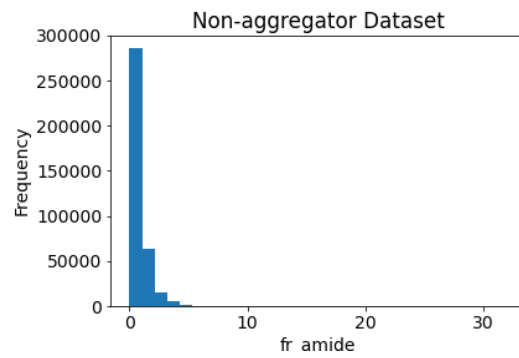
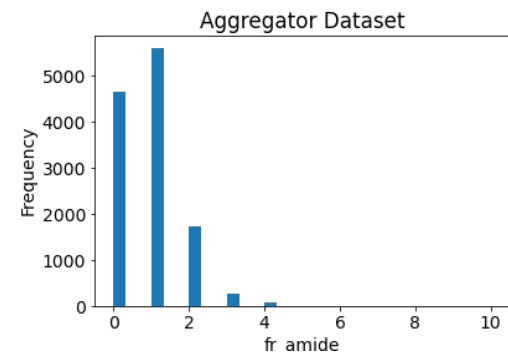
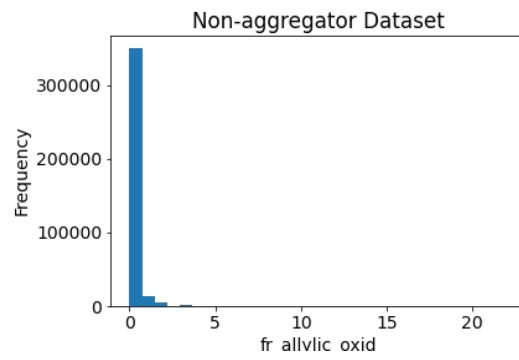
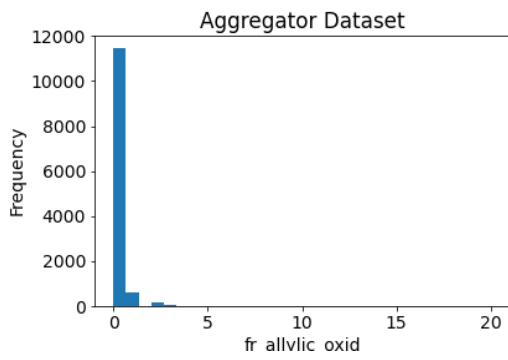
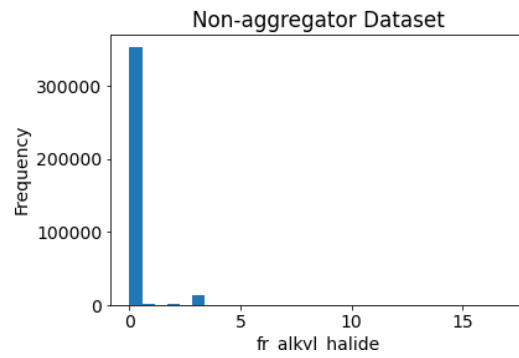
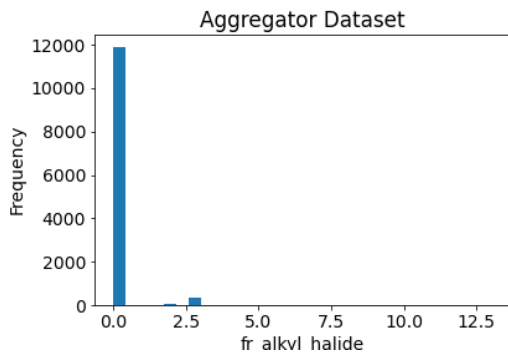
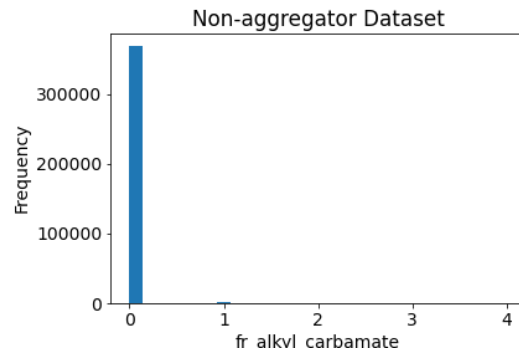
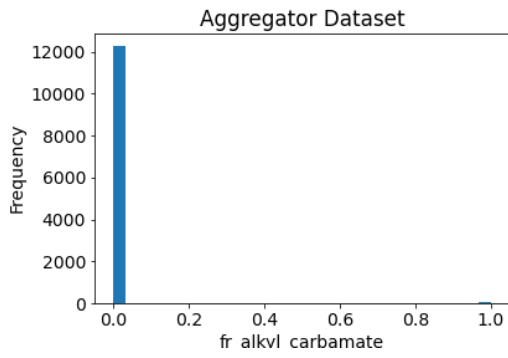


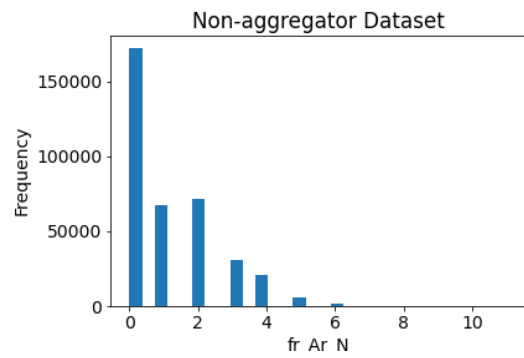
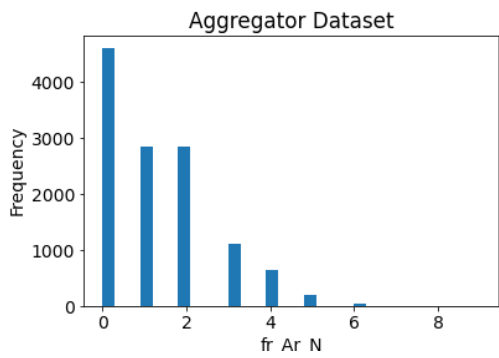
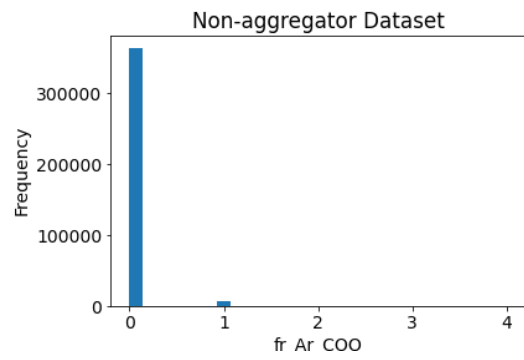
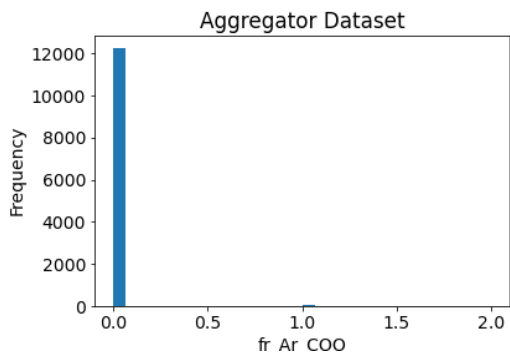
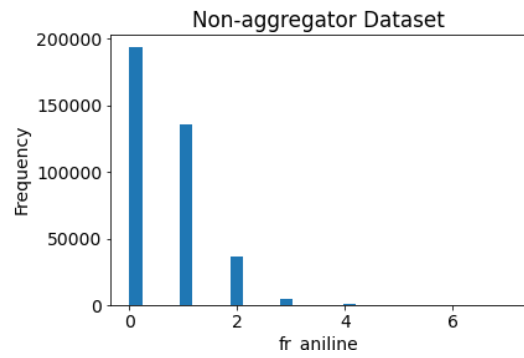
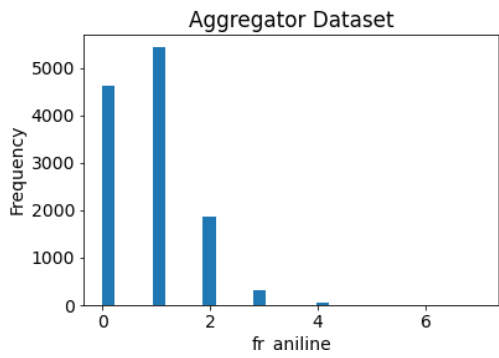
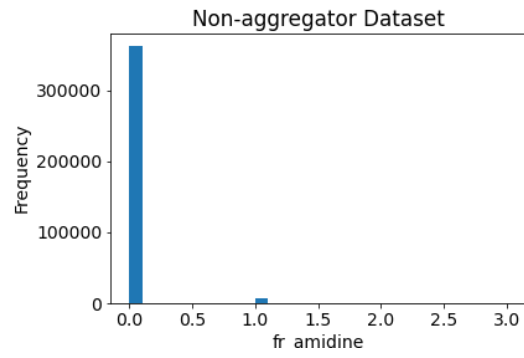
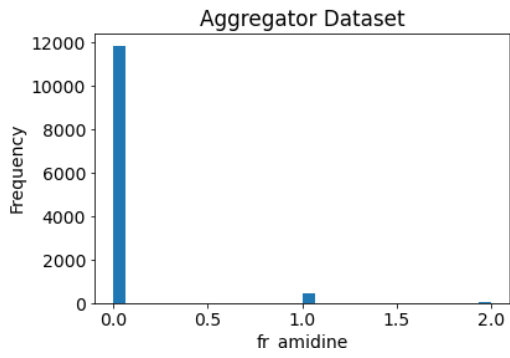


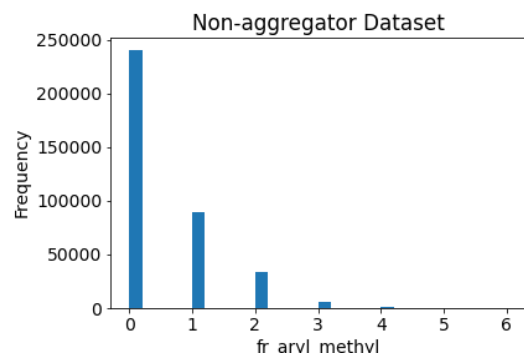
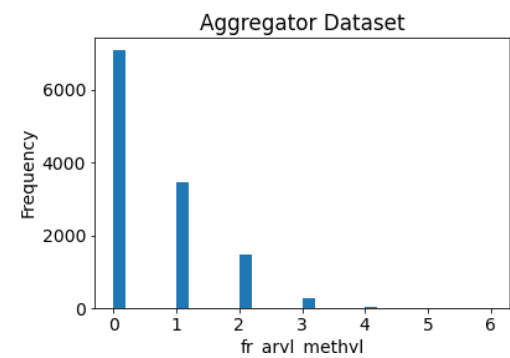
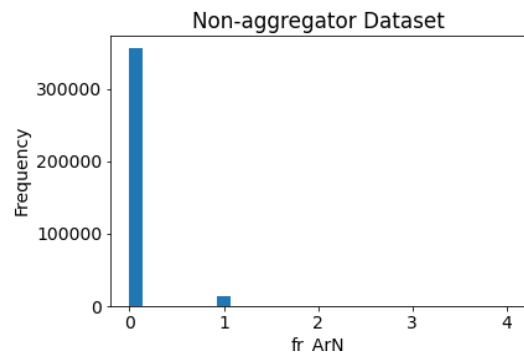
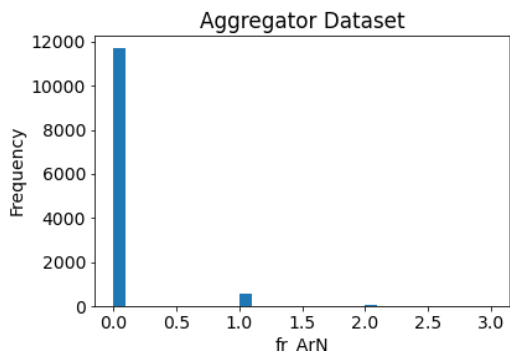
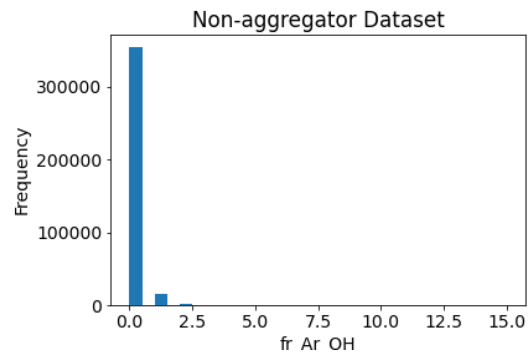
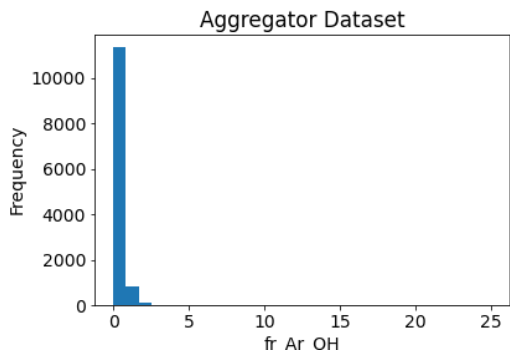
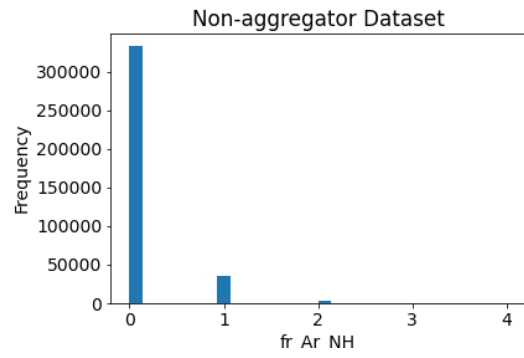
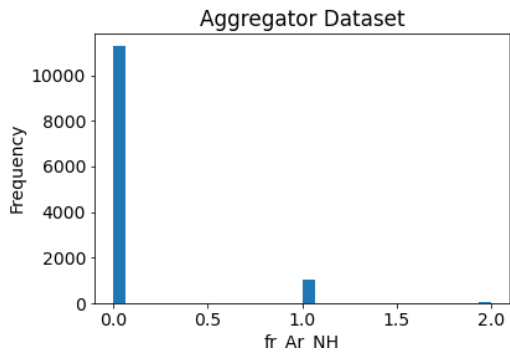


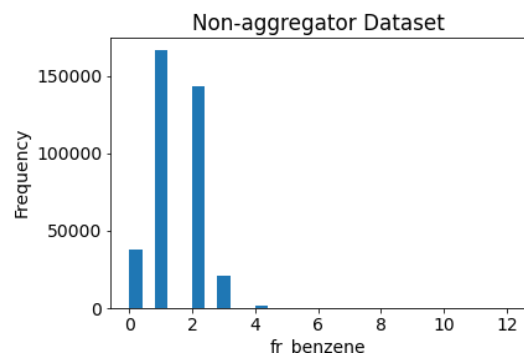
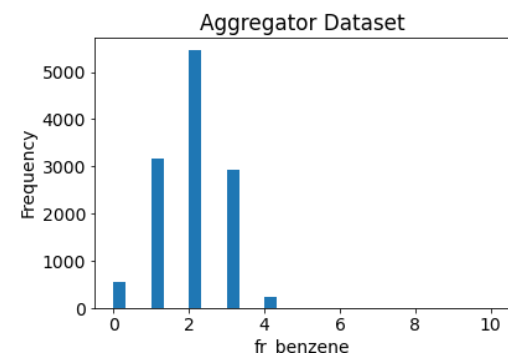
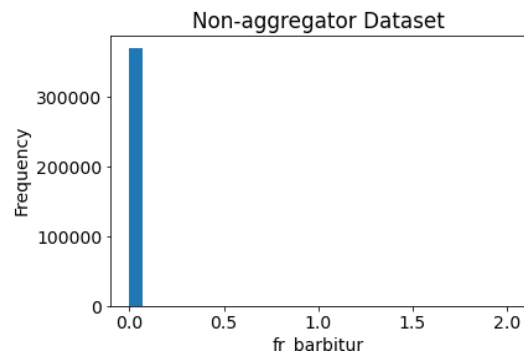
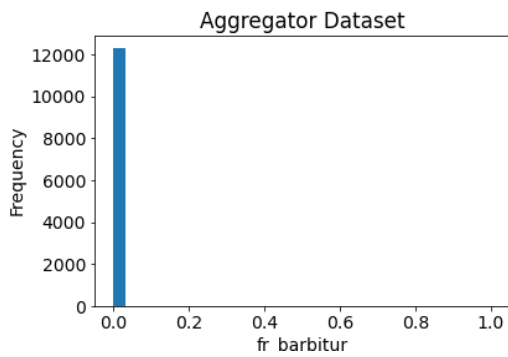
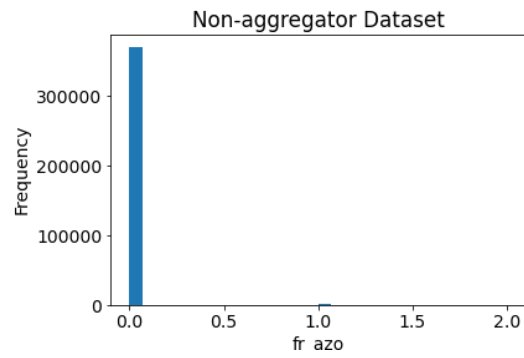
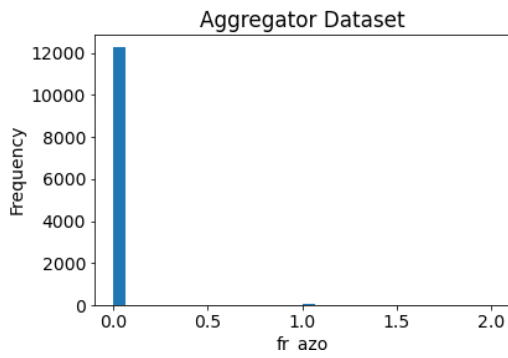
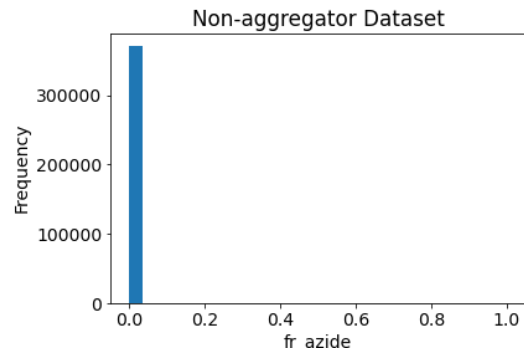
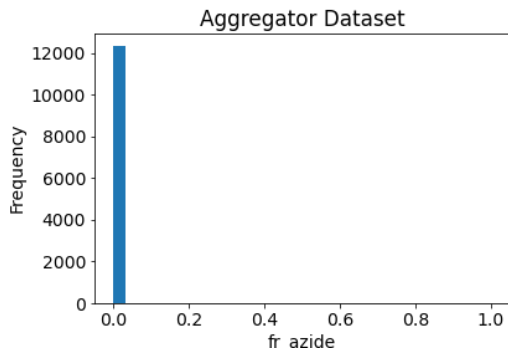
SIV. Histograms of fragment molecular descriptors for the aggregator and non-aggregator datasets.

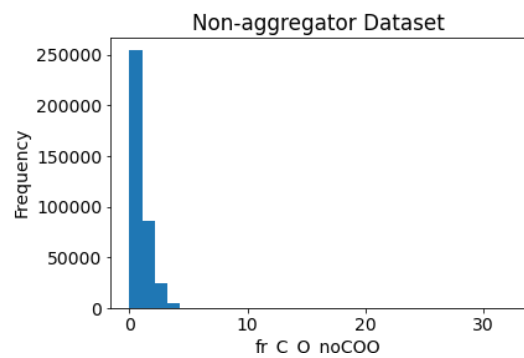
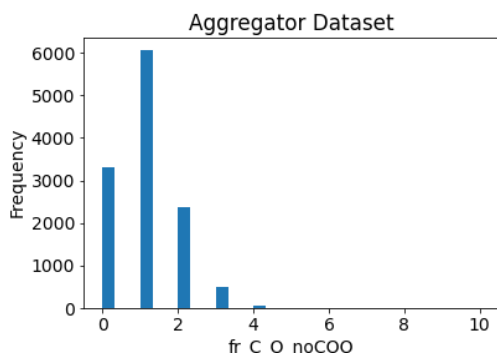
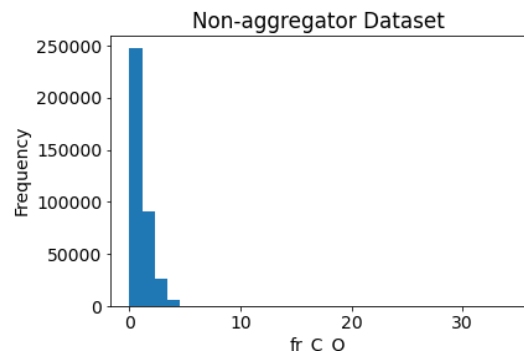
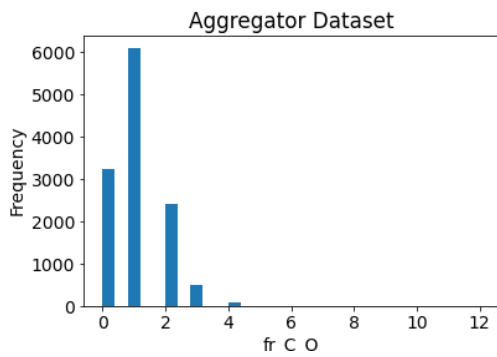
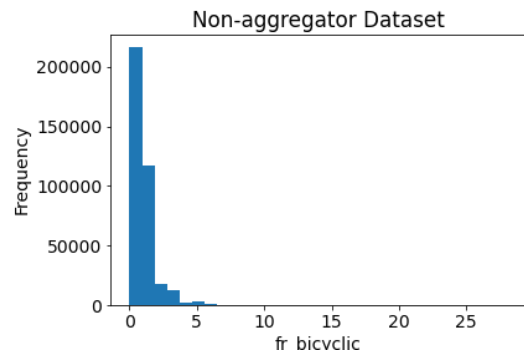
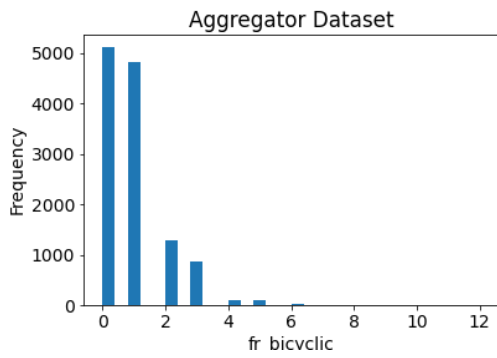
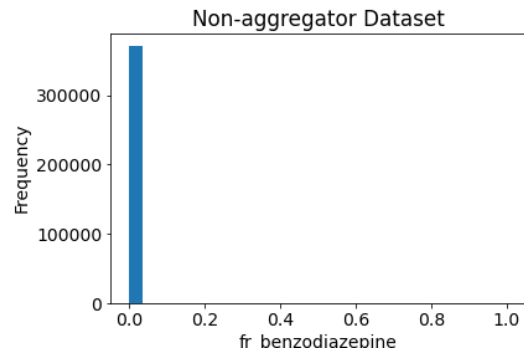
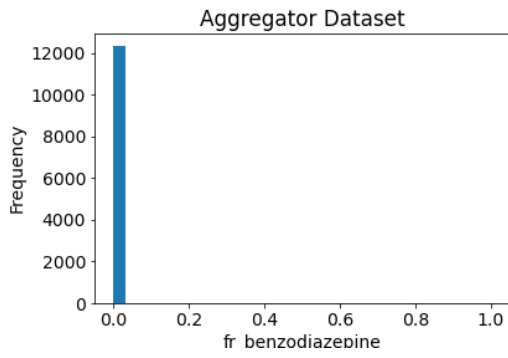


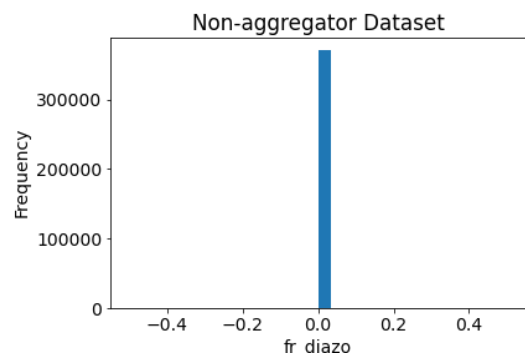
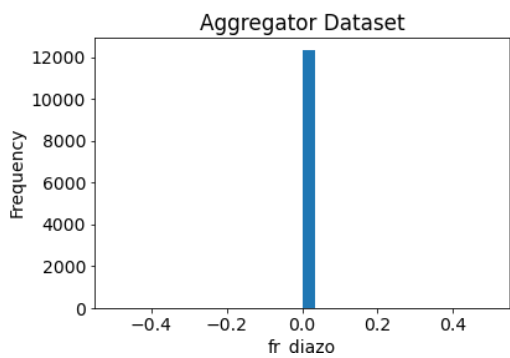
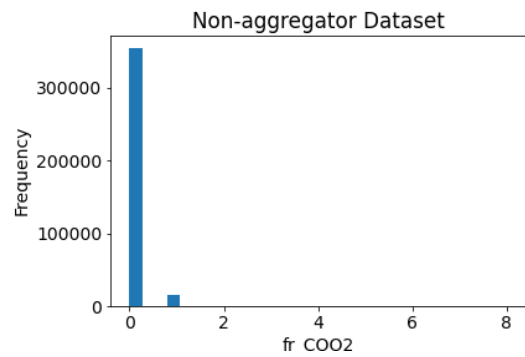
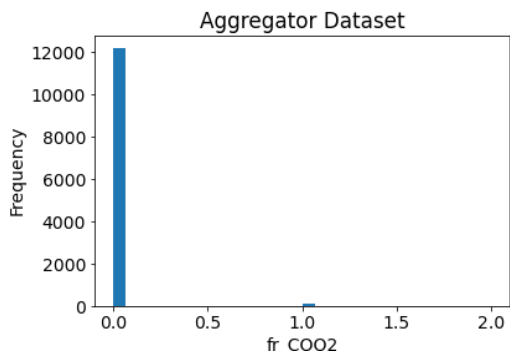
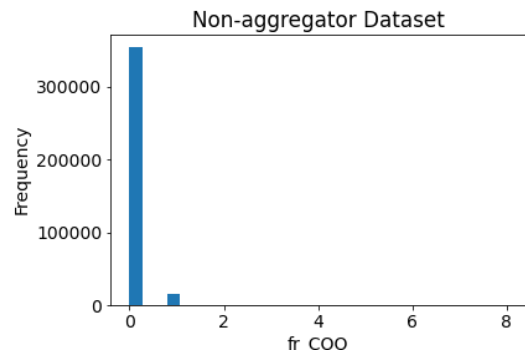
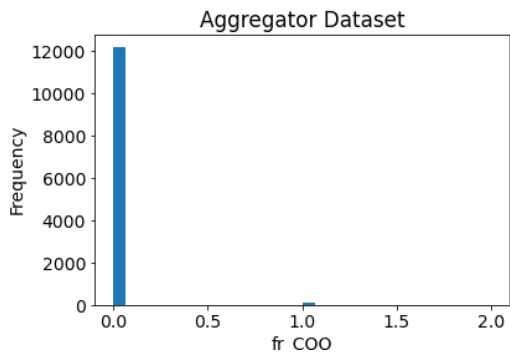
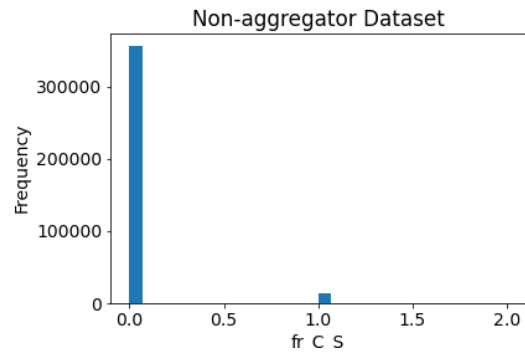
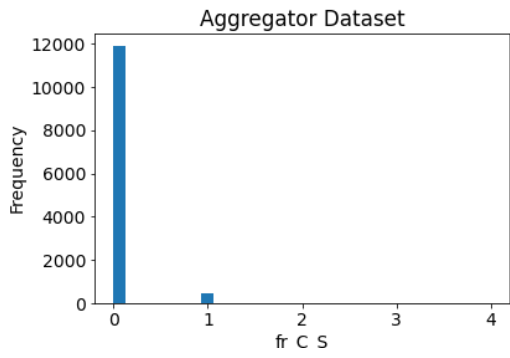


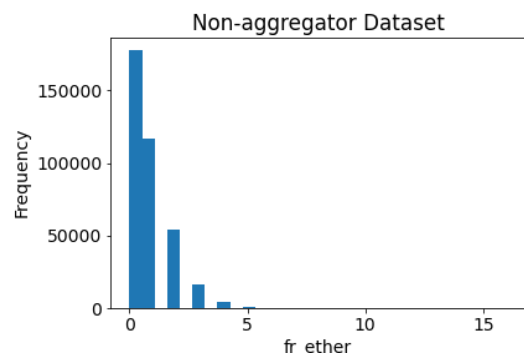
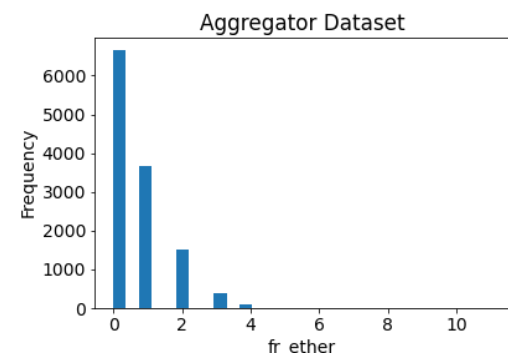
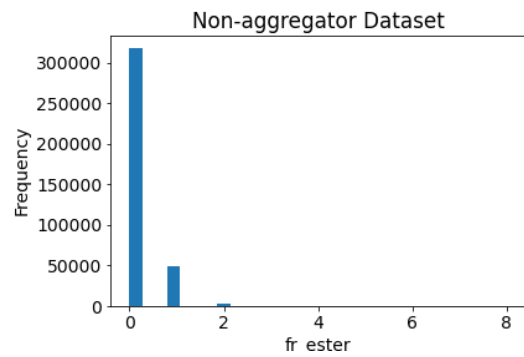
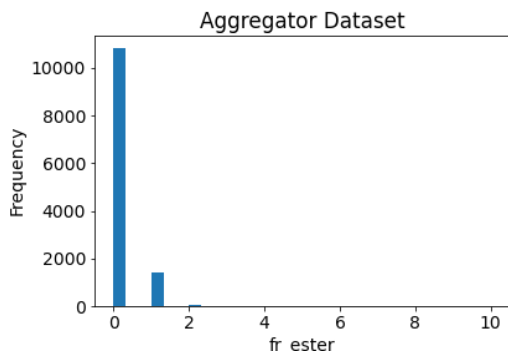
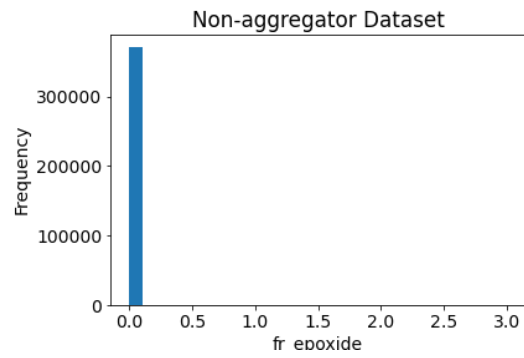
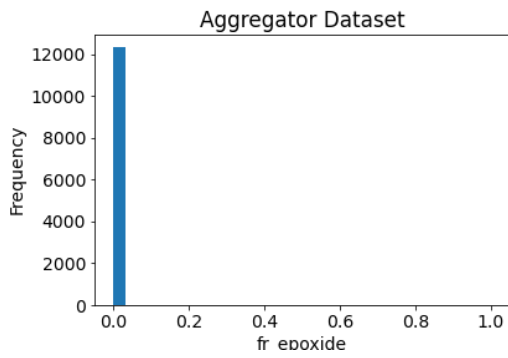
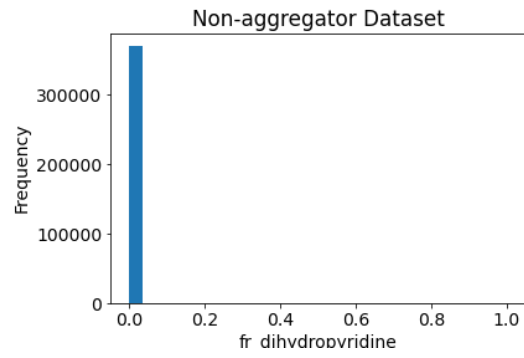
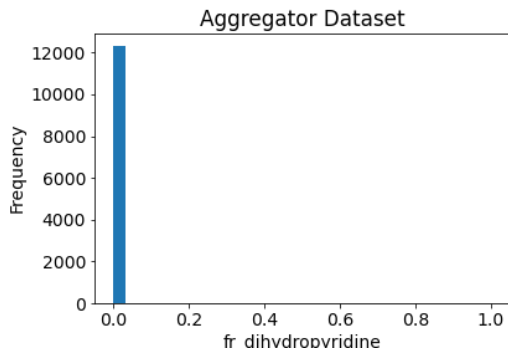


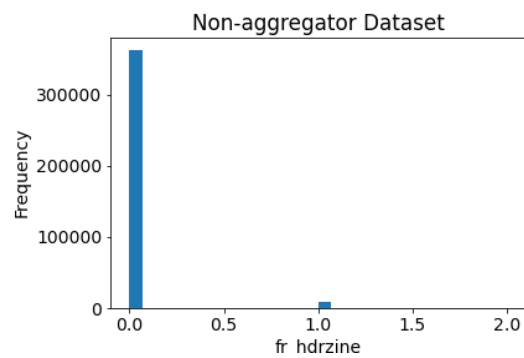
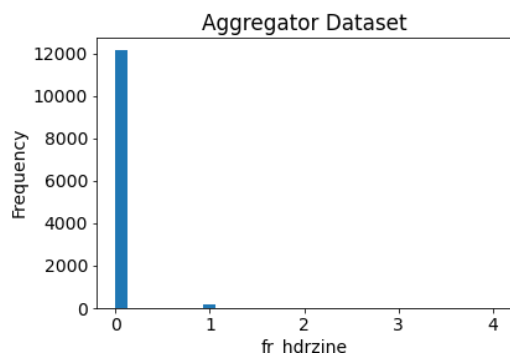
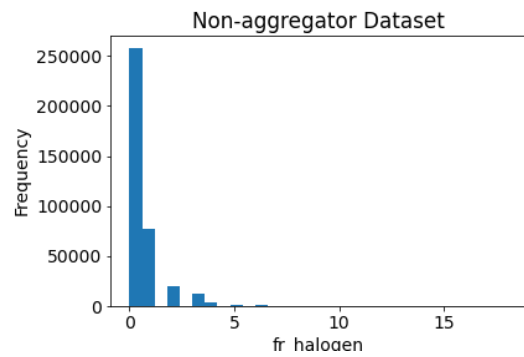
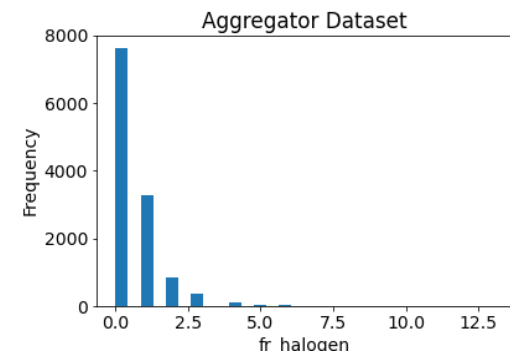
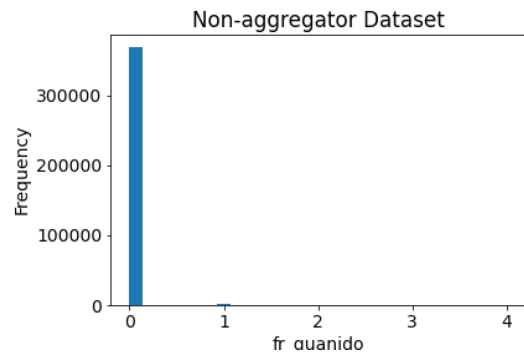
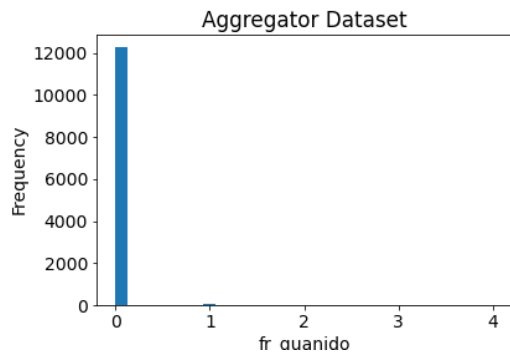
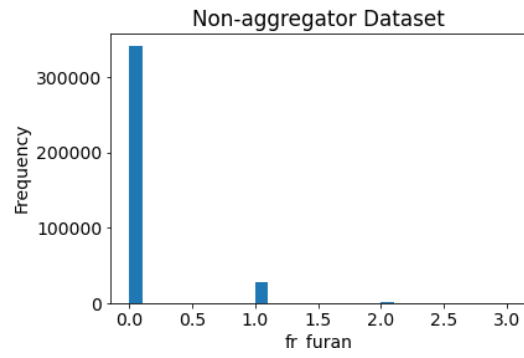
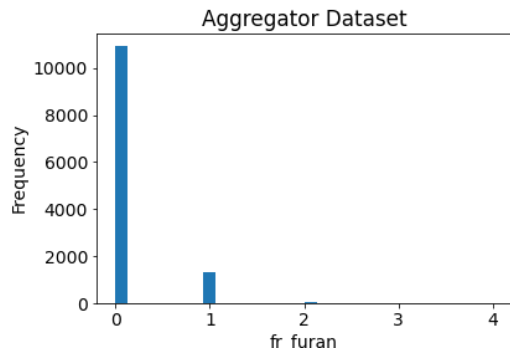


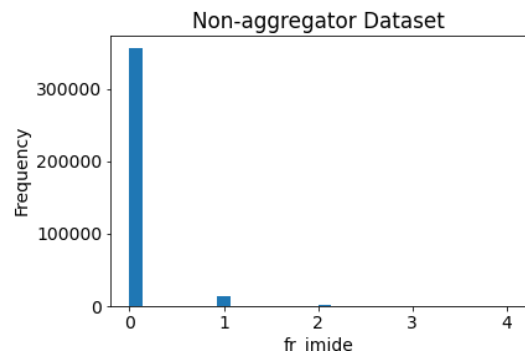
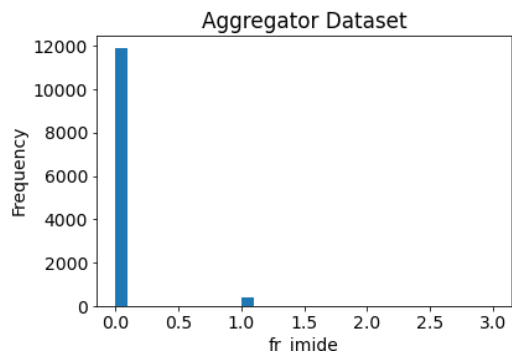
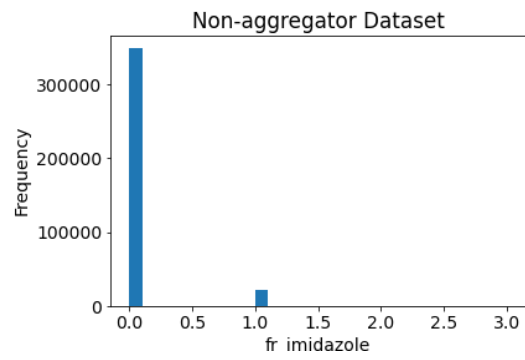
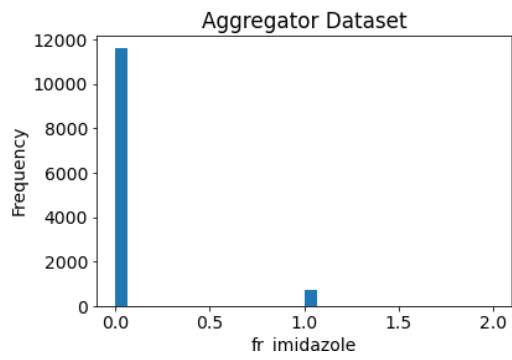
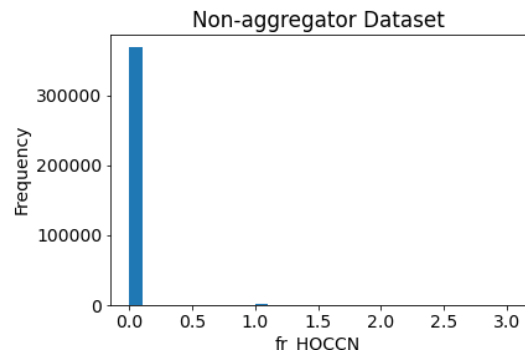
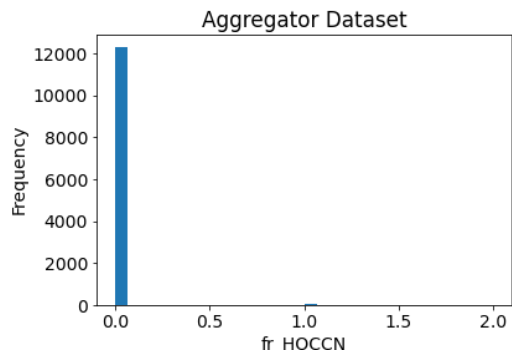
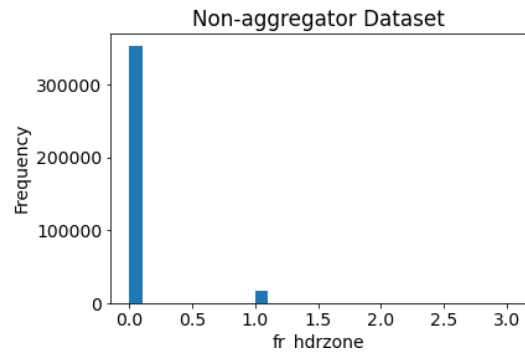
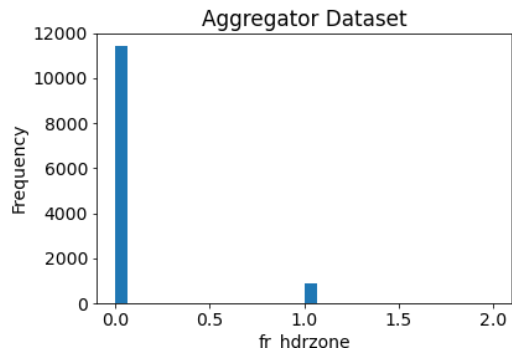


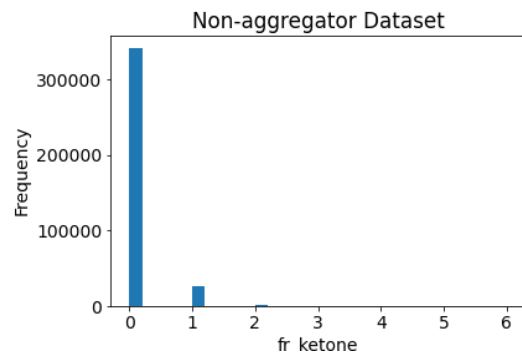
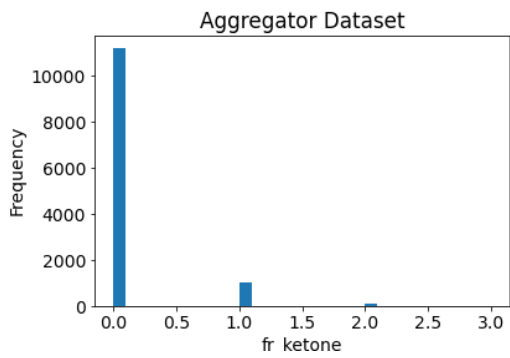
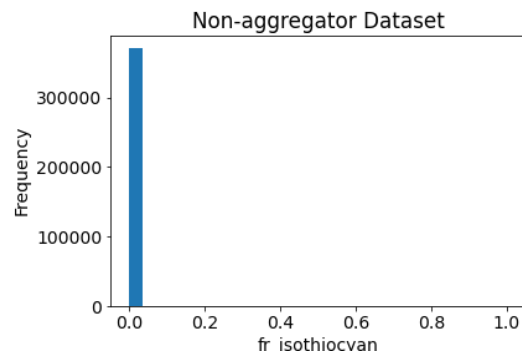
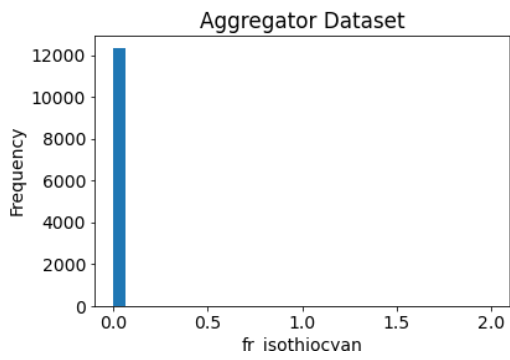
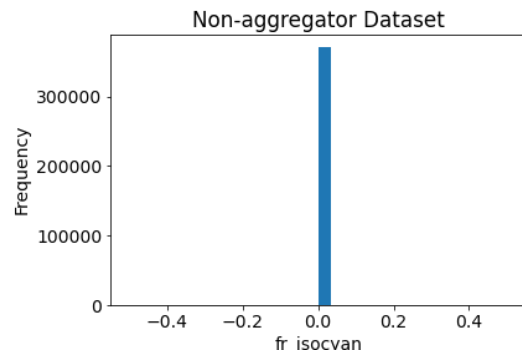
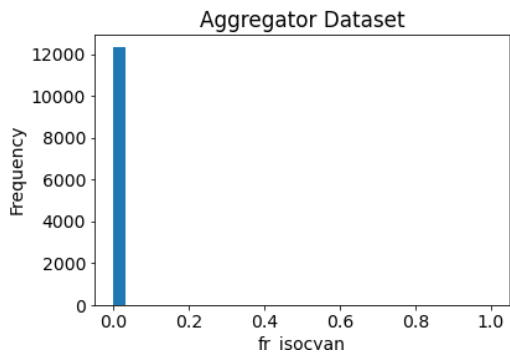
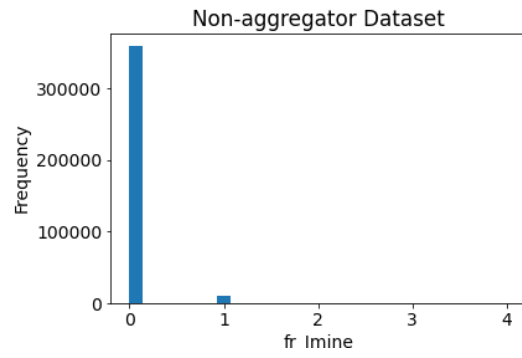
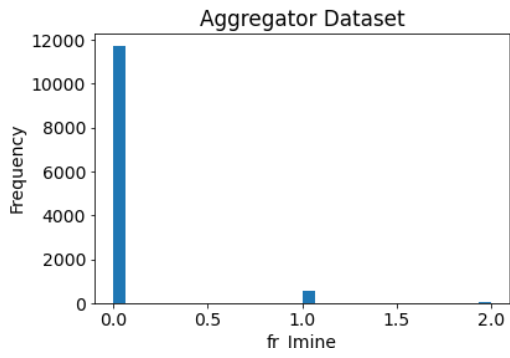


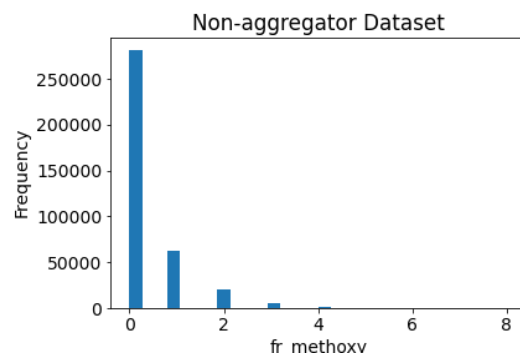
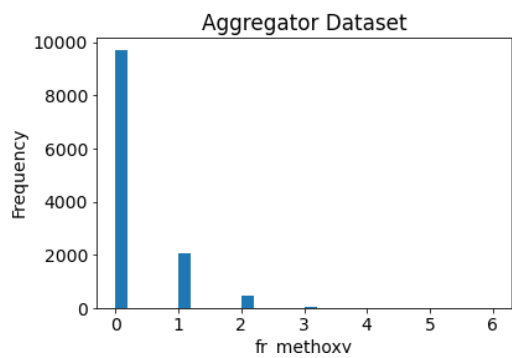
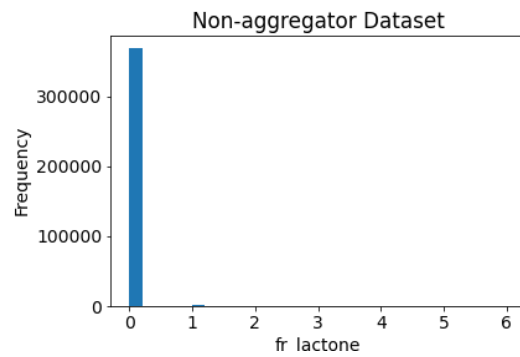
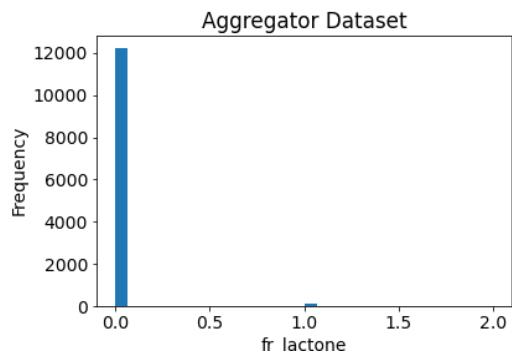
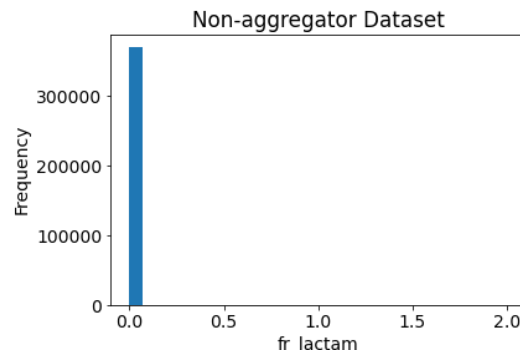
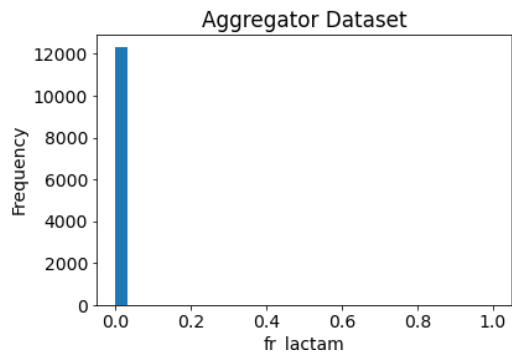
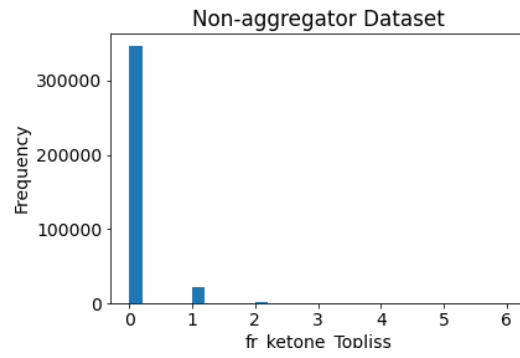
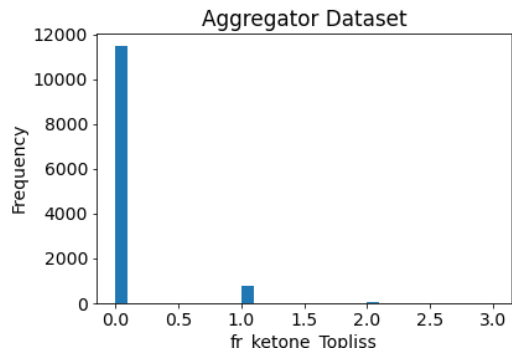


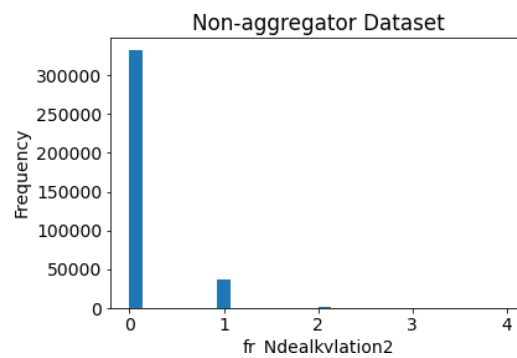
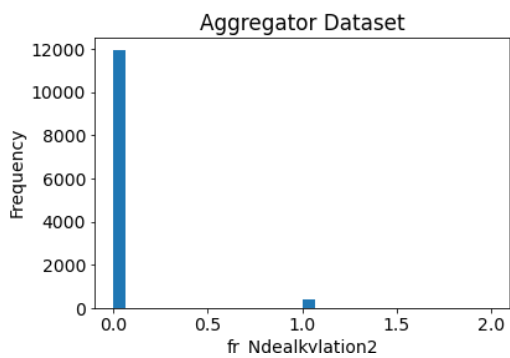
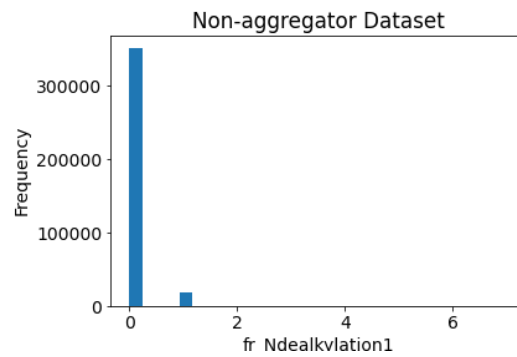
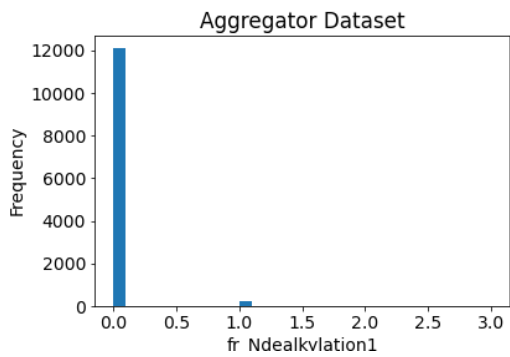
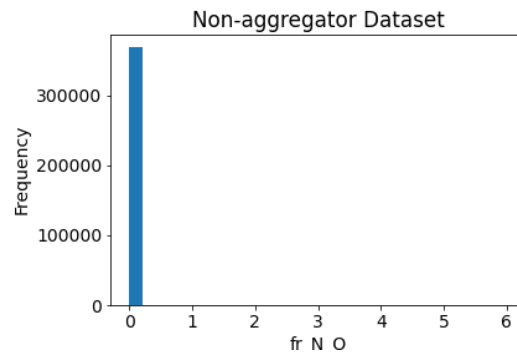
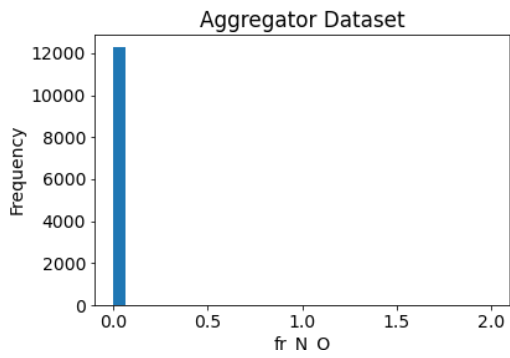
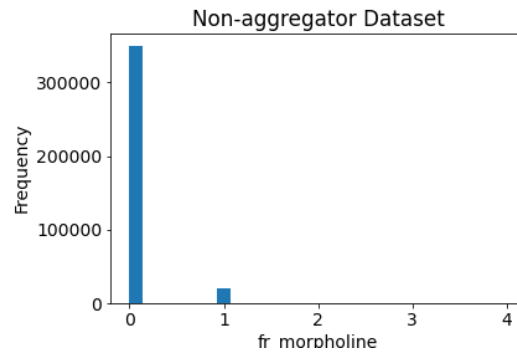
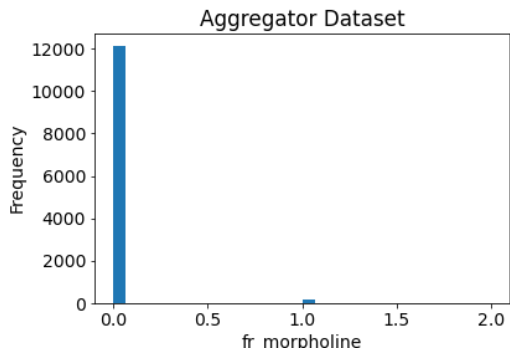


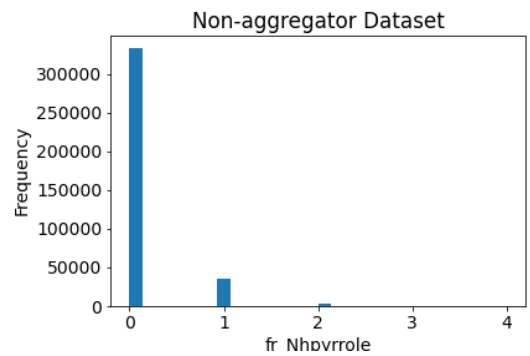
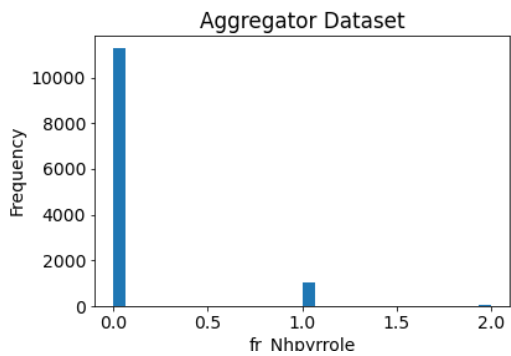
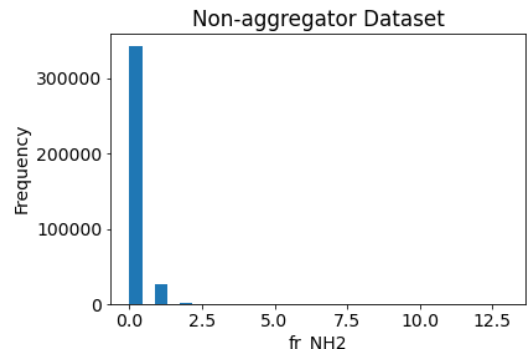
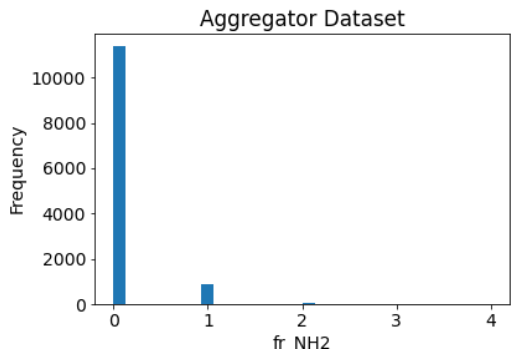
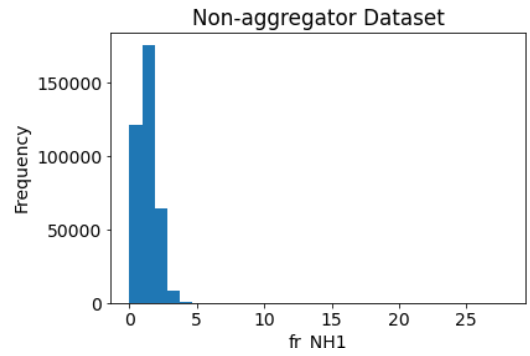
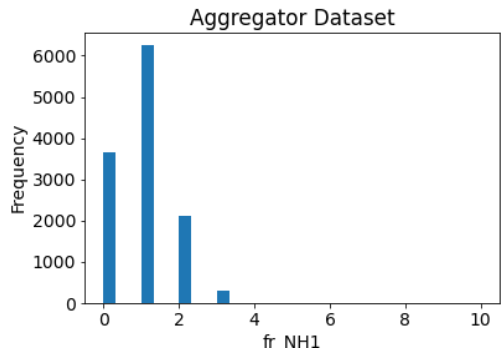
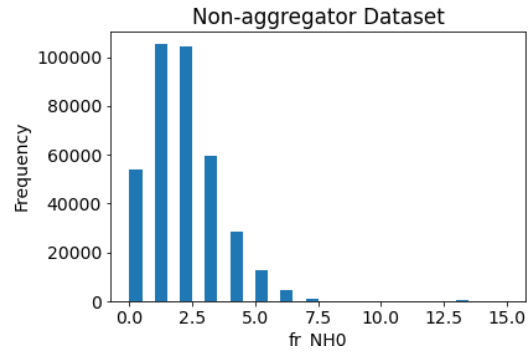
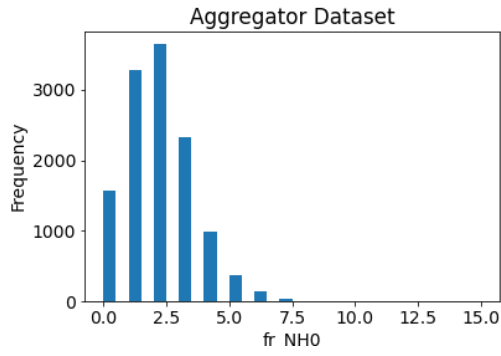


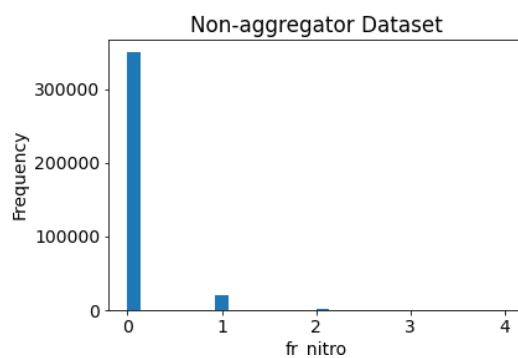
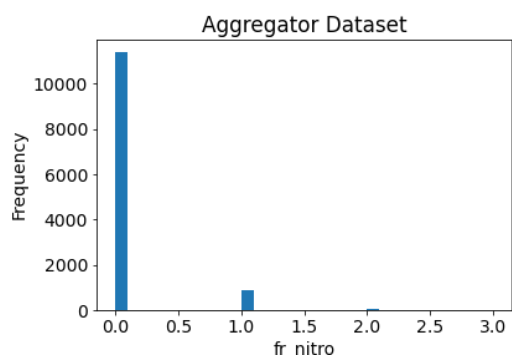
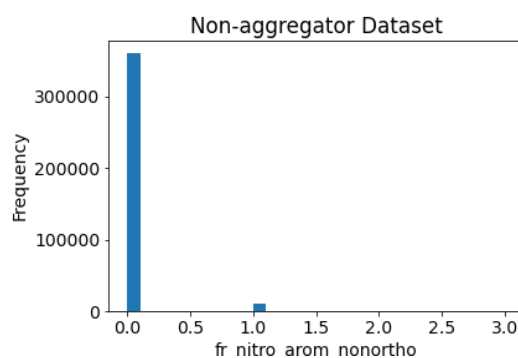
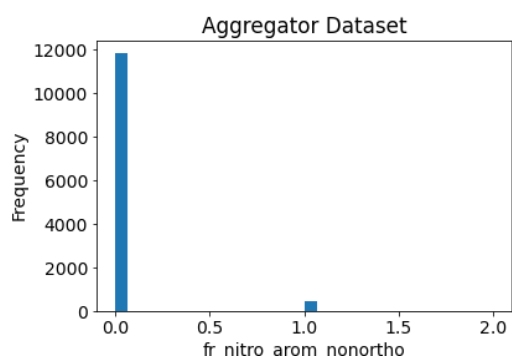
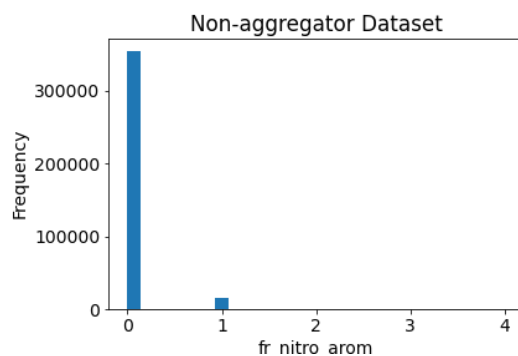
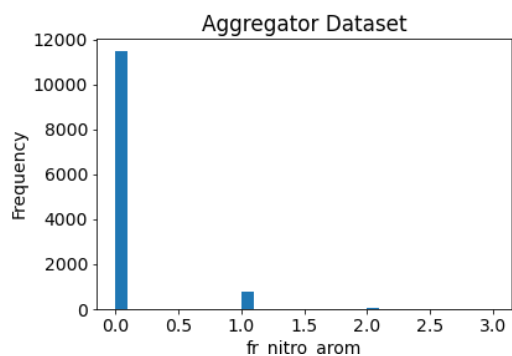
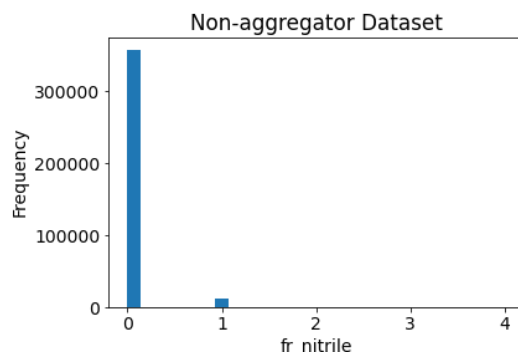
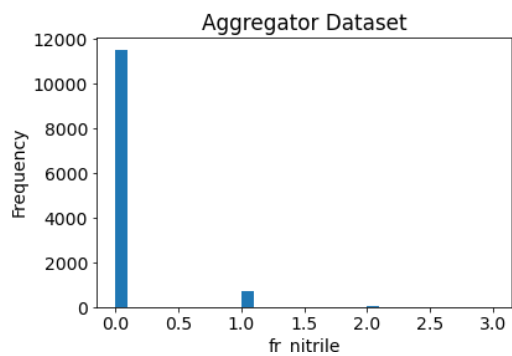


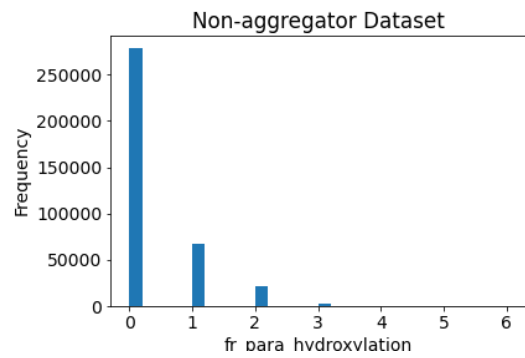
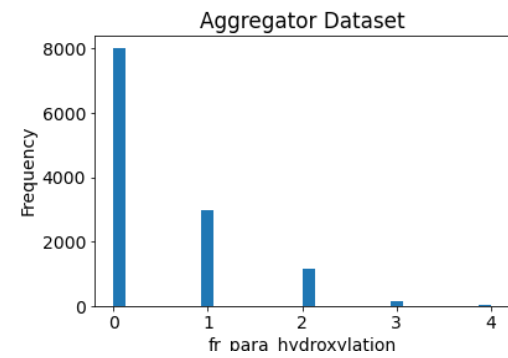
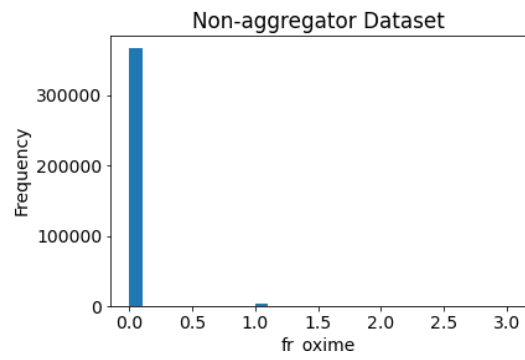
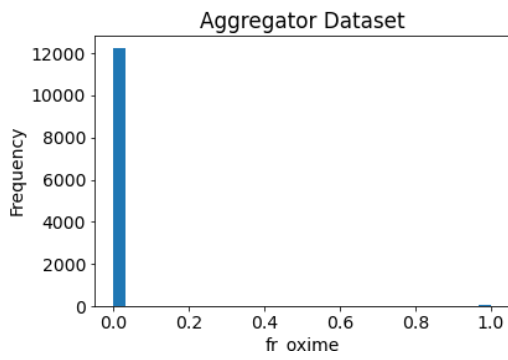
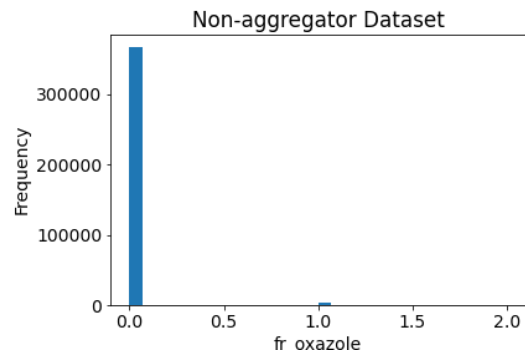
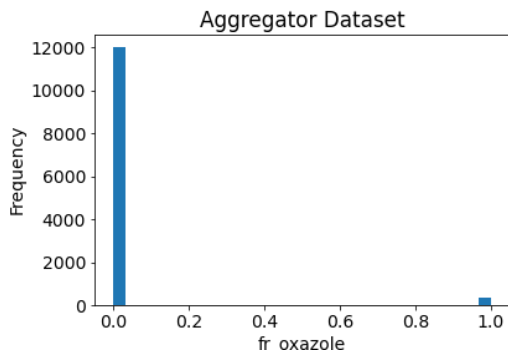
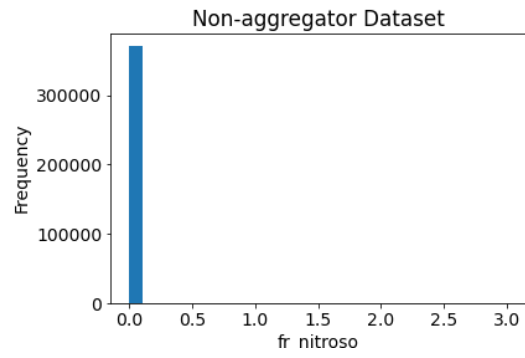
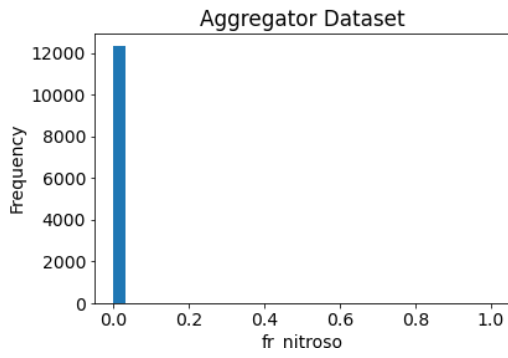


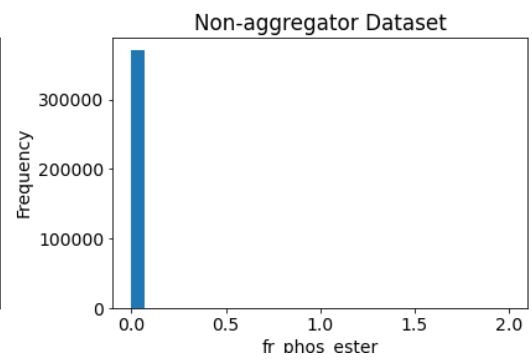
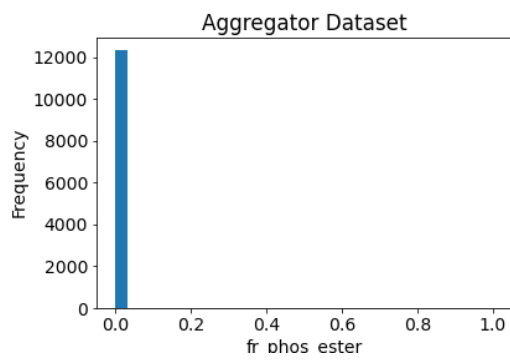
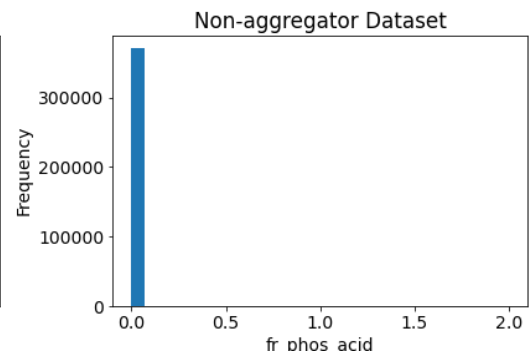
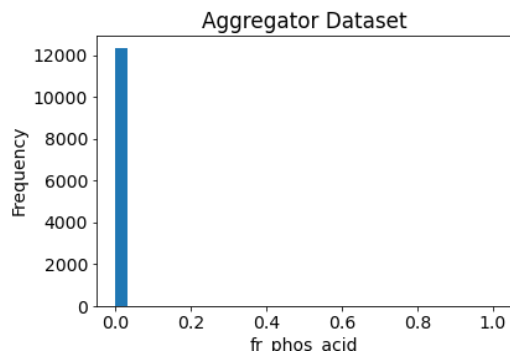
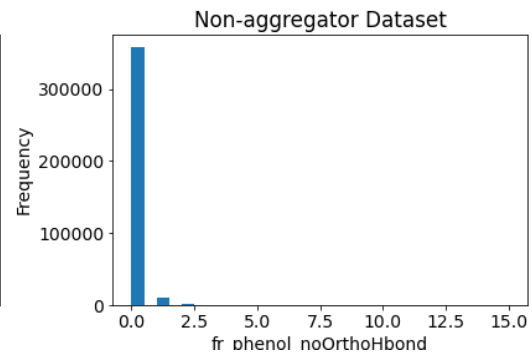
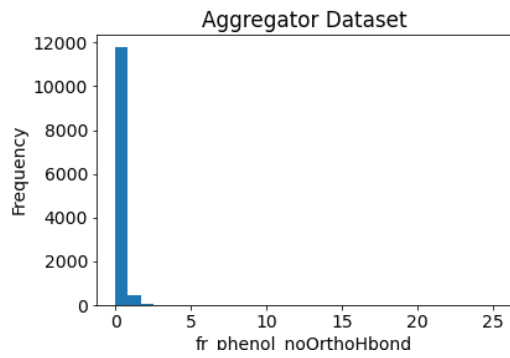
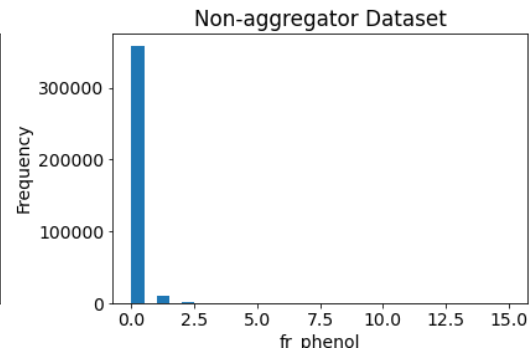
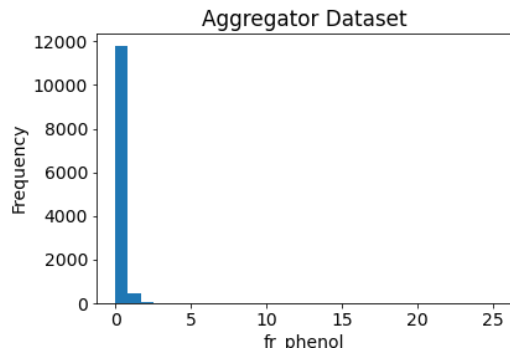


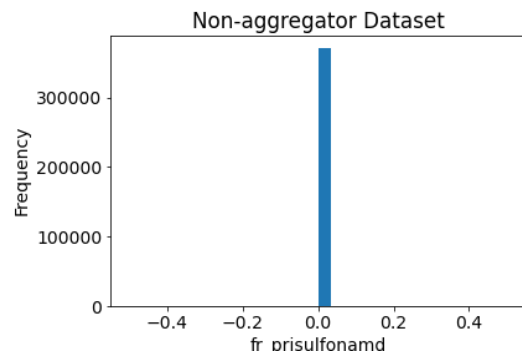
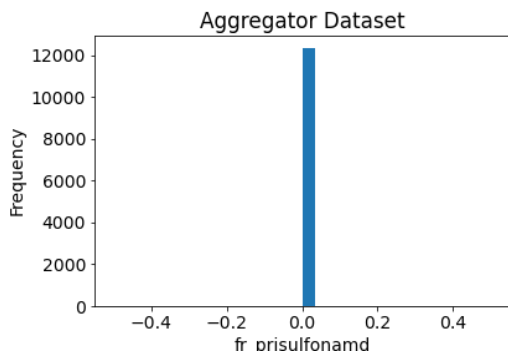
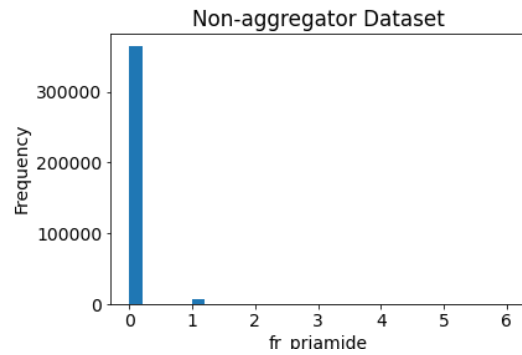
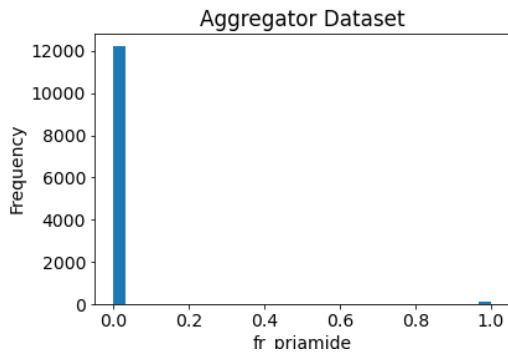
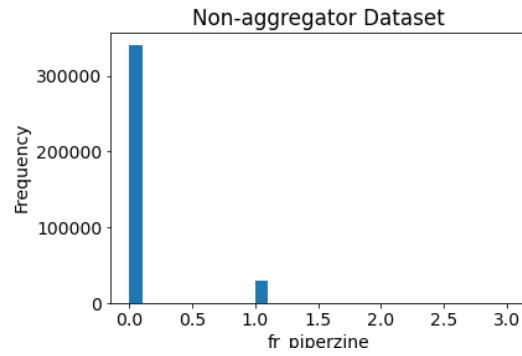
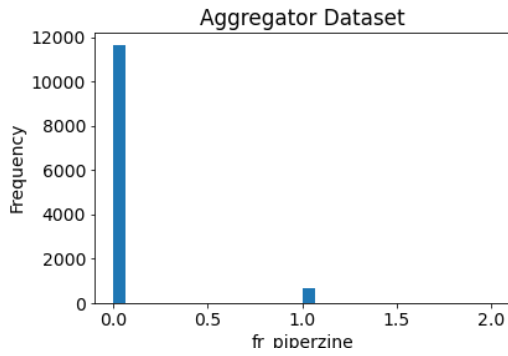
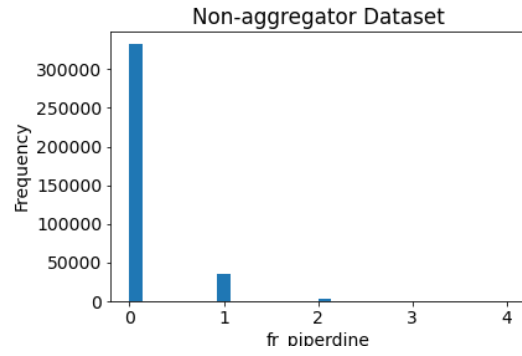
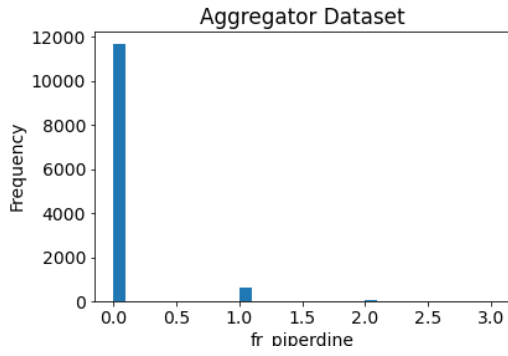


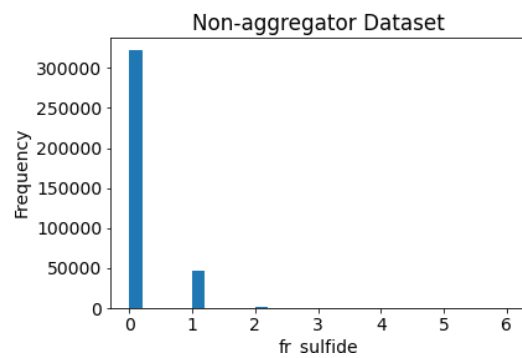
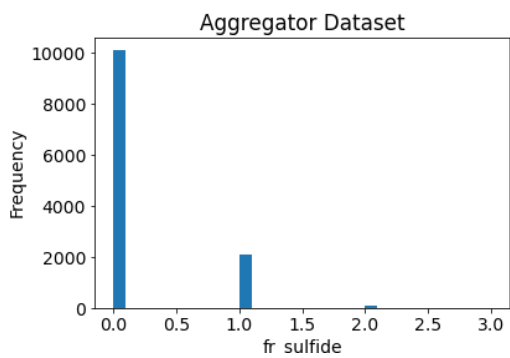
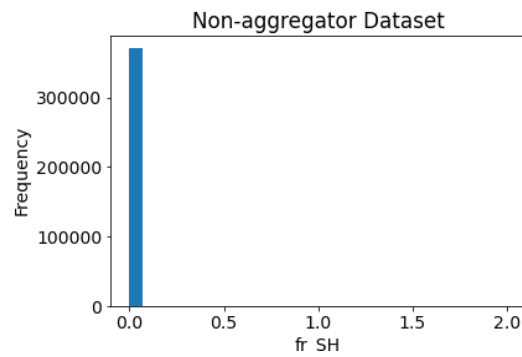
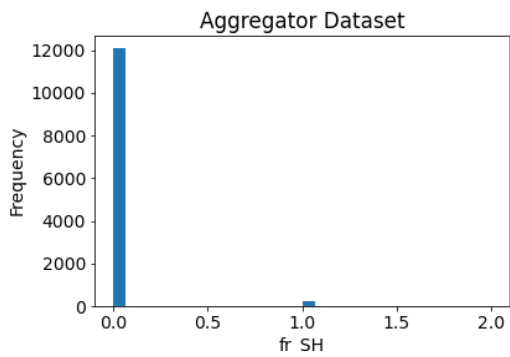
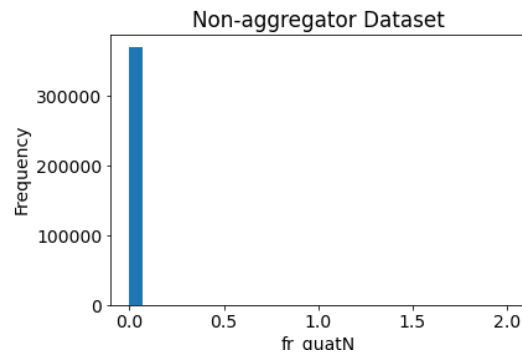
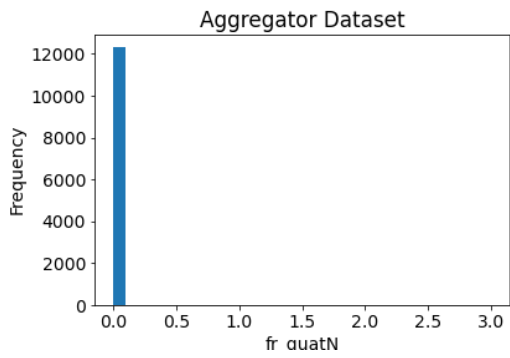
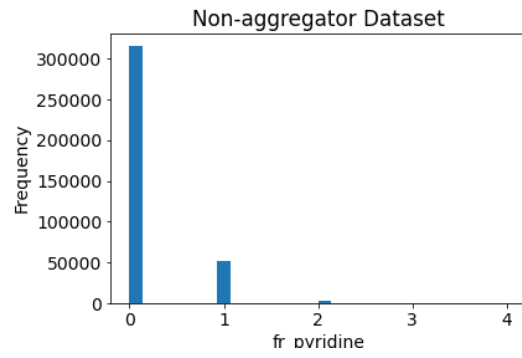
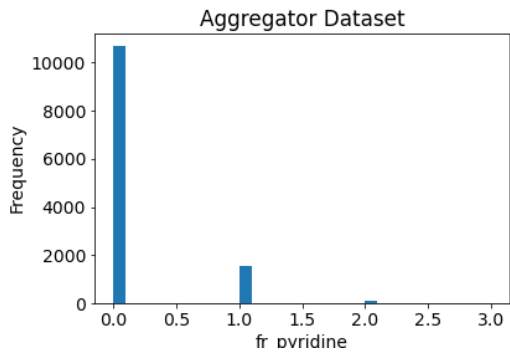


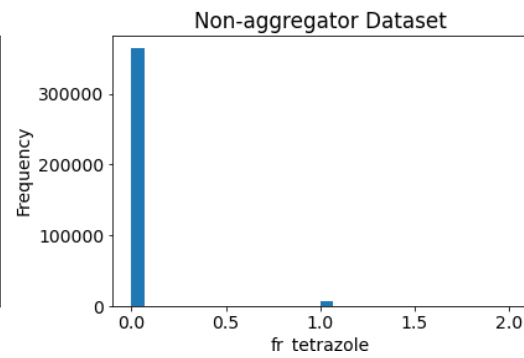
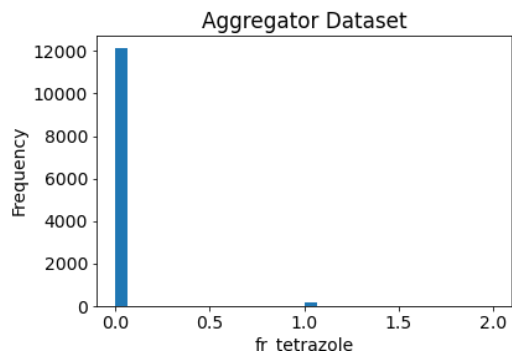
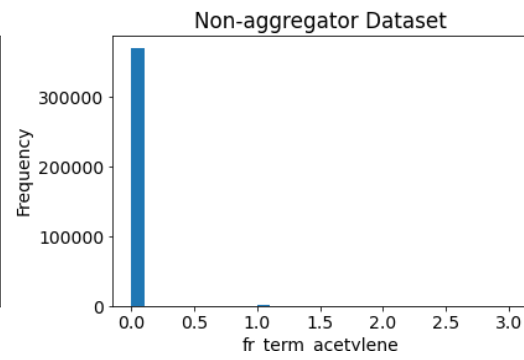
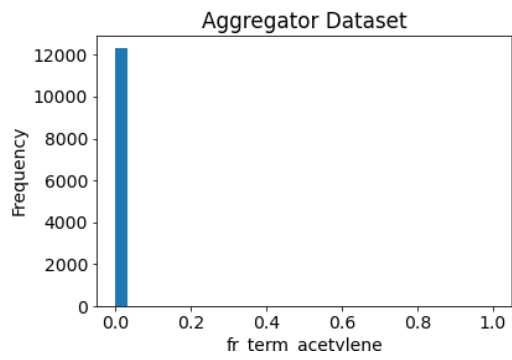
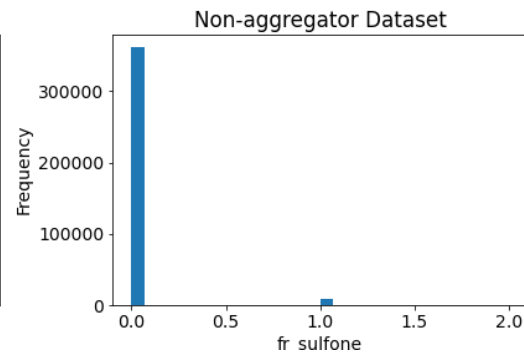
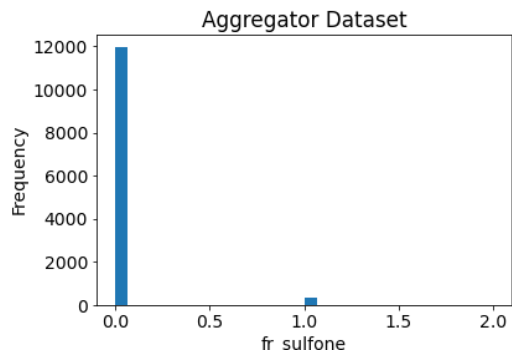
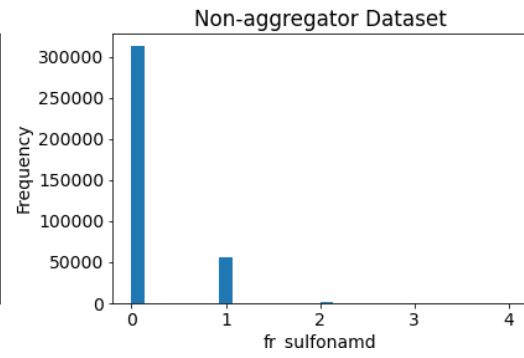
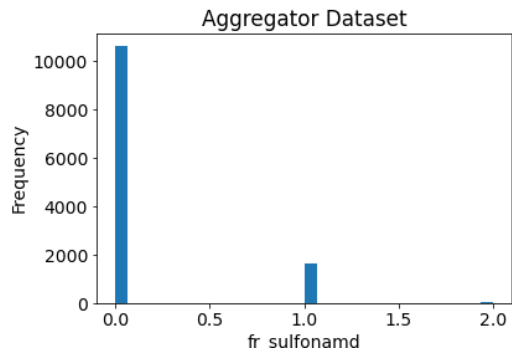


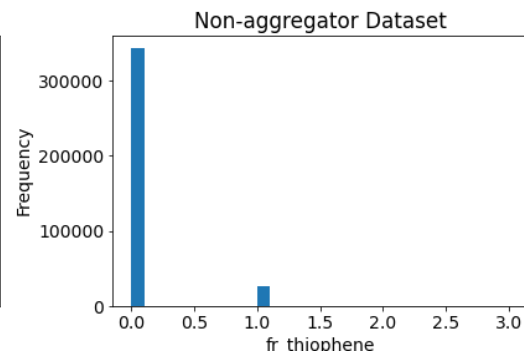
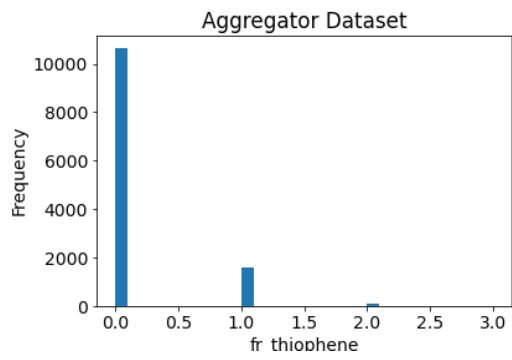
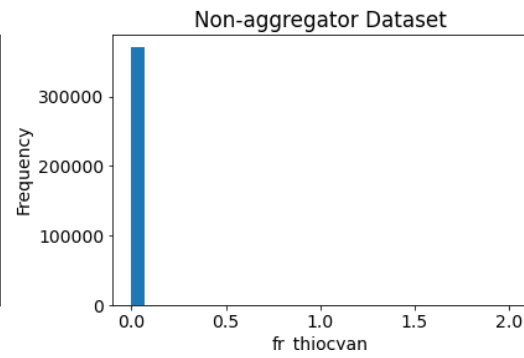
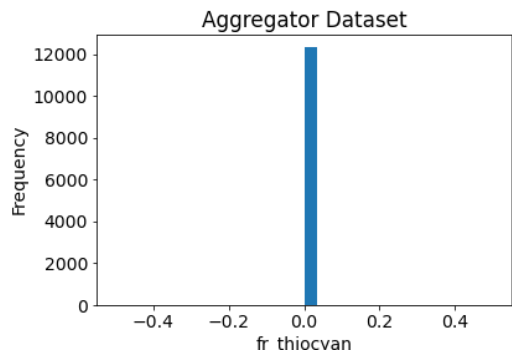
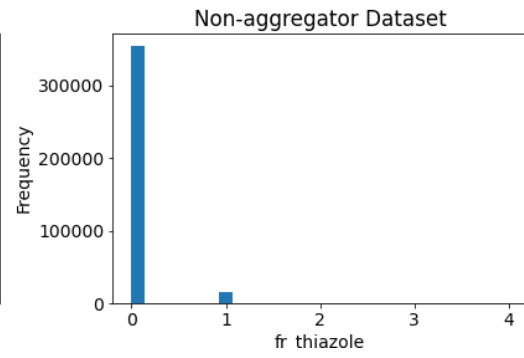
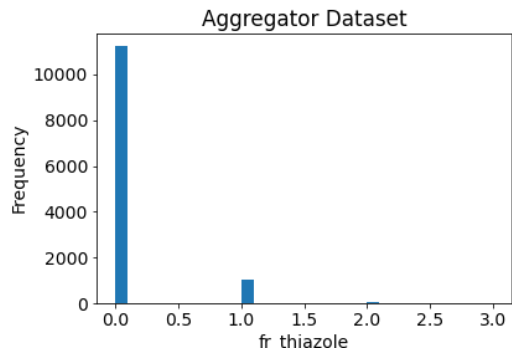


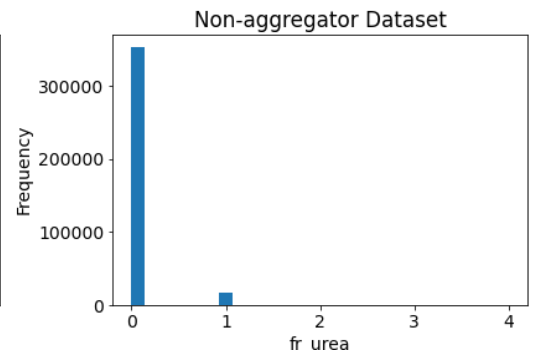
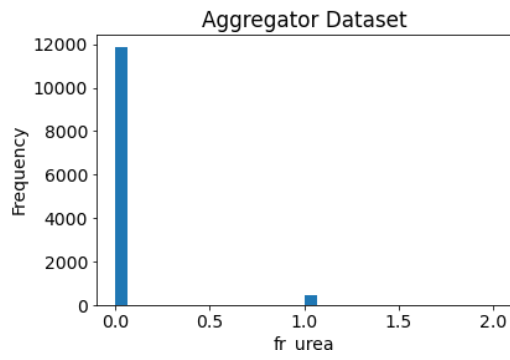
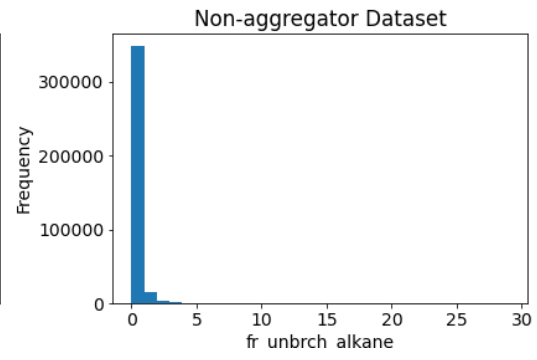
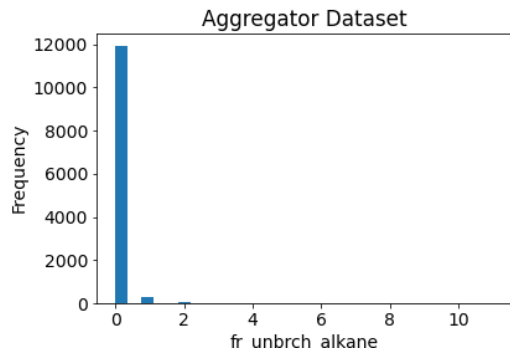










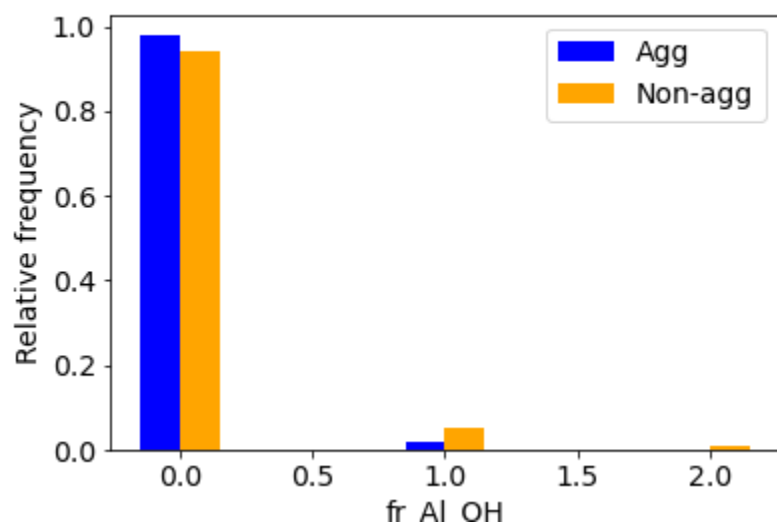
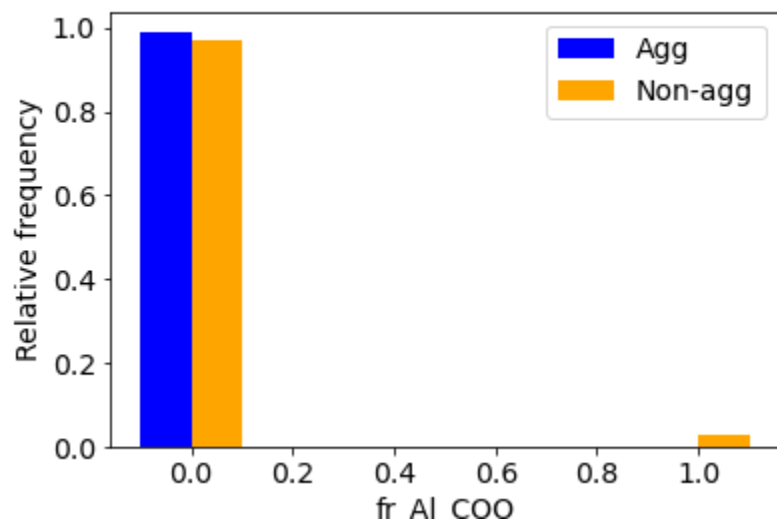


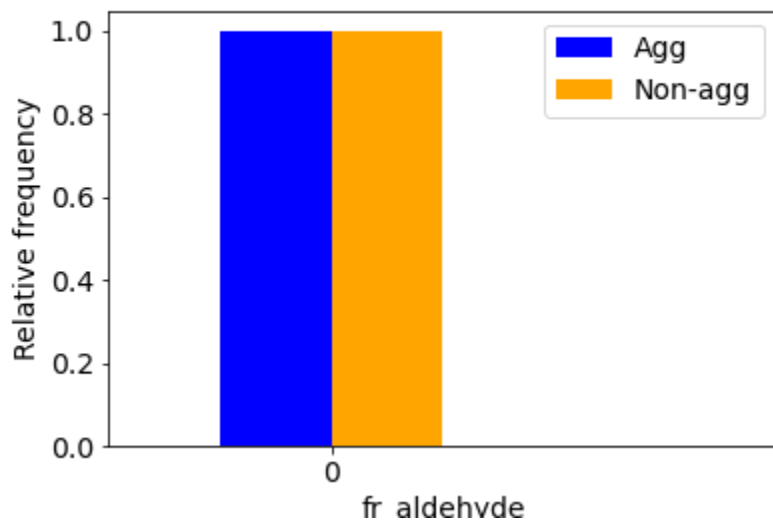
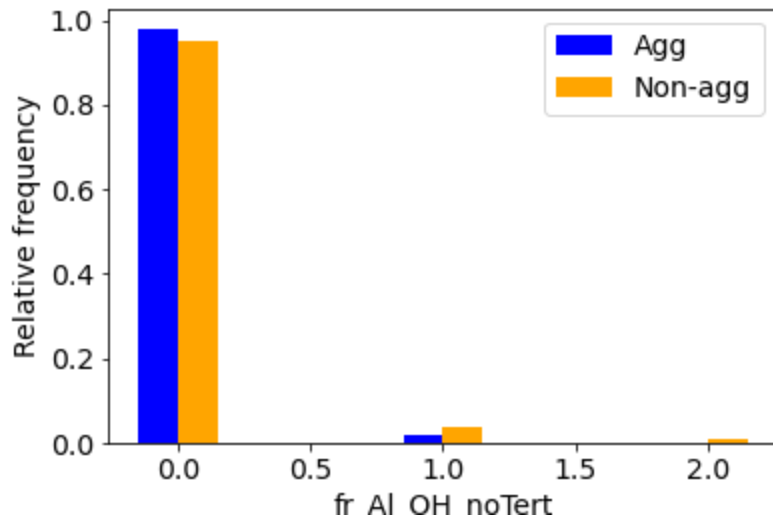
SV. p-values, means, standard deviations and Cohen's d values for the 16 general molecular descriptors calculated for the aggregator and non-aggregator datasets.

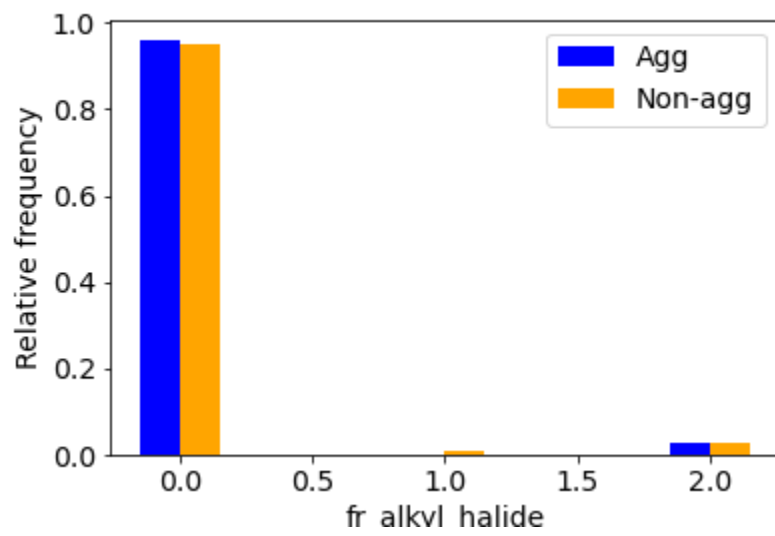
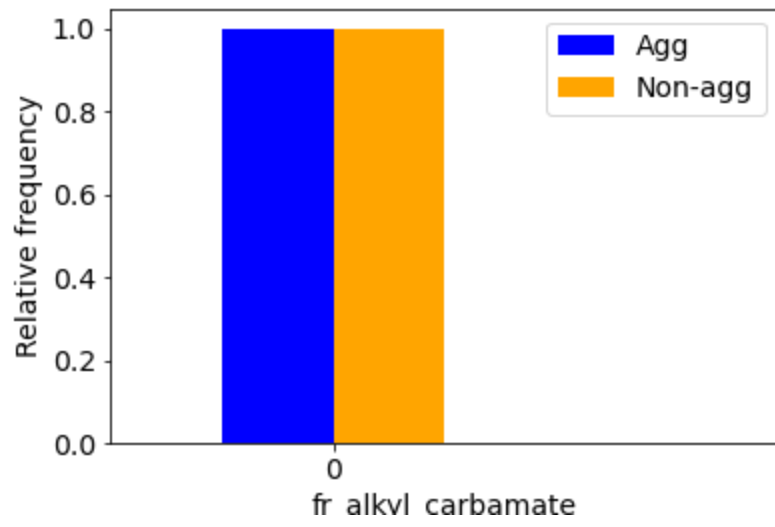
Table S1. Statistics for the 16 general molecular descriptors calculated for the aggregator and non-aggregator datasets.

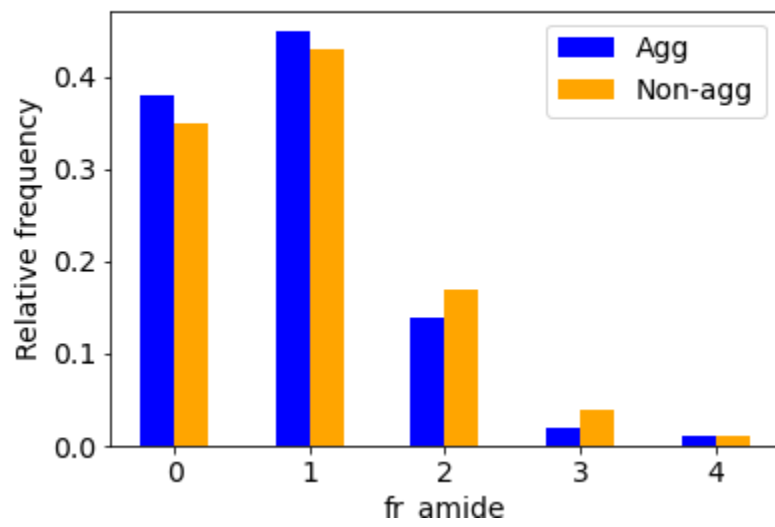
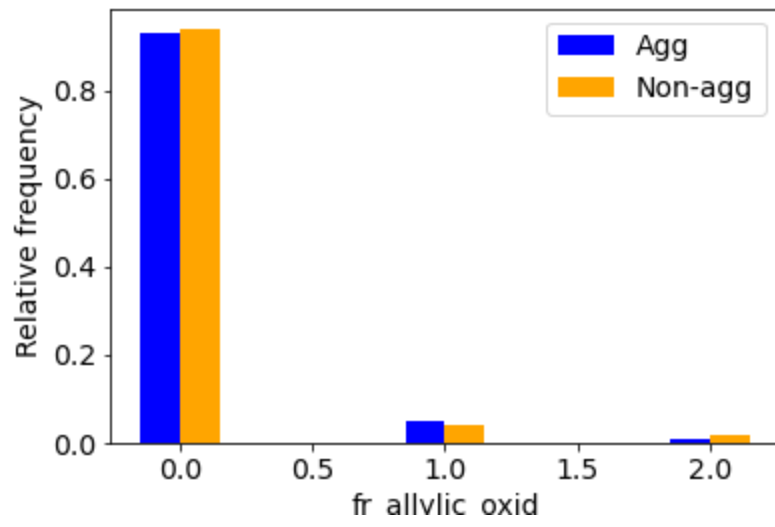
| Molecular Descriptor | p-Value | Aggregators Mean | Aggregators Std. Dev. | Non-aggregators Mean | Non-aggregators Std. Dev. | Cohen's D | Cohen's_D |
|------------------------|---------|------------------|-----------------------|----------------------|---------------------------|-----------|-----------|
| MolLogP | 0.000 | 4.098 | 1.293 | 2.991 | 1.291 | 0.857 | 0.857 |
| NumAromaticRings | 0.000 | 3.026 | 0.959 | 2.278 | 0.948 | 0.786 | 0.786 |
| NumAromaticCarbocycles | 0.000 | 1.939 | 0.873 | 1.413 | 0.769 | 0.640 | 0.640 |
| FractionCSP3 | 0.000 | 0.208 | 0.143 | 0.308 | 0.180 | -0.618 | 0.618 |
| RingCount | 0.000 | 3.680 | 1.022 | 3.078 | 1.033 | 0.586 | 0.586 |
| MolMR | 0.000 | 108.108 | 20.145 | 97.985 | 22.947 | 0.469 | 0.469 |
| HeavyAtomMolWt | 0.000 | 377.776 | 74.077 | 345.086 | 81.052 | 0.421 | 0.421 |
| LabuteASA | 0.000 | 164.940 | 30.715 | 151.659 | 35.252 | 0.402 | 0.402 |
| ExactMolWt | 0.000 | 396.709 | 76.916 | 365.005 | 85.830 | 0.389 | 0.389 |
| HeavyAtomCount | 0.000 | 27.696 | 5.375 | 25.561 | 6.110 | 0.371 | 0.371 |
| NumValenceElectrons | 0.000 | 141.817 | 27.813 | 133.917 | 32.631 | 0.261 | 0.261 |
| NumHAcceptors | 0.000 | 5.118 | 1.826 | 4.912 | 1.907 | 0.110 | 0.110 |
| NOCcount | 0.000 | 5.771 | 1.920 | 5.957 | 2.138 | -0.092 | 0.092 |
| NumHeteroatoms | 0.000 | 7.074 | 2.168 | 6.970 | 2.332 | 0.046 | 0.046 |
| NumRotatableBonds | 0.000 | 4.962 | 2.104 | 5.052 | 2.497 | -0.039 | 0.039 |
| TPSA | 0.005 | 74.321 | 27.357 | 75.069 | 29.338 | -0.026 | 0.026 |

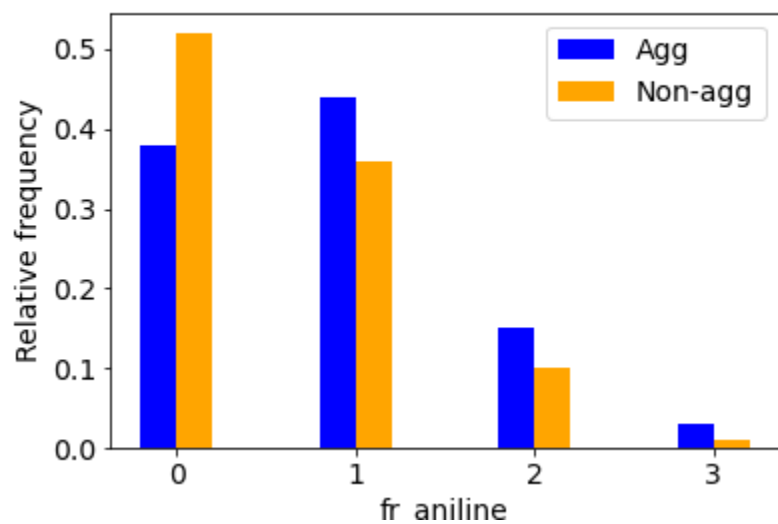
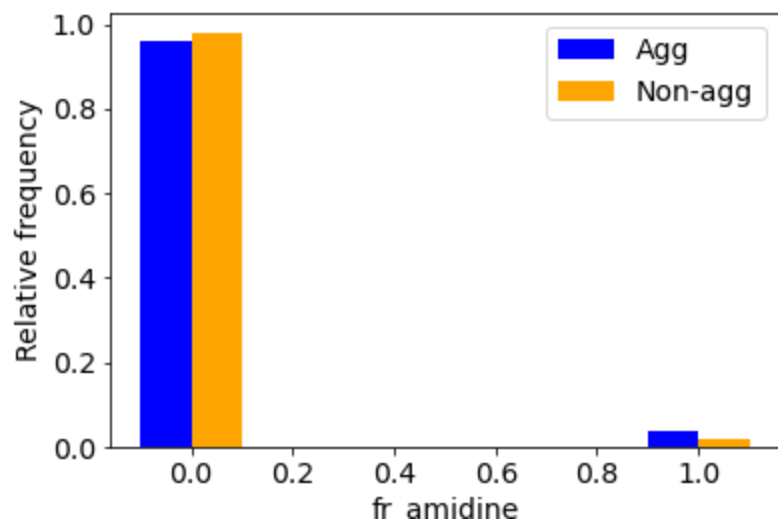
SVI. Comparison of the relative frequency of each of the fragments described by the fragment descriptors for the aggregator and non-aggregator molecules.

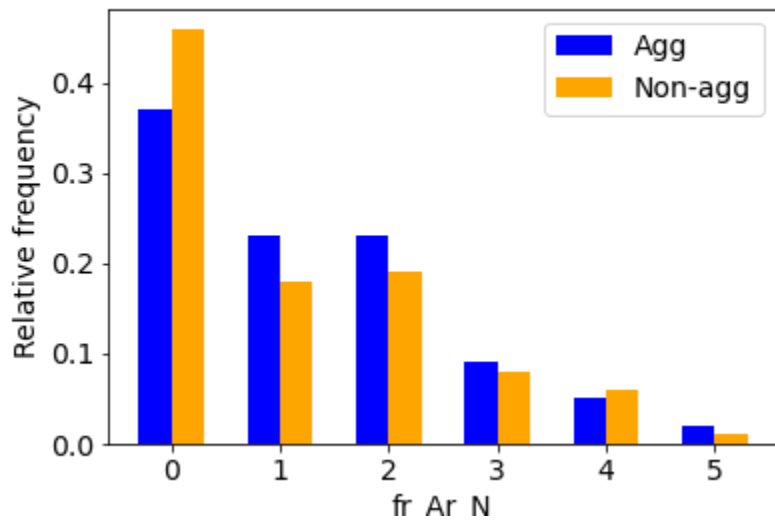
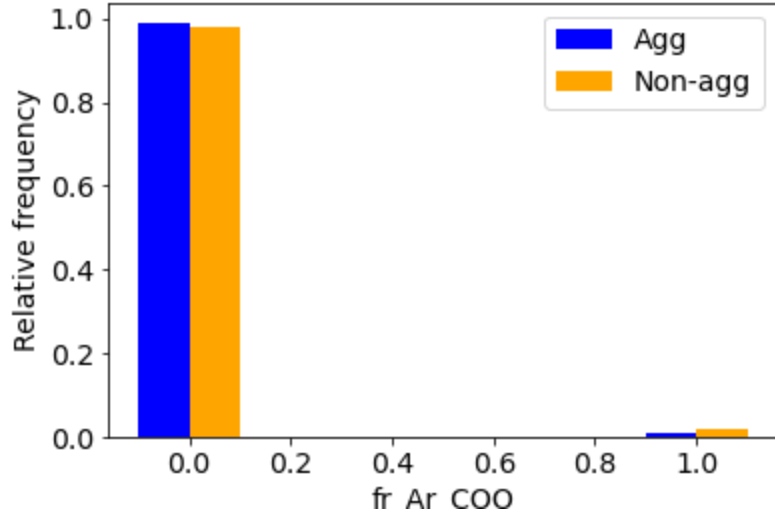


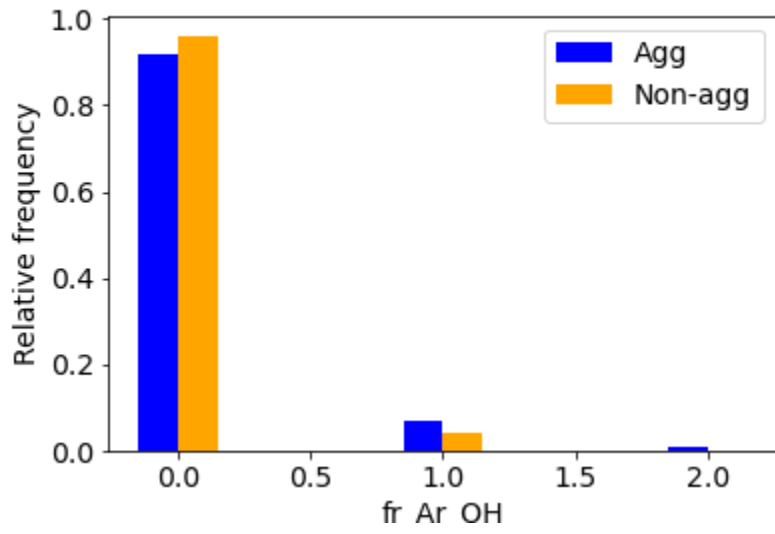
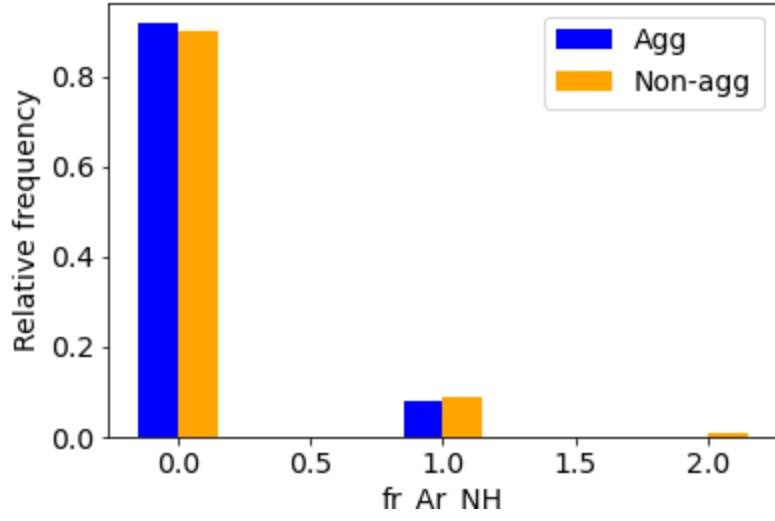


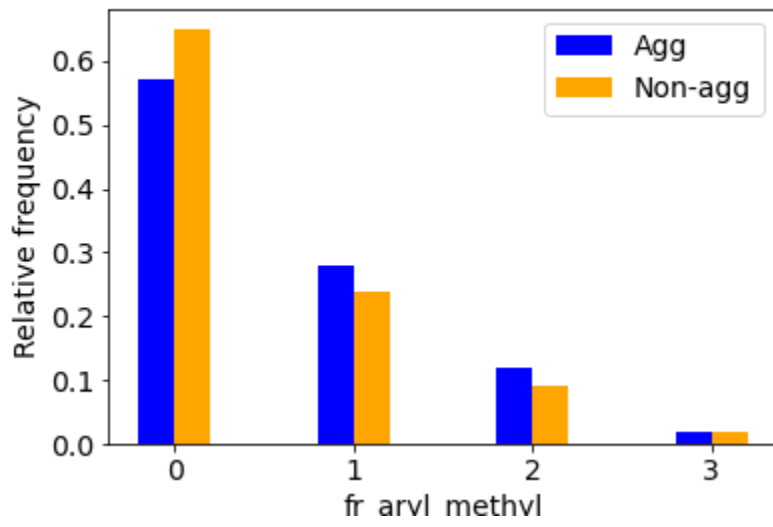
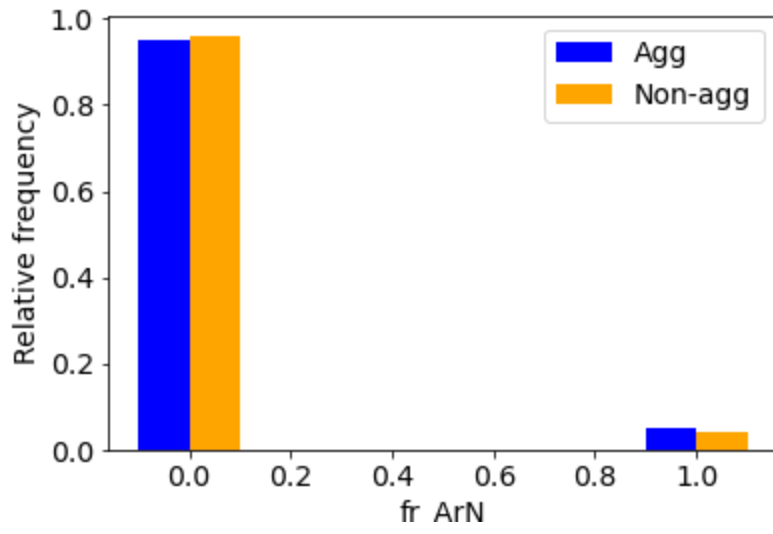


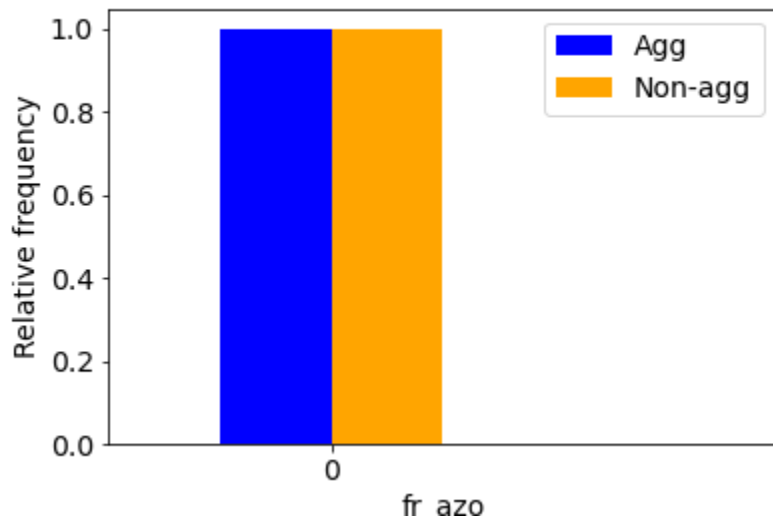
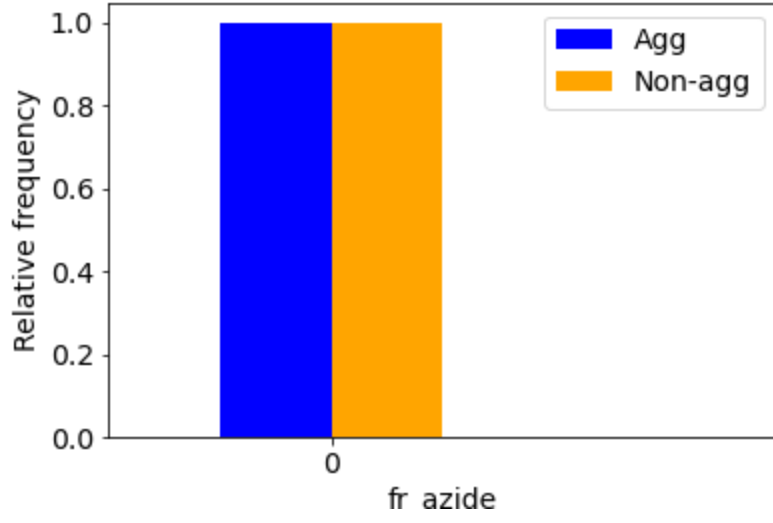


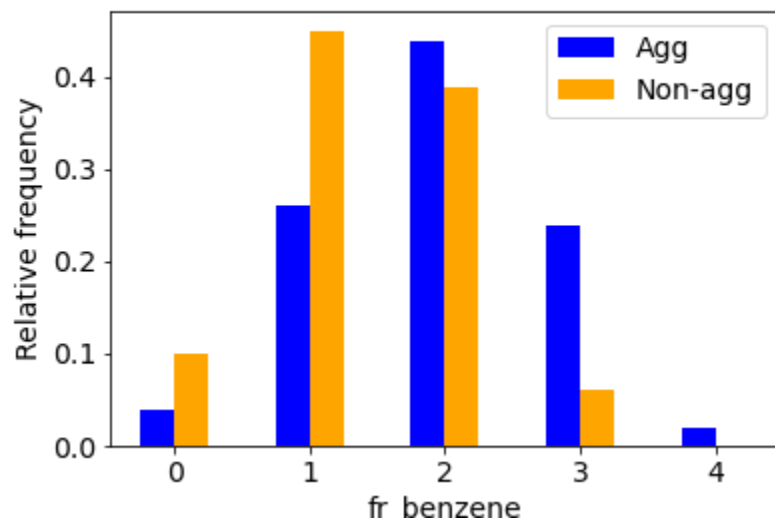
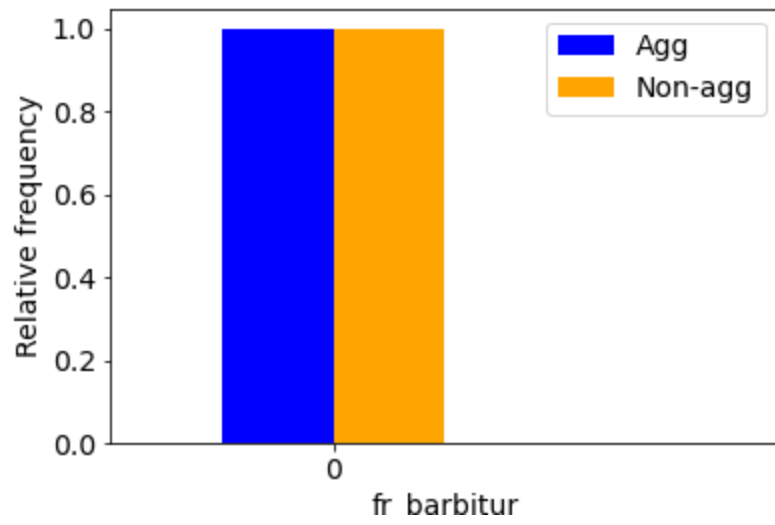


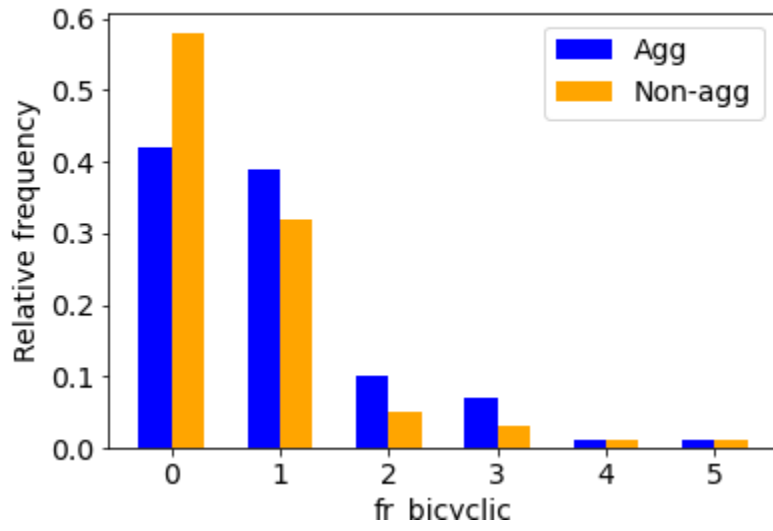
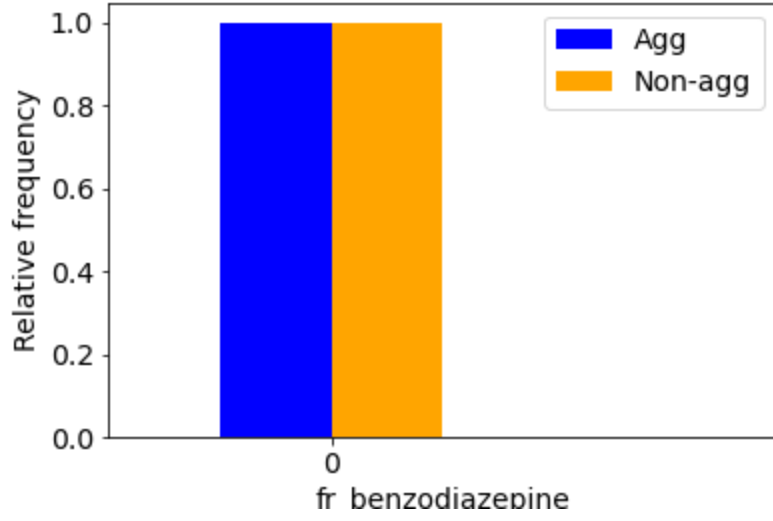


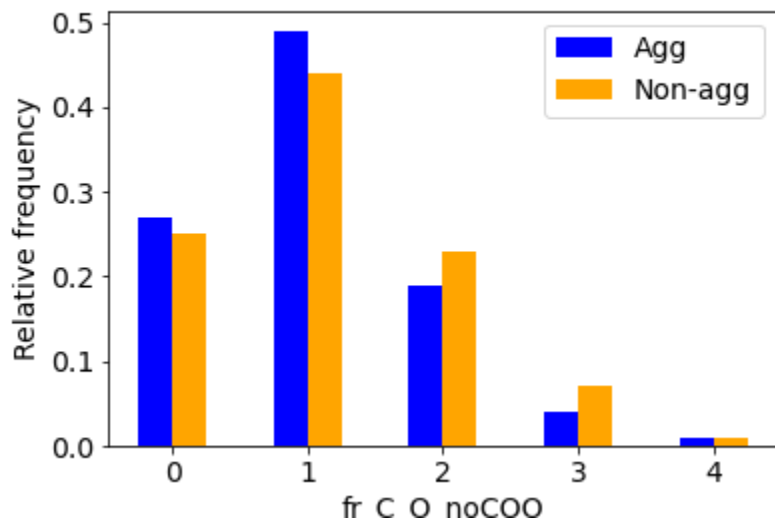
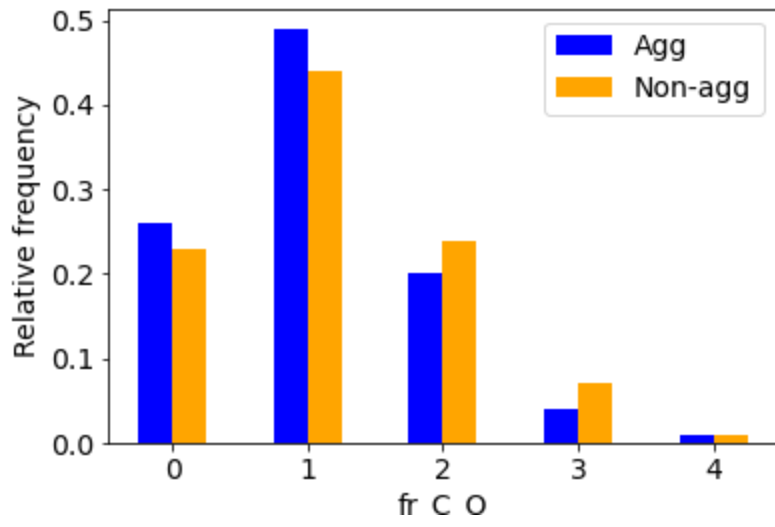


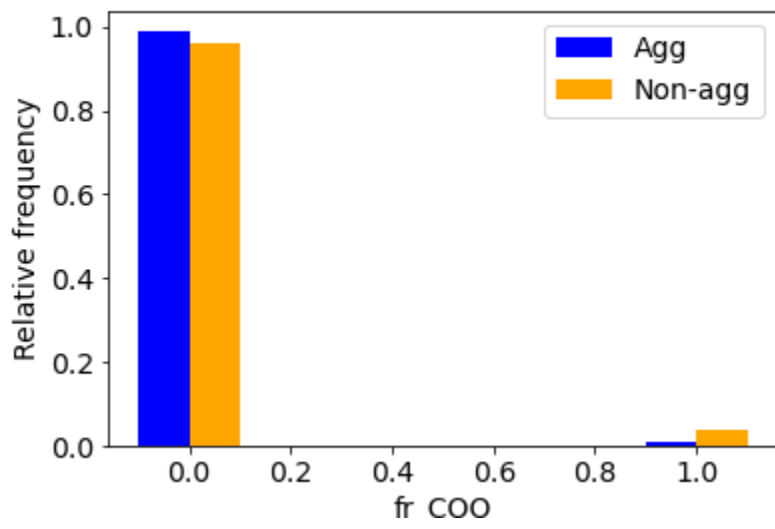
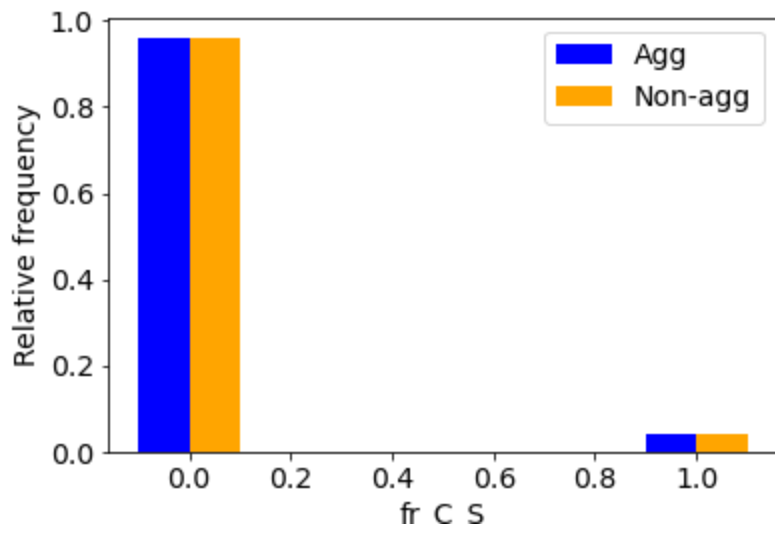


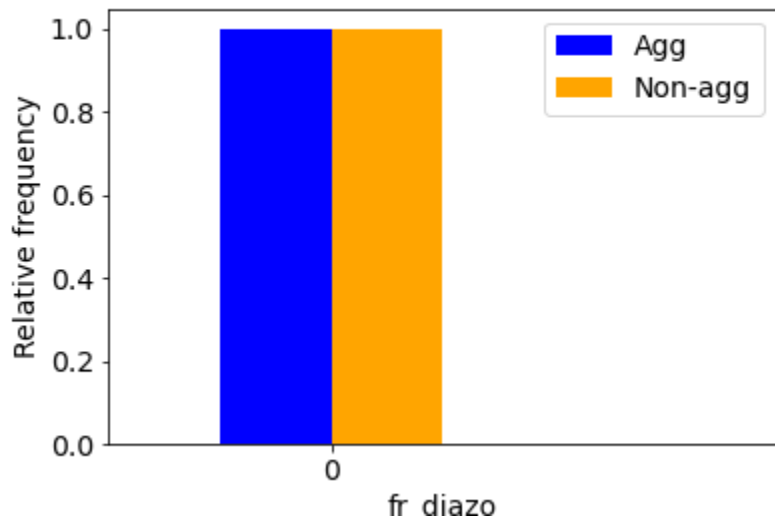
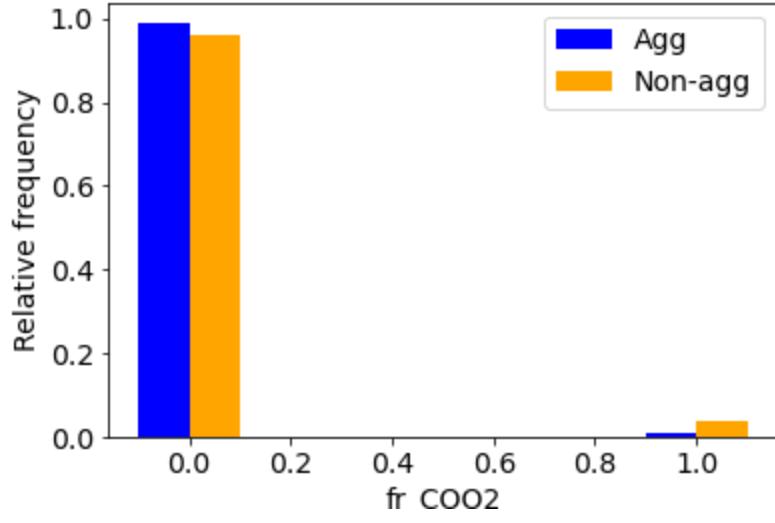


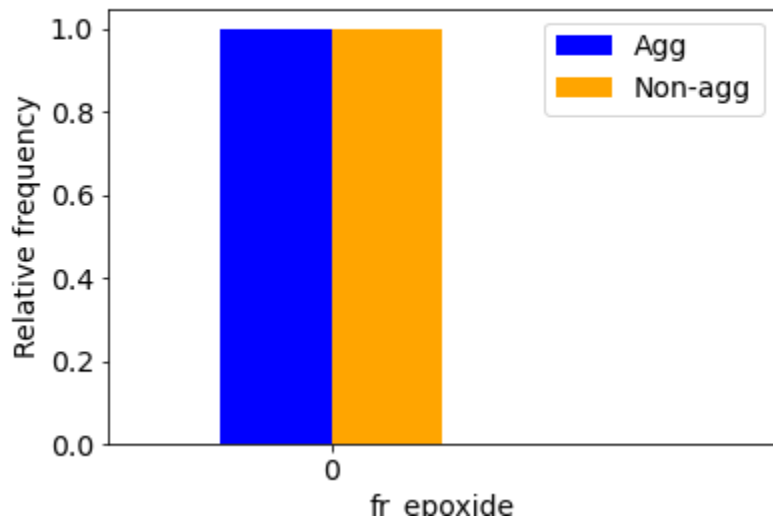
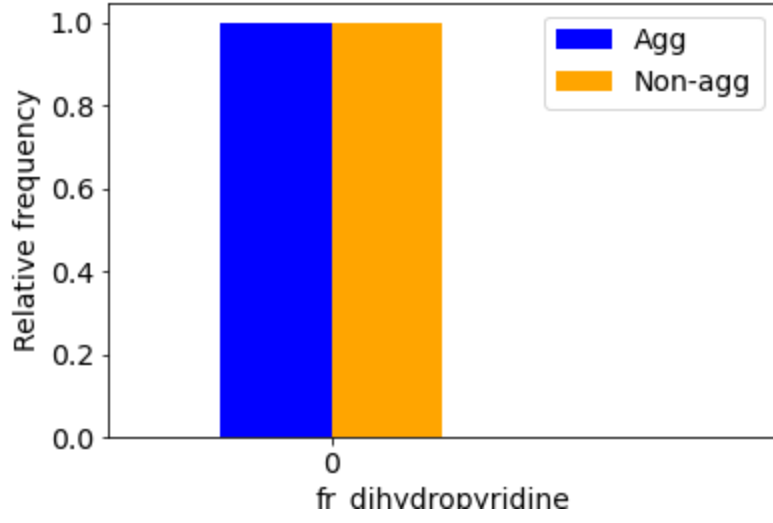


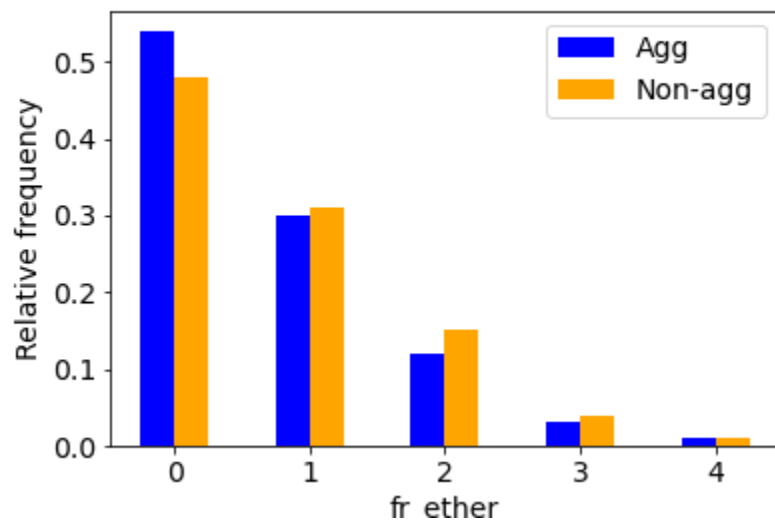
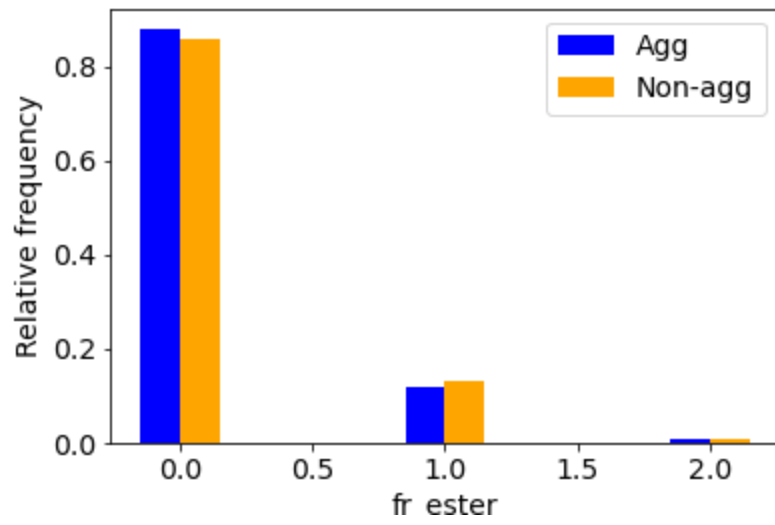


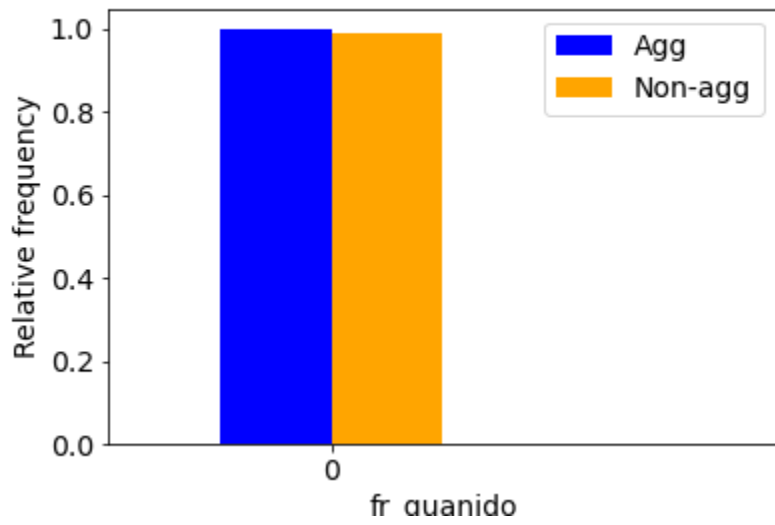
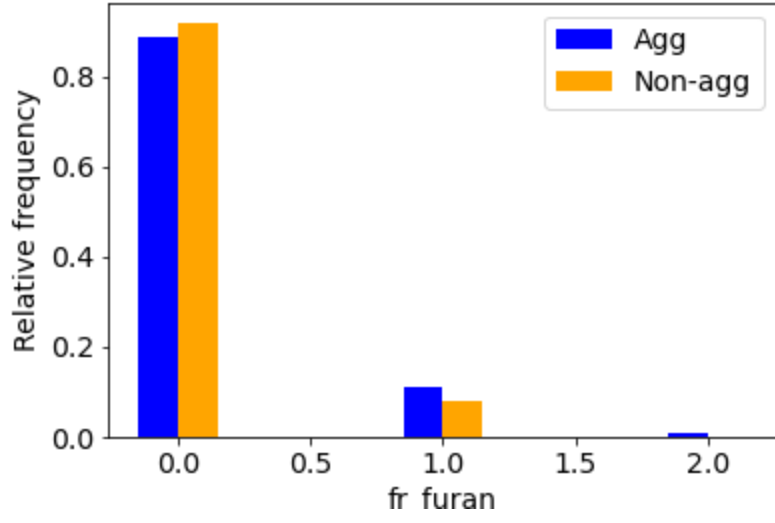


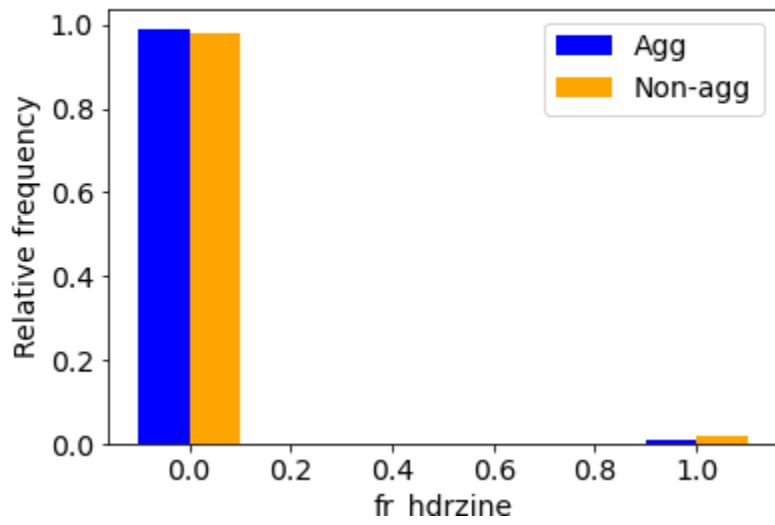
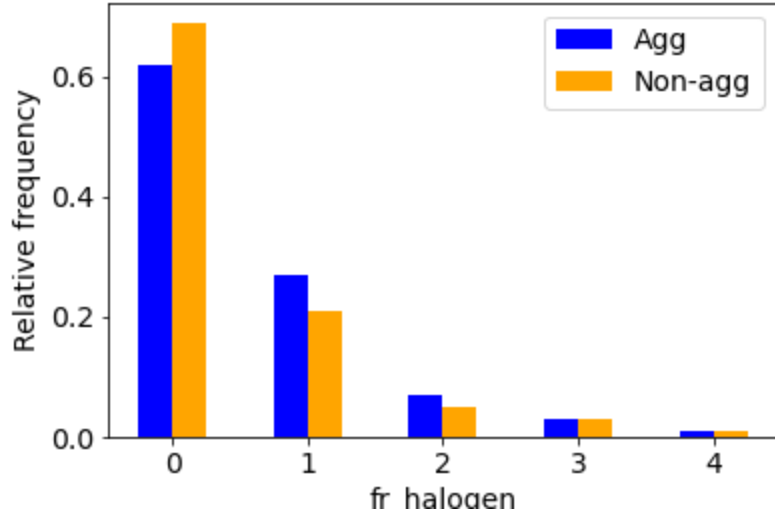


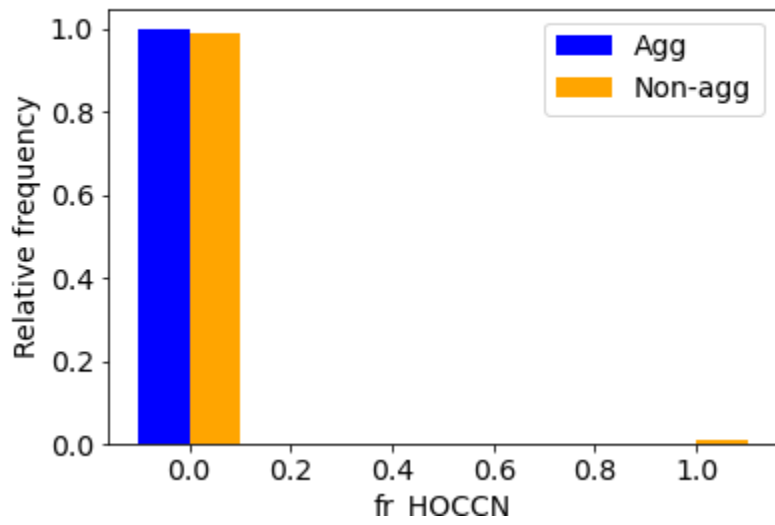
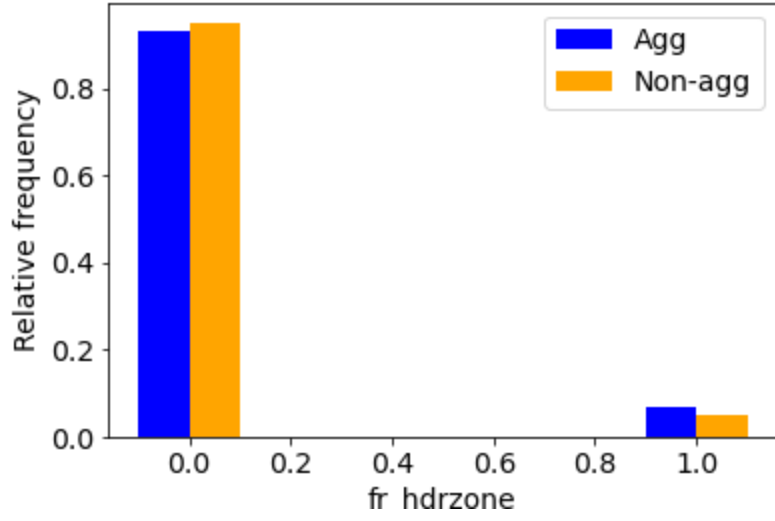


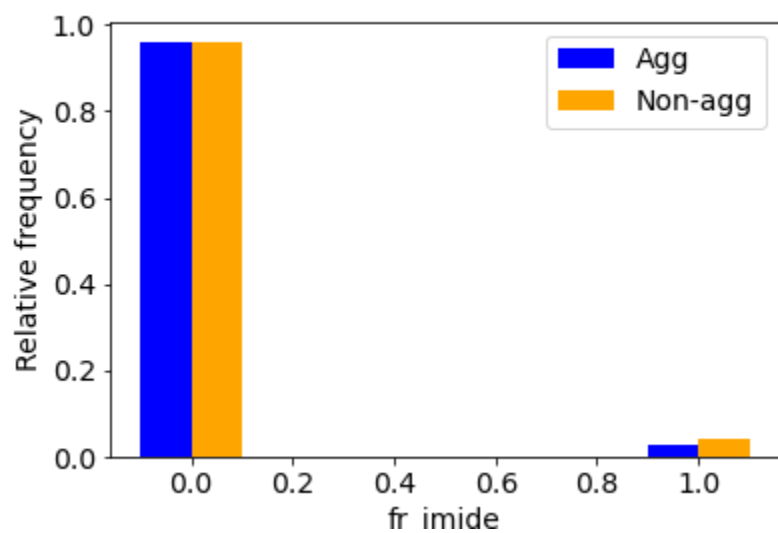
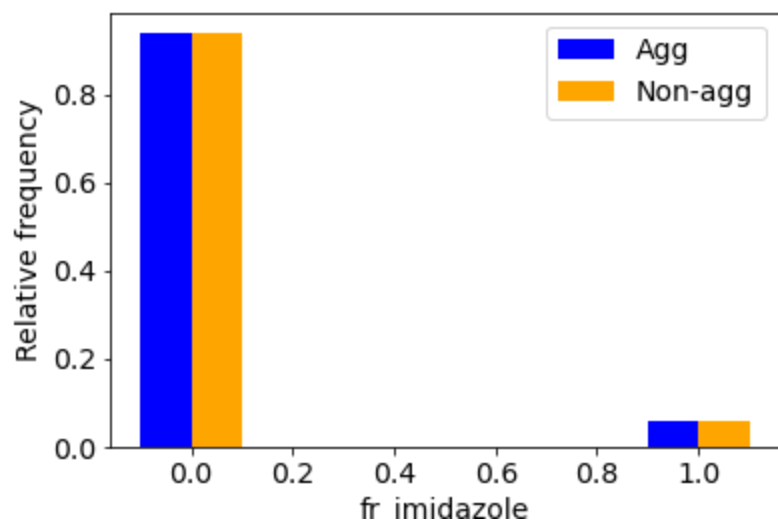


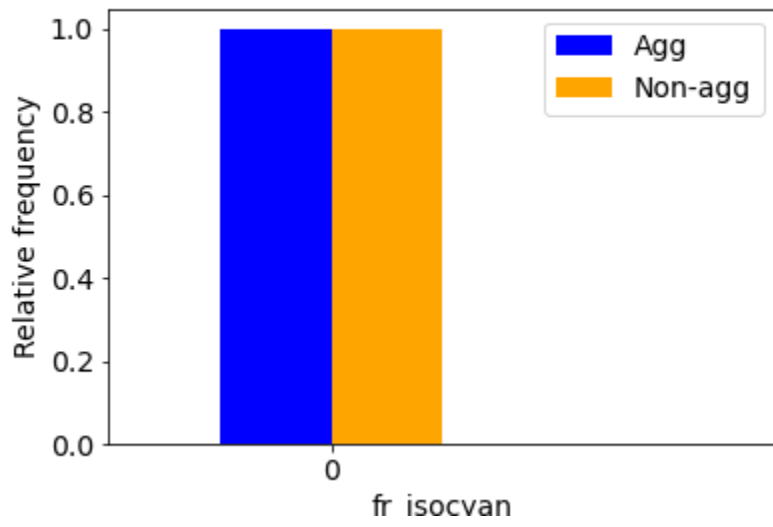
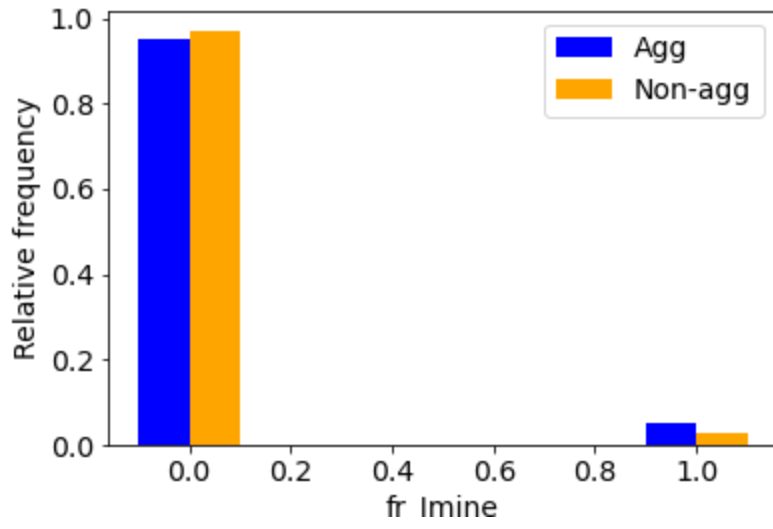


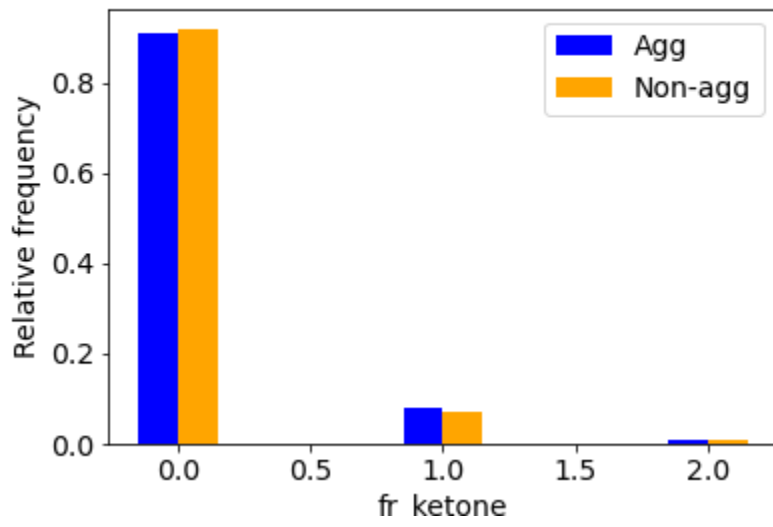
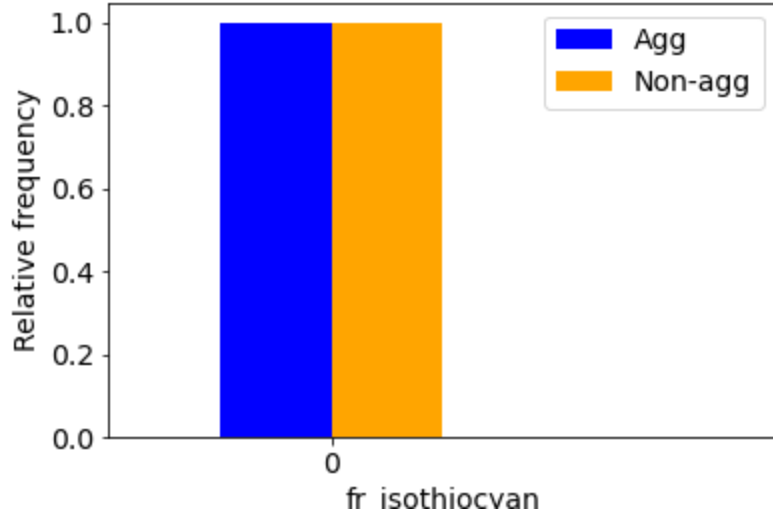


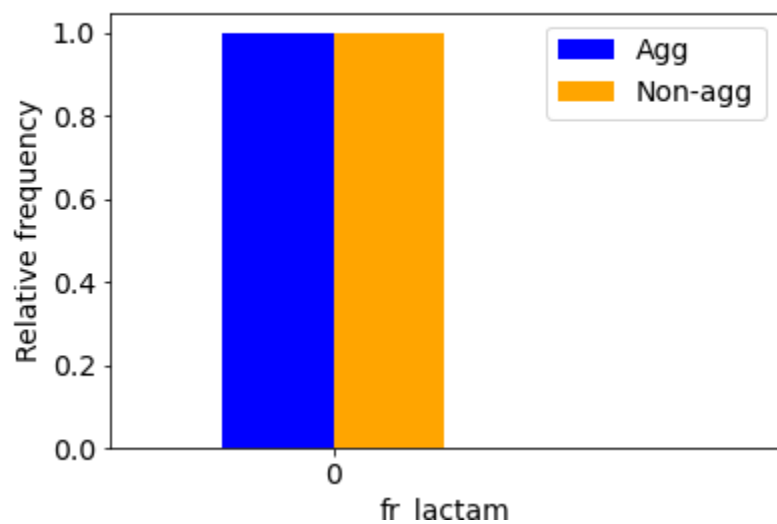
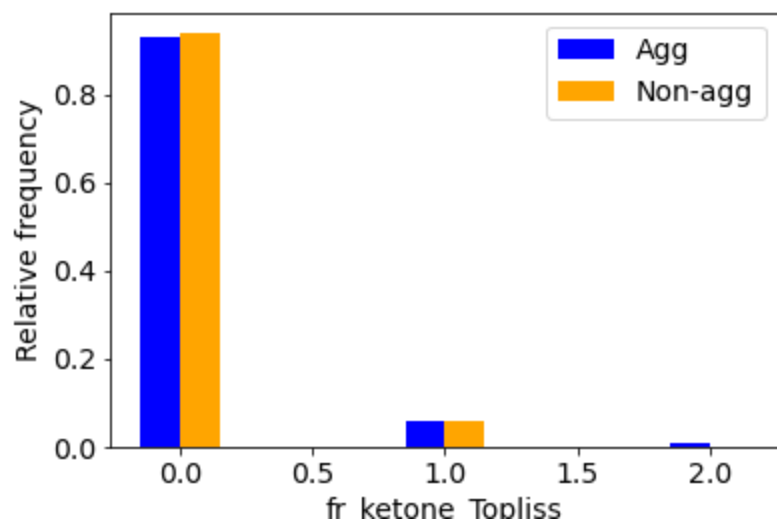


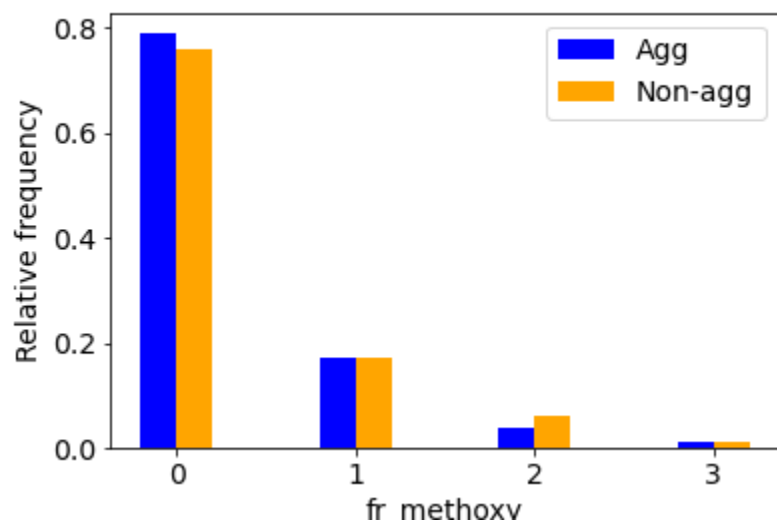
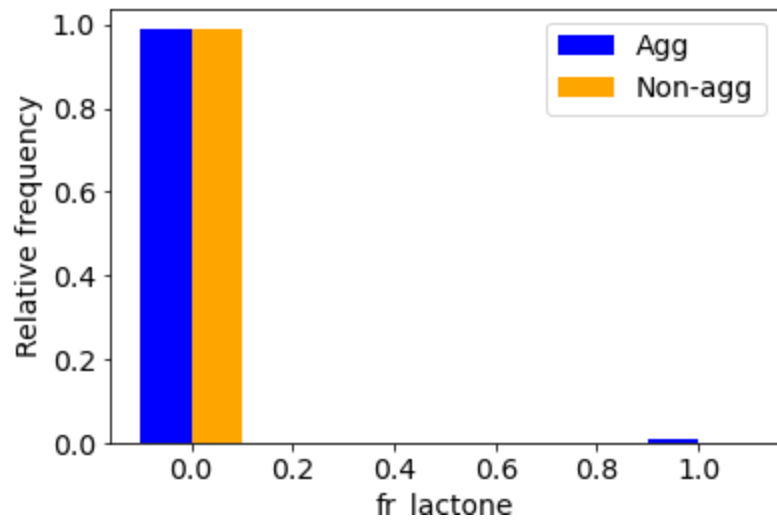


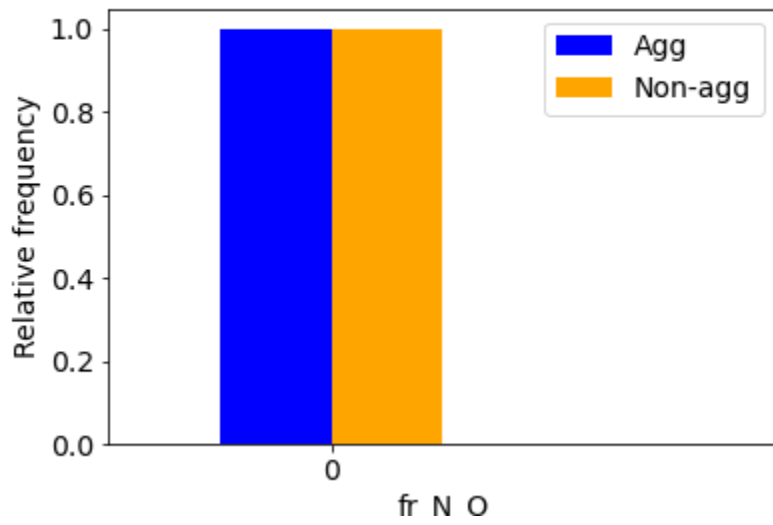
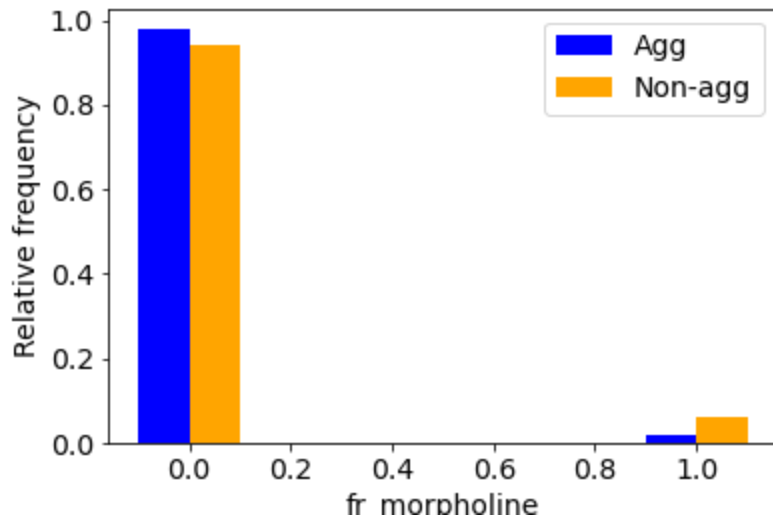


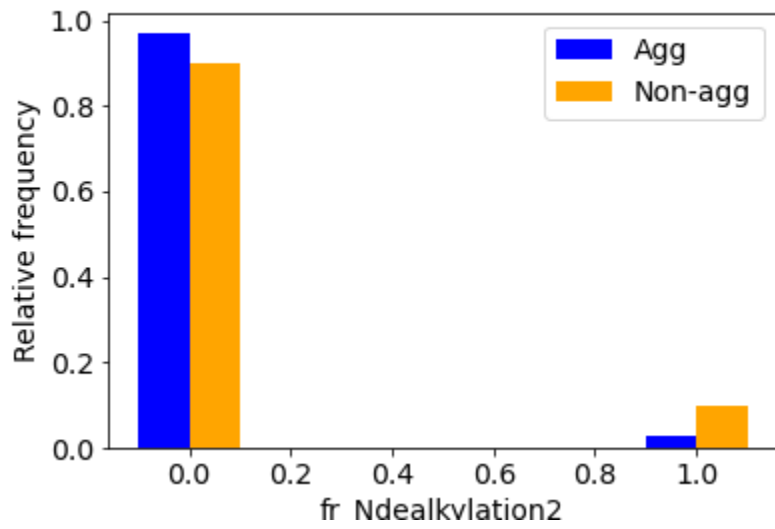
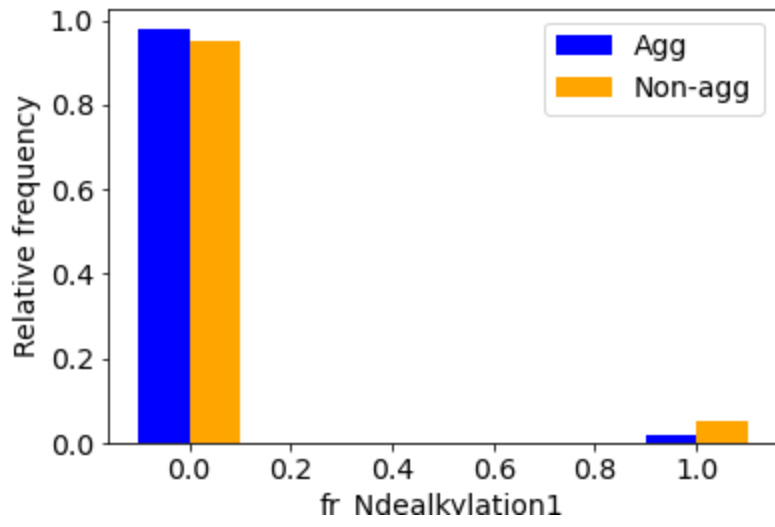


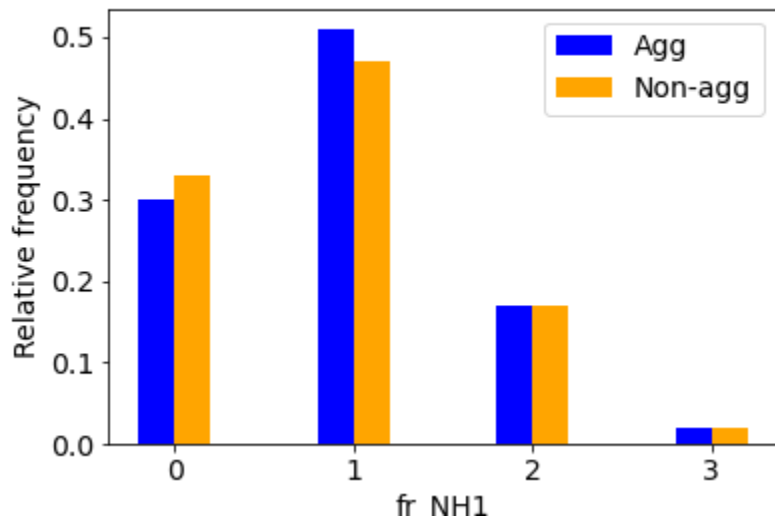
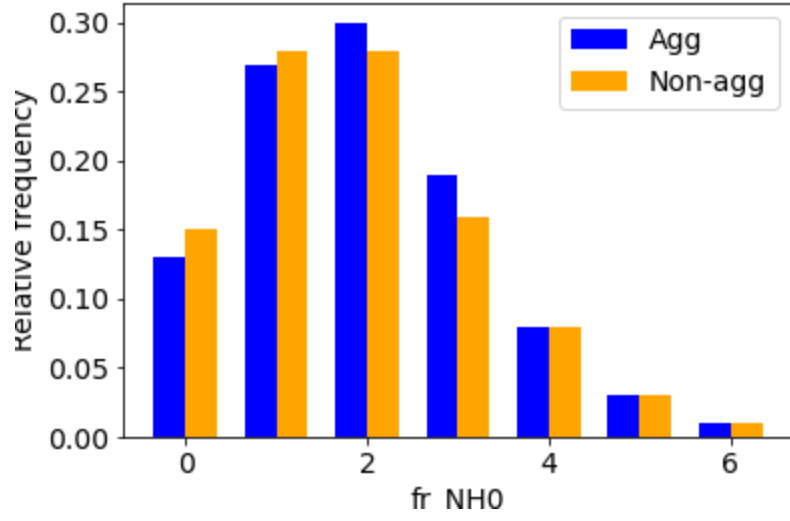


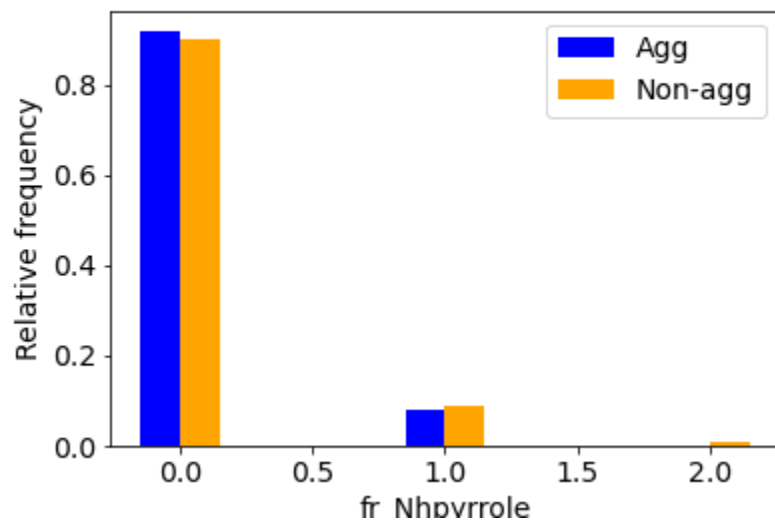
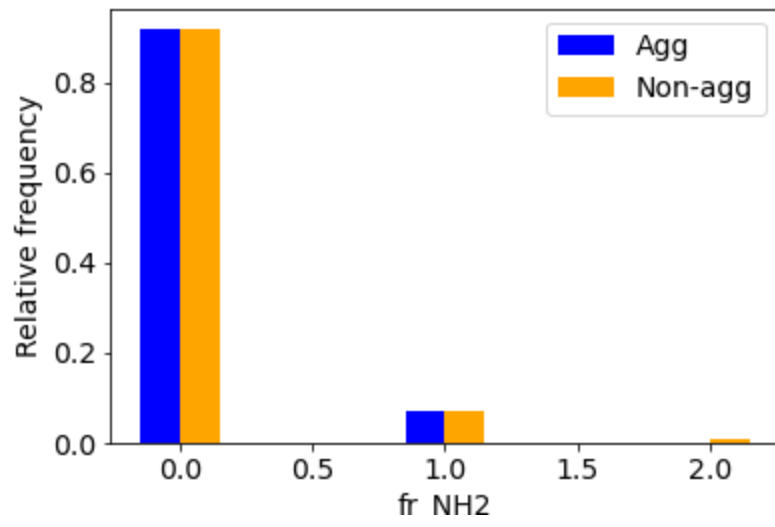


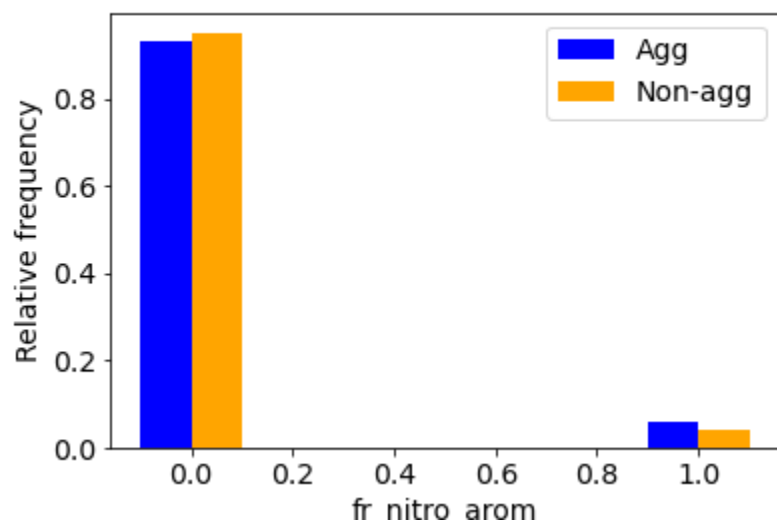
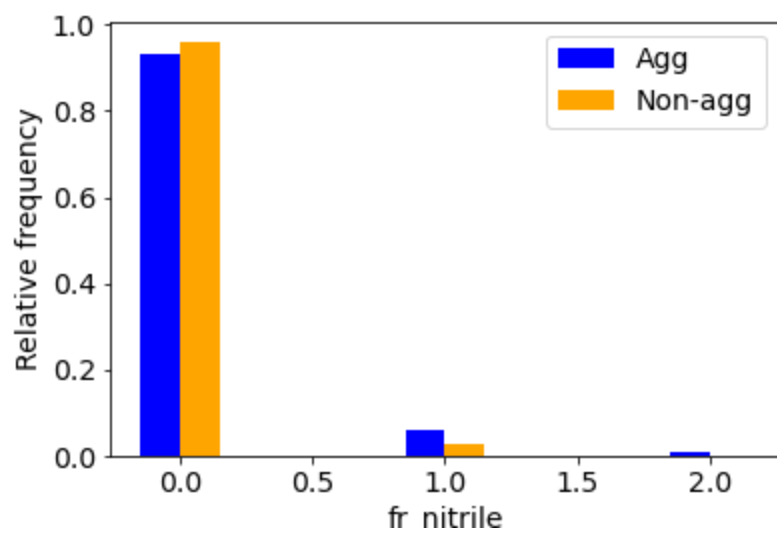


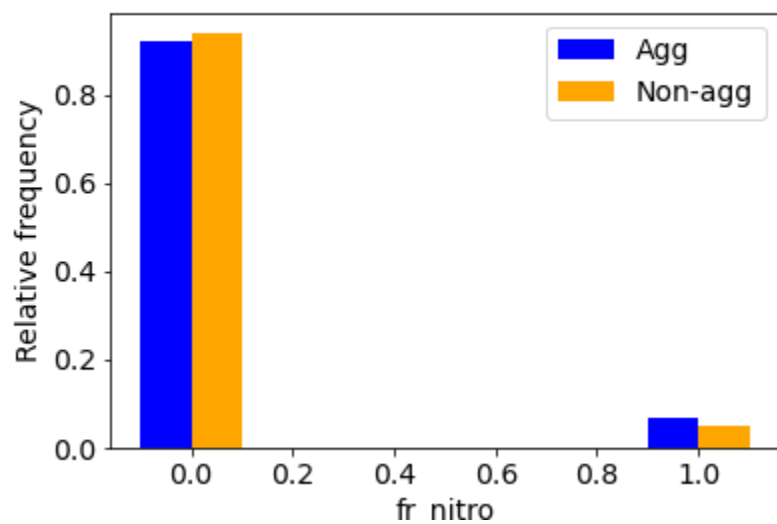
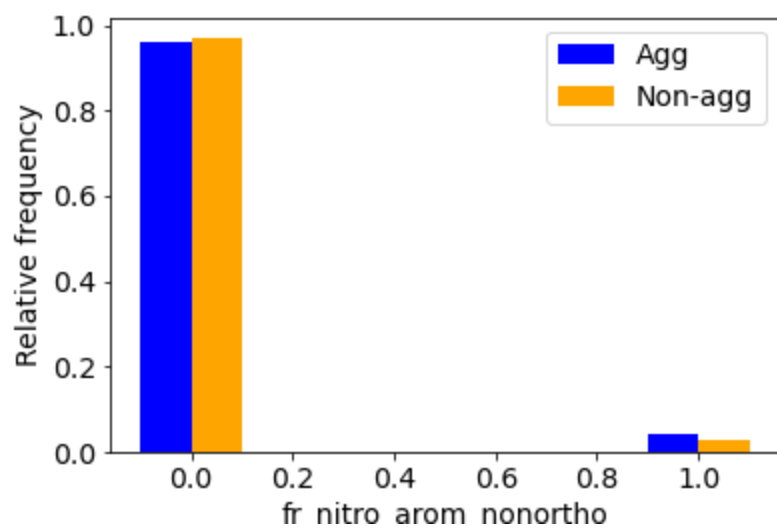


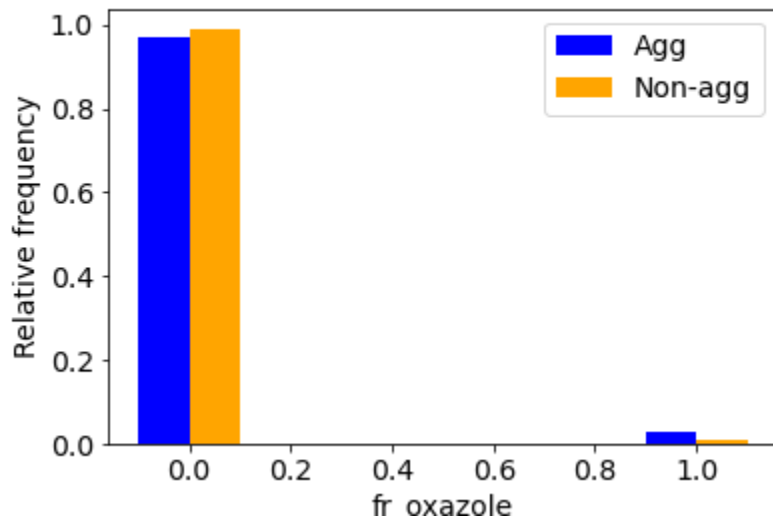
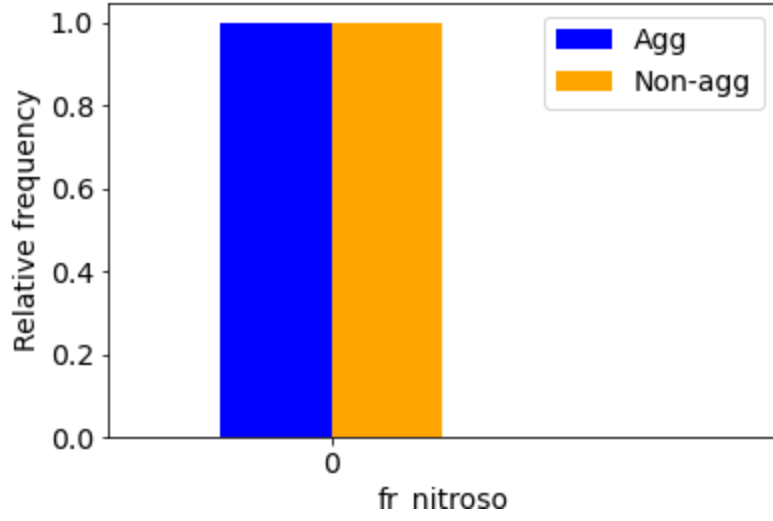


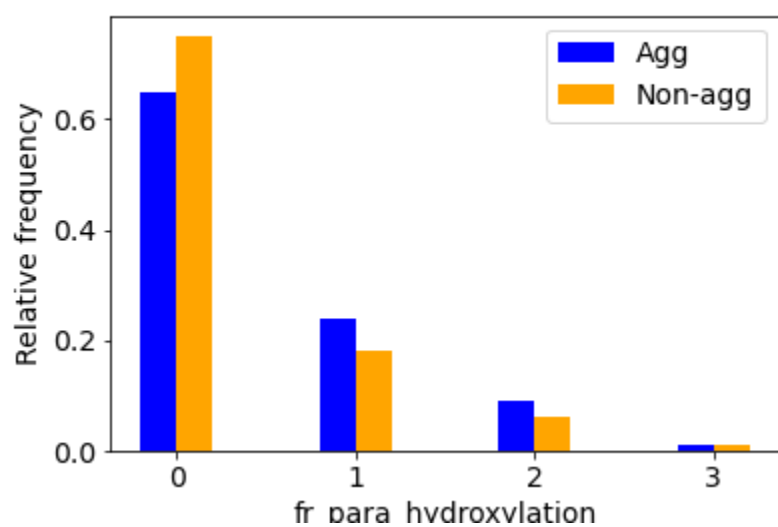
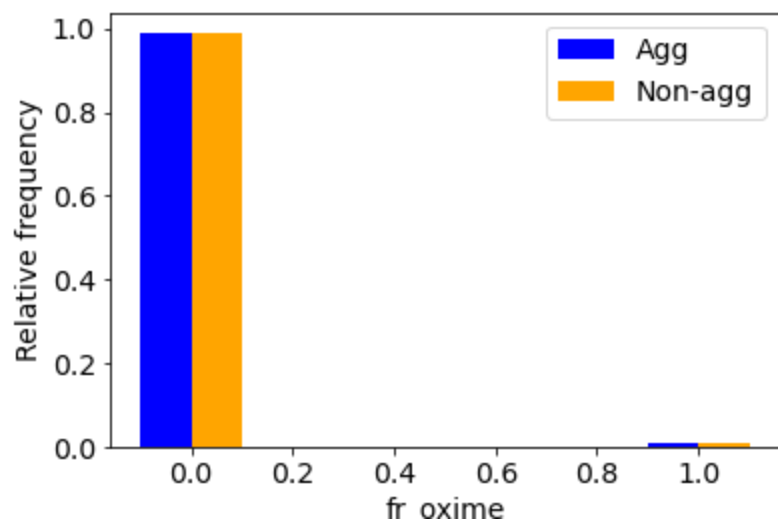


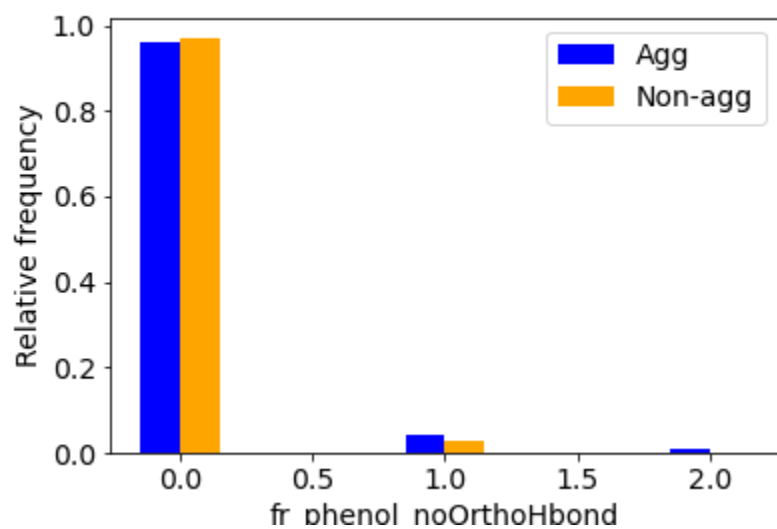
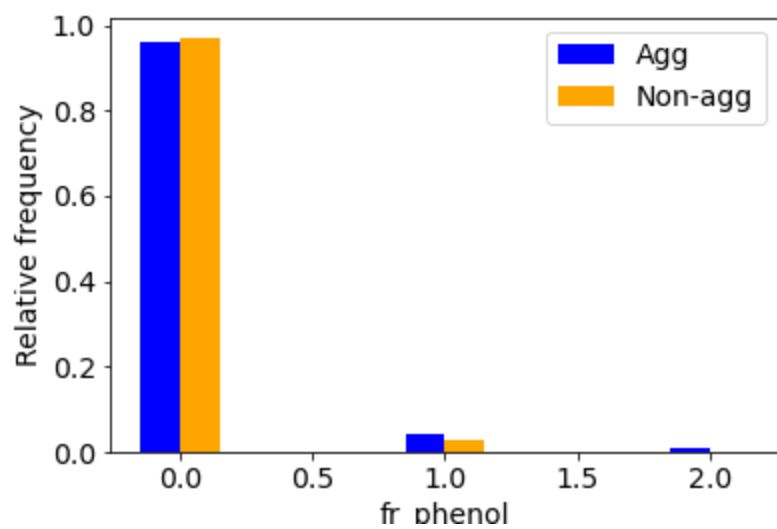


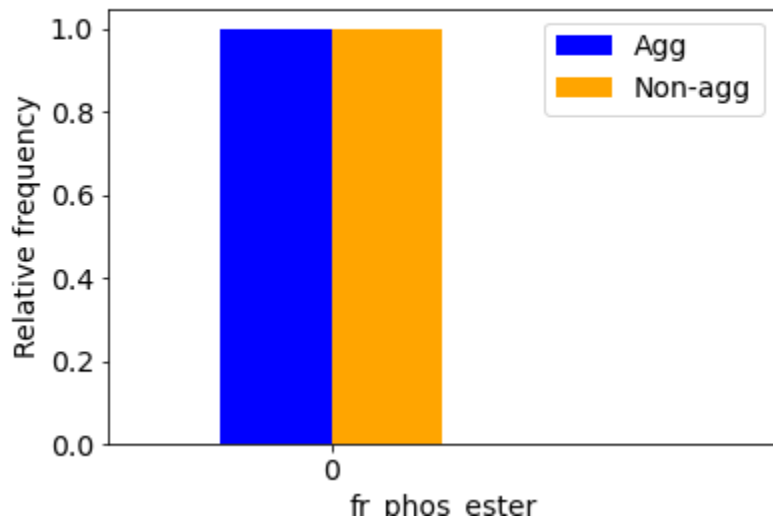
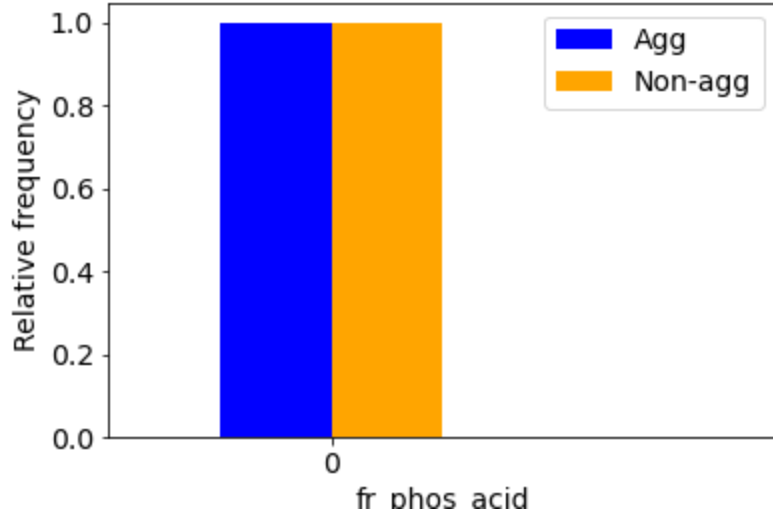


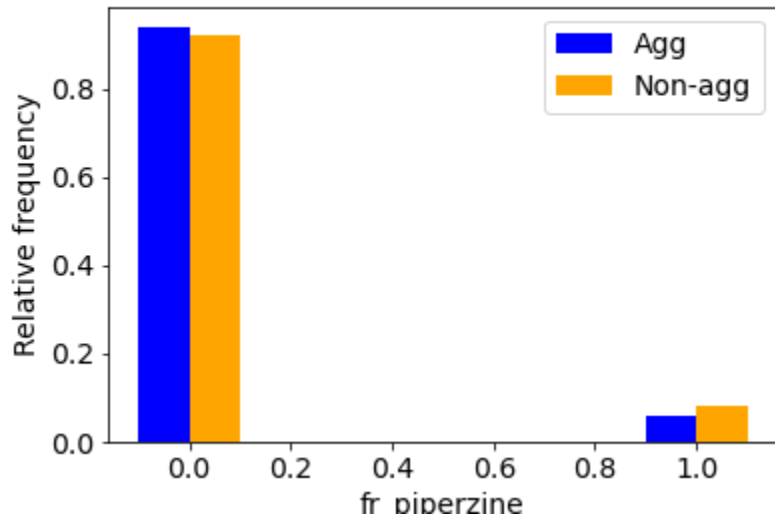
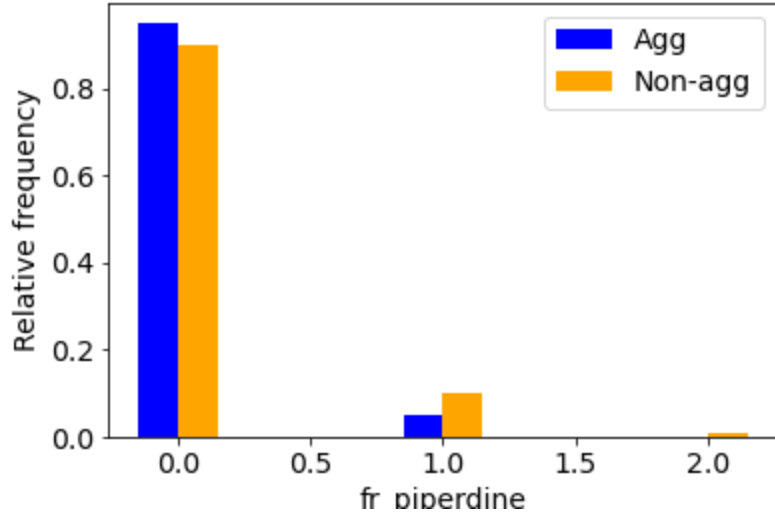


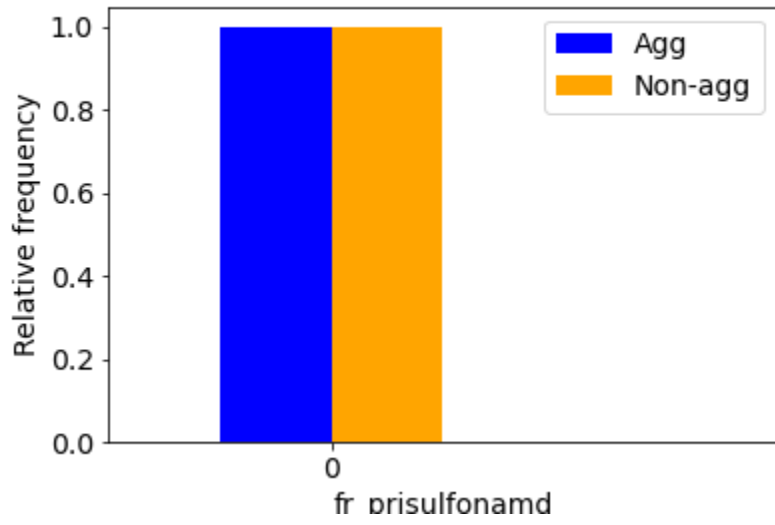
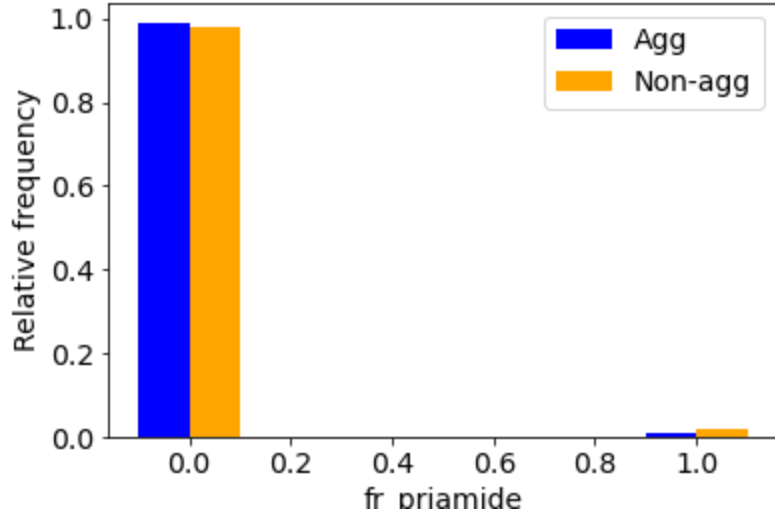


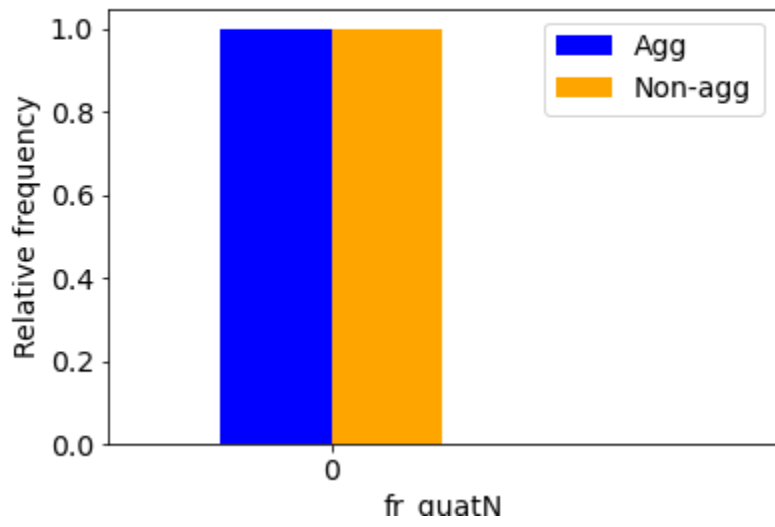
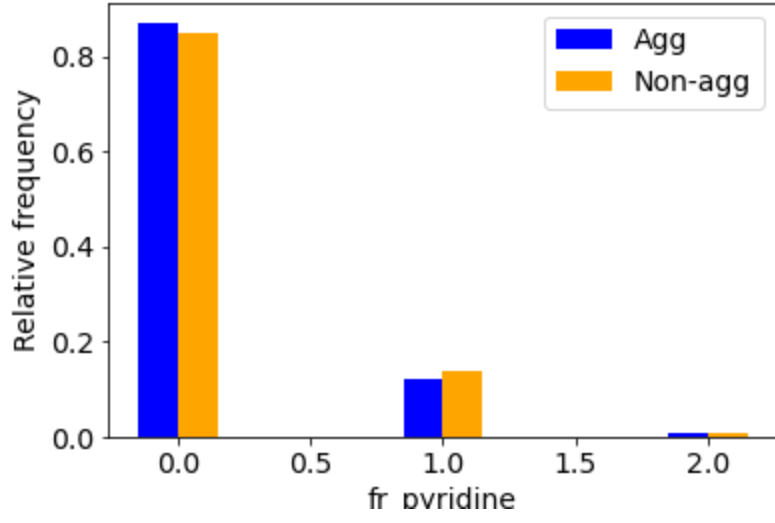


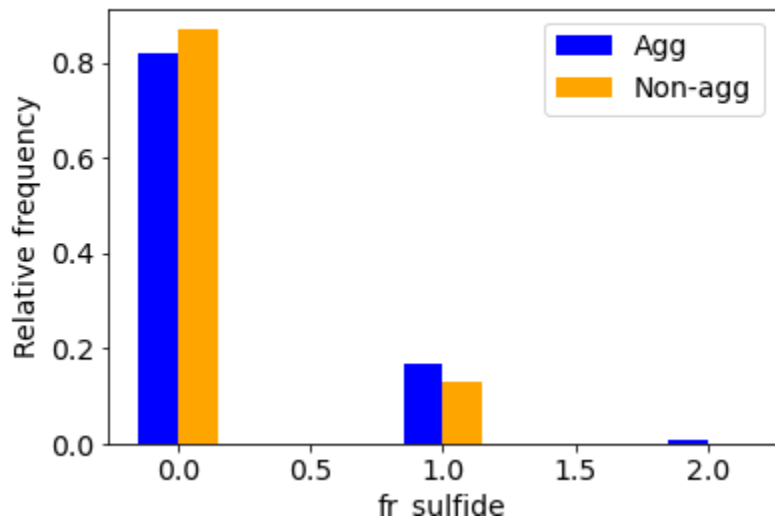
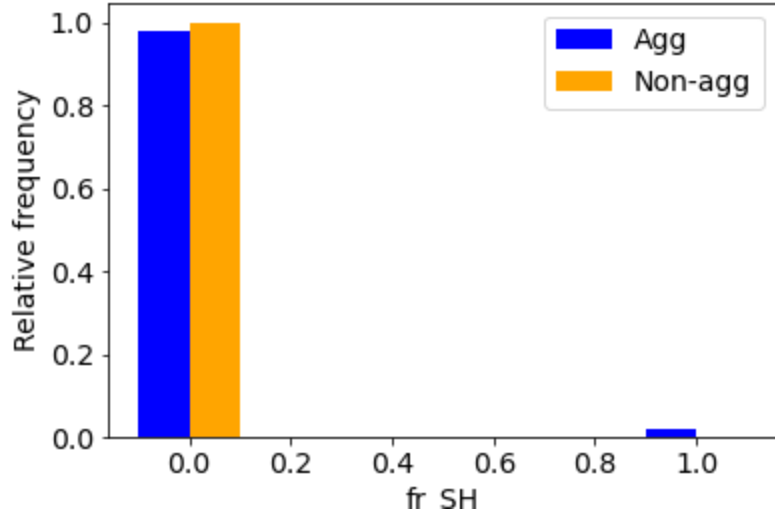


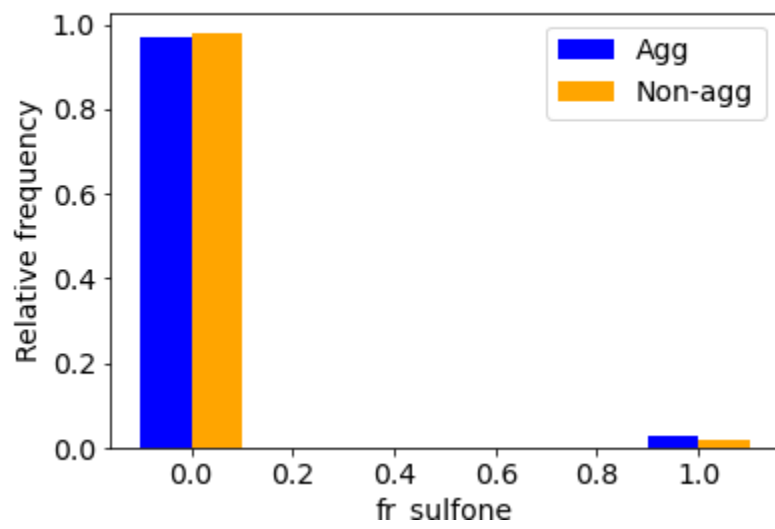
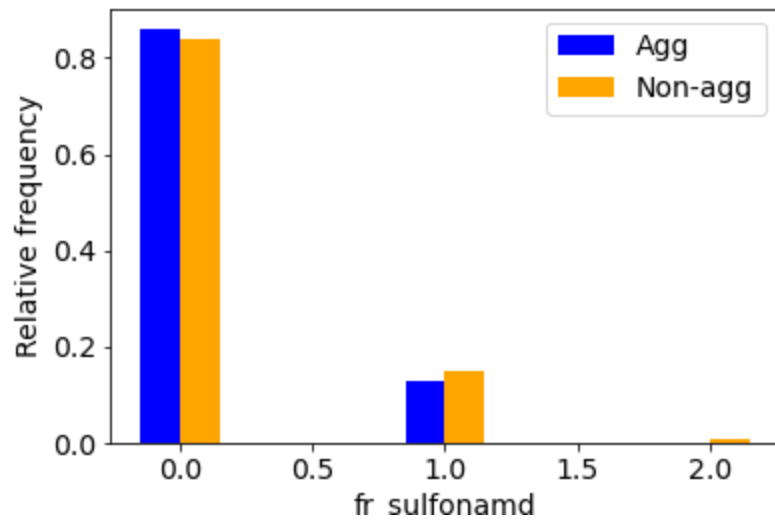


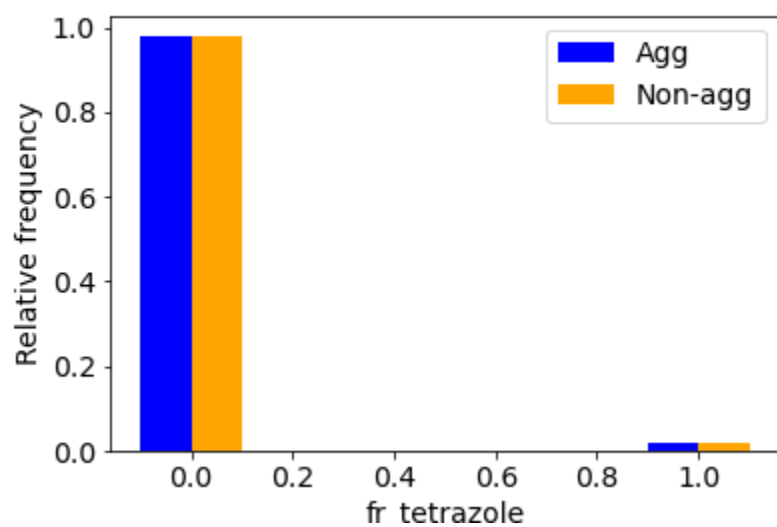
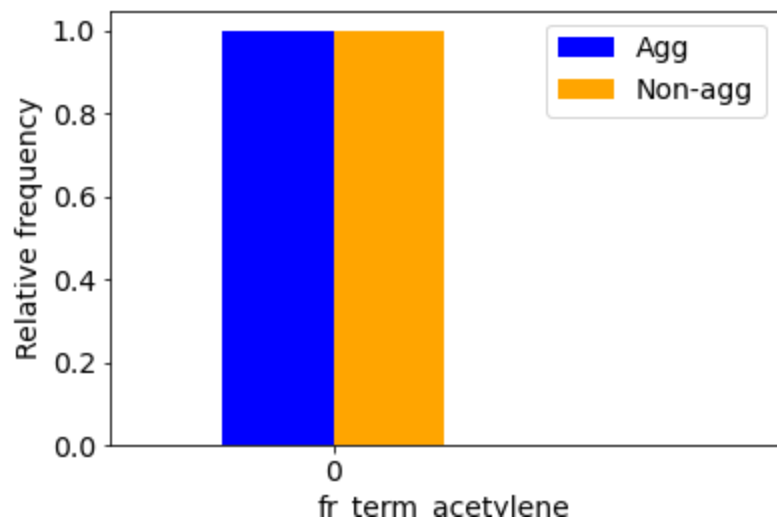


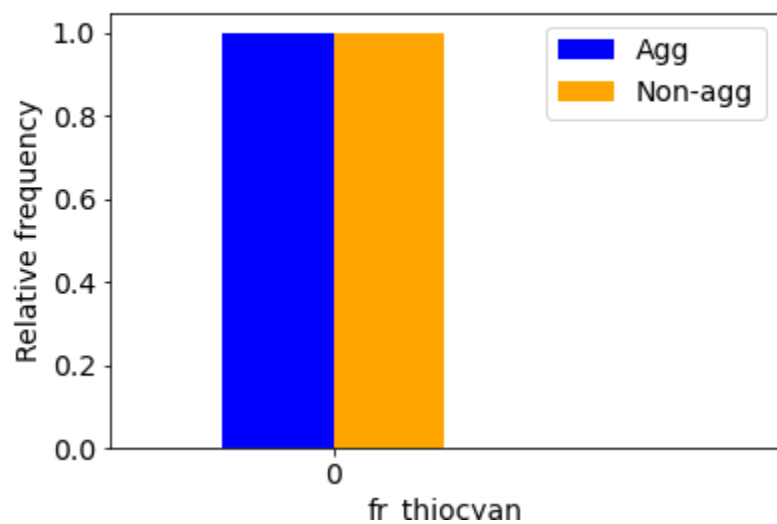
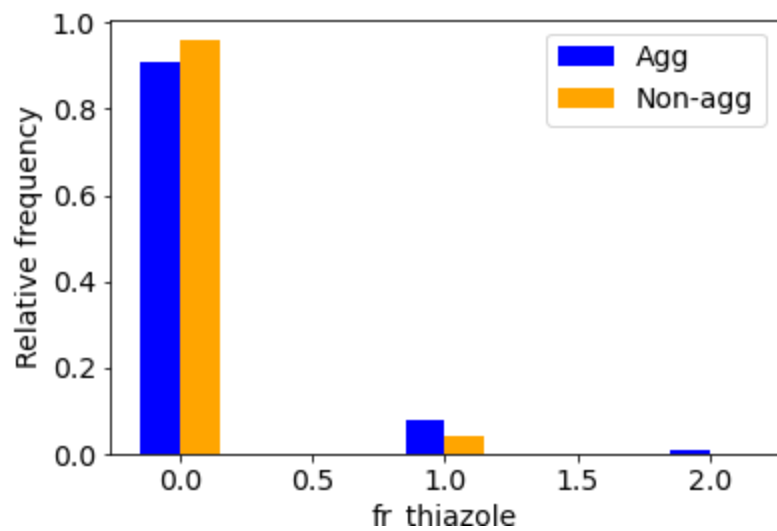












SVII. ChatGPT Explanations

When looking at the counterfactuals, we have noticed that a very common strategy to flip the label is to modify sulfur groups. Adding specific sulfur groups is often times used to flip the label from “non-aggregator” to “aggregator” while removing or inhibiting sulfur groups is often used to flip from “aggregator” to “non-aggregator”.

One possible explanation for this is that this reflects a bias in the dataset. However, assuming that it is not a bias, we have asked ChatGPT to provide possible explanations about why these groups specifically might be so important for aggregation behavior. We will collect these explanations with ChatGPT in the following sections:

J

The molecule I am looking at is classified as an aggregator it contains the following substructure "N=C(S)N". When the sulfur atom is removed "N=CN" it does not longer aggregate. What could be an explanation for this?



The difference in aggregation behavior between the two substructures, "N=C(S)N" and "N=CN," can be attributed to the presence or absence of the sulfur atom (S).



Aggregation is often driven by noncovalent interactions, such as hydrogen bonding, pi-pi stacking, and hydrophobic interactions. The addition or removal of a specific atom can disrupt or alter these interactions, leading to different aggregation tendencies.

In the case of the "N=C(S)N" substructure, the presence of the sulfur atom introduces additional opportunities for intermolecular interactions. The sulfur atom can participate in hydrogen bonding and form favorable interactions with other molecules or parts of the same molecule. These interactions contribute to the aggregation behavior observed.

However, when the sulfur atom is removed, as in the "N=CN" substructure, the potential for these specific interactions decreases. This change in the molecular structure reduces the propensity for aggregation since the sulfur atom can no longer participate in the favorable interactions that promote aggregation.

In summary, the presence of the sulfur atom in the "N=C(S)N" substructure likely facilitates specific intermolecular interactions, leading to aggregation behavior. When the sulfur atom is removed, as in the "N=CN" substructure, the favorable interactions are no longer possible, resulting in a diminished tendency for aggregation.

J

Why and how do sulfur atoms specifically cause opportunities for such aggregation-inducing interactions when compared to other functional groups such as oxygen and nitrogen?



Sulfur atoms can exhibit unique properties that make them more prone to participate in aggregation-inducing interactions compared to other functional groups such as oxygen and nitrogen. These properties include:



1. **Size and polarizability:** Sulfur is a larger atom compared to oxygen and nitrogen, which means it has more electrons and a larger atomic radius. This larger size and higher polarizability enable sulfur atoms to interact with other molecules over a larger surface area, leading to stronger intermolecular interactions.
2. **Lone pair availability:** Sulfur, like oxygen and nitrogen, possesses lone pairs of electrons. These lone pairs can participate in hydrogen bonding and other intermolecular interactions. However, the larger size and lower electronegativity of sulfur atoms compared to oxygen can make the sulfur lone pairs more accessible and more prone to engage in interactions with other molecules.
3. **Hydrophobic properties:** Sulfur is less electronegative than oxygen, making it more hydrophobic. Hydrophobic interactions play a significant role in aggregation processes, as nonpolar regions of molecules tend to associate with each other to minimize exposure to water. The hydrophobic nature of sulfur can contribute to favorable interactions between molecules in aggregating systems.
4. **Aromaticity and pi interactions:** Sulfur-containing groups, such as thiols (R-SH) and thioethers (R-S-R), can participate in pi interactions and pi-stacking interactions. These interactions involve the overlapping of pi orbitals, which can stabilize molecular assemblies and promote aggregation.
5. **Metal coordination:** Sulfur atoms can readily form coordination bonds with metal ions. This property is particularly relevant in the context of metalloproteins and metal-containing complexes, where the presence of sulfur can facilitate aggregation through metal-sulfur coordination interactions.

It's important to note that the aggregation-inducing properties of sulfur are not exclusive to sulfur alone. Other functional groups, such as oxygen and nitrogen, can also participate in intermolecular interactions that promote aggregation. The specific contribution of each functional group depends on the molecular context and the nature of the interactions involved.

J

I have another set of molecules, the first one contains a sulfur double bonded to a carbon "C=S" and it does not aggregate. If that part of the molecule is changed to a single bond "C-S" it does aggregate however. Please give a detailed description why this could be the case.



The difference in aggregation behavior between the two molecules, one containing a sulfur double bonded to a carbon (C=S) and the other with a sulfur single bonded to a carbon (C-S), can be explained by considering the electronic and steric factors associated with the bonding arrangement.



In the case of the molecule with the C=S bond:

1. **Electronic Factors:** The double bond between carbon and sulfur in C=S results in a strong pi bond formed by the overlap of p orbitals. This pi bond holds the atoms closer together, reducing the available space for intermolecular interactions. The electron density is primarily localized in the pi bond, making it less accessible for interactions with other molecules. Consequently, the molecule is less prone to aggregation because the interactions required for aggregation, such as hydrogen bonding or pi stacking, have limited opportunities.
2. **Steric Factors:** The double bond in C=S introduces rigidity into the molecule due to the planar arrangement of the bond. This rigidity restricts the conformational flexibility of the molecule, limiting its ability to adopt favorable orientations for aggregation.

In contrast, in the molecule with the C-S bond:

1. **Electronic Factors:** The single bond between carbon and sulfur in C-S allows for greater electron density around the sulfur atom, making it more available for interactions. The electron density is more evenly distributed between the carbon and sulfur atoms, enabling the sulfur atom to engage in intermolecular interactions with neighboring molecules.
2. **Steric Factors:** The single bond in C-S introduces more flexibility into the molecule, allowing it to adopt different conformations and orientations favorable for intermolecular interactions. This increased conformational freedom enhances the opportunities for aggregation-inducing interactions, such as hydrogen bonding, pi stacking, and other noncovalent interactions.

In summary, the presence of a double bond between carbon and sulfur (C=S) limits the availability of electron density for intermolecular interactions and introduces rigidity into the molecule, reducing its propensity for aggregation. On the other hand, a single bond between carbon and sulfur (C-S) provides more electron density and flexibility, allowing for increased intermolecular interactions and facilitating aggregation.